



UNIVERSITÀ DEGLI STUDI DI TRIESTE

XXIX ciclo

PhD corso in Nanotecnologie

INTRACELLULAR DNA DELIVERY USING POLYMERIC NANOPARTICLES FOR LYSOSOMAL STORAGE DISORDERS GENE THERAPY

Settore scientifico-disciplinare: **BIO/13 BIOLOGIA APPLICATA**

**DOTTORANDA
Eleonora De Martino**

**COORDINATORE
Prof.ssa Lucia Pasquato**

**SUPERVISORE DI TESI
Prof.ssa Serena Bonin**

Dott. Giovanni Maria Severini



IRCCS BURLO GAROFOLO - TRIESTE
dott. Giovanni Maria Severini

ANNO ACCADEMICO 2015/2016

Summary

SUMMARY	1
1 ABSTRACT	5
2 INTRODUCTION	8
2.1 TRANSPOSABLE ELEMENTS	9
2.1.1 <i>Tc1/mariner superfamily</i>	10
2.1.2 <i>Sleeping Beauty</i>	10
2.1.2.1 Transposase	11
2.1.2.2 Transposon	12
2.1.2.3 Cut and Paste mechanism	13
2.1.3 <i>Sleeping Beauty applications</i>	16
2.2 BLOOD BRAIN BARRIER	17
2.2.1 <i>Mechanism to cross the blood brain barrier</i>	18
2.2.2 <i>Strategy of drugs delivery</i>	19
2.2.3 <i>Synthetic opioid peptide g7</i>	21
2.3 ALTERNATIVE ROUTES OF ADMINISTRATION	22
2.3.1 <i>Ependymal barrier</i>	22
2.3.2 <i>Intranasal drug delivery</i>	23
2.4 NANOPARTICLES	24
2.4.1 <i>Polymeric nanoparticles</i>	25
2.4.1.1 PLGA	28
2.4.1.2 PLGA nanoparticles and plasmid DNA	29
2.4.1.3 Polysaccharide nanoparticles	30
2.4.1.4 Chitosan	31
2.4.1.5 Chitosan and plasmid DNA	33
2.5 GLOBOID CELLS LEUKODYSTROPHY (OR KRABBE'S DISEASE)	35
2.5.1 <i>Pathogenic Mechanisms</i>	37
2.5.2 <i>Therapy</i>	38
2.5.3 <i>Animal Models</i>	39
3 OBJECTIVE	41
4 MATERIALS AND METHODS	43
4.1 PLASMIDS	44
4.2 PLASMIDS SEQUENCING	47
4.3 CELL CULTURE	48
4.4 CELL TRANSFECTION	49

4.5	LUCIFERASE ASSAY	49
4.6	DNA EXTRACTION	50
4.7	RNA EXTRACTION AND RT	50
4.8	REAL TIME PCR	50
4.8.1	<i>Absolute Real-Time quantification</i>	50
4.8.2	<i>Relative Real-Time quantification</i>	51
4.9	PROTEIN EXTRACTION AND QUANTIFICATION	52
4.10	ENZYMATIC ASSAY	52
4.11	PLASMID LABELING	52
4.12	CELL LABELING AND FIXATION.....	53
4.13	CELL VIABILITY ASSAY	53
4.14	ANIMALS	54
4.15	THE G7 OPIOID PEPTIDE BOUND TO PLGA NANOPARTICLES.....	54
4.15.1	<i>The g7-PLGA nanoparticles preparation and characterization</i>	54
4.15.2	<i>In vivo imaging</i>	54
4.16	CHITOSAN	55
4.16.1	<i>Chitosan/plasmid DNA nanoplexes preparation</i>	55
4.16.2	<i>Gel retardation assay</i>	56
4.16.3	<i>Cellular uptake</i>	56
4.16.4	<i>Chitosan/TPP-hyaluronic acid nanoparticles preparation</i>	57
4.16.5	<i>Chitosan/TPP-hyaluronic acid nanoparticles characterization</i>	58
4.16.6	<i>Chitosan/TPP-hyaluronic acid nanoparticles encapsulation efficiency</i>	58
4.16.7	<i>Chitosan/TPP-hyaluronic acid nanoparticles up-take efficiency</i>	58
4.17	STATISTICAL ANALYSIS.....	59
5	RESULTS	60
5.1	<i>IN VITRO EXPERIMENTS</i>	61
5.1.1	<i>Cell transfection</i>	61
5.1.2	<i>Luciferase assay</i>	62
5.1.3	<i>Absolute Quantitative Real time PCR</i>	66
5.1.4	<i>Relative quantitative Real Time PCR</i>	69
5.1.5	<i>Enzymatic activity</i>	71
5.2	PLASMID LABELING	73
5.3	G7 OPIOID PEPTIDE BOUND TO PLGA NANOPARTICLES.....	75
5.3.1	<i>g7-PLGA nanoparticles preparation and characterization</i>	75
5.3.2	<i>In vivo Imaging</i>	76
5.4	CHITOSAN NANOPLEXES AND CHITOSAN/TPP-HYALURONIC ACID NANOPARTICLES.....	77

5.4.1	<i>Preparation of chitosan/plasmid DNA nanoplexes</i>	78
5.4.2	<i>Gel retardation assay of the chitosan nanoplexes</i>	79
5.4.3	<i>Cell viability of the chitosan nanoplexes</i>	80
5.4.4	<i>Cellular uptake of the chitosan nanoplexes</i>	81
5.4.5	<i>Synthesis and characterization of Chitosan/TPP-hyaluronic acid nanoparticles</i>	82
5.4.6	<i>Cellular uptake of the chitosan/TPP-hyaluronic acid nanoparticles</i>	84
6	DISCUSSION	86
6.1	PLASMIDS MODIFICATIONS AND <i>IN VITRO</i> TRANSPOSASE EFFICIENCY	88
6.2	RELATIVE EXCISION EFFICIENCY	89
6.3	SLEEPING BEAUTY SYSTEM EFFICACY	90
6.4	THE ABILITY OF G7 OPIOID PEPTIDE TO CROSS THE BLOOD BRAIN BARRIER	90
6.4.1	<i>g7 bound to PLGA nanoparticles synthesis and characterization</i>	91
6.4.2	<i>In vivo imaging</i>	91
6.5	CHITOSAN POLYSACCHARIDE AS GENE DELIVERY	91
6.5.1	<i>Nanoplexes preparation, cellular up-take and cytotoxicity</i>	92
6.5.2	<i>Chitosan/TPP-hyaluronic acid nanoparticles synthesis and characterization</i>	92
6.5.3	<i>Chitosan/TPP-hyaluronic acid nanoparticles cellular uptake</i>	93
7	CONCLUSION	94
8	ACKNOWLEDGMENTS	97
9	BIBLIOGRAPHY	99

1 Abstract

INTRODUCTION: Gene therapy can be currently performed by viral or non-viral vectors. Although viral ones have already come to a clinical translation, concerns remain about both safety and the industrial applicability of this system.

We therefore started the study of a transposon-based gene transfer system. We used nanoparticles (NPs) as vector to carry the transposon within the blood stream, then in cells. These had to be able to hold large plasmids, such as transposon. The NPs must then be able to reach the tissue most affected by the genetic disorder. Coating the NPs with specific peptides, they acquire the ability to accumulate in the target tissue, in our case the Central Nervous System (CNS) penetrating the blood-brain barrier (BBB). We started to develop a non-viral gene therapy approach in order to treat a neurological disease, globoid cell leukodystrophy in (GLD), an inherited, rapidly fatal disorder affecting myelin.

METHODS: We tested the ability of a transposon-based system called Sleeping Beauty (SB), to convey the luciferase marker gene in the control cells. Then we modified the transposon cloning the GALC codifying sequence and we tested its ability to integrated the gene of interest in the cellular genome.

We then verified the ability of NPS of chitosan to contain large plasmids. We then verified the quality (size, shape) of the NPS obtained and the ability to go into the cells.

Lastly, we verified the ability of a heptameric synthetic glycopeptide, of opioid origin, g7, to convey inside the CNS NPs of Poly Lactic-Co-Glycolic Acid (PLGA). We injected PLGA NPs coated with g7 in tail vein's Balb/c mice and followed through optical imaging their distribution.

RESULTS: We verified the high SB transduction efficiency on control cells by their expression of luciferase marker gene. We then assessed the copies number of the integrated gene. We demonstrated the high transduction efficiency of the transgene within the genome of fibroblasts grown from biopsies of patients with GLD. We assessed the quality and features of chitosan-SB NPs. We could observe that g7 coated PLGA NPs accumulate in the CNS 10 minutes after infusion, with accumulation even and up to 2 hours.

DISCUSSION: SB demonstrated high efficiency in stable transduction of control cells. So we thought to encapsulate SB in chitosan NPs. These have proven to be highly efficient in stably transducing deficient fibroblasts. We can confirm that g7 is today the best way to address the NPs to the CNS.

CONCLUSIONS: Future studies will test the ability of g7 to coat the NPs of chitosan, verify its efficiency in conveying the chitosan NPs to the CNS as well as they did for PLGA NPs. Finally, by cloning into SB the gene whose mutation causes GLD, can be assessed the therapeutic efficacy of the system in the mouse model of the disease.

2 Introduction

2.1 Transposable elements

Transposable elements (TE) were discovered by McClintok during the analysis of maize's unstable mutations in the 1940s [1]. The TE biological value is confirmed from the evidence that they are highly conserved among taxonomic groups, for example the 45% of the human genome is made of transposable elements [2]. The movable genetic elements are divided in two classes in respect of the transposition mechanism. The class I, or retro-transposons, use a “copy and paste” mechanism, in which the TE is firstly transcribed from DNA to RNA and then the RNA is reverse transcribed to DNA. The copied DNA is inserted into the genome. Whereas the class II, or DNA transposons, are able to remove the gene of interest (GOI) from the donor site and integrate it into the target site using a “cut and paste” mechanism (Figure 1). Both of the two classes are divided in different groups [3, 4]. Class I is commonly grouped into three orders: TEs with long terminal repeats (LTRs); long interspersed nuclear elements (LINEs, LINE-1s or L1s); short interspersed nuclear elements. Class II is divided in families in correspondence of their TEs sequence. The families themselves are separated in Subclass I (Tc1/mariner, PIF/Harbinger, hAT, Mutator, Merlin, Transib, P, piggyBac and CACTA), and Subclass II (Helitron and Maverick) [6].

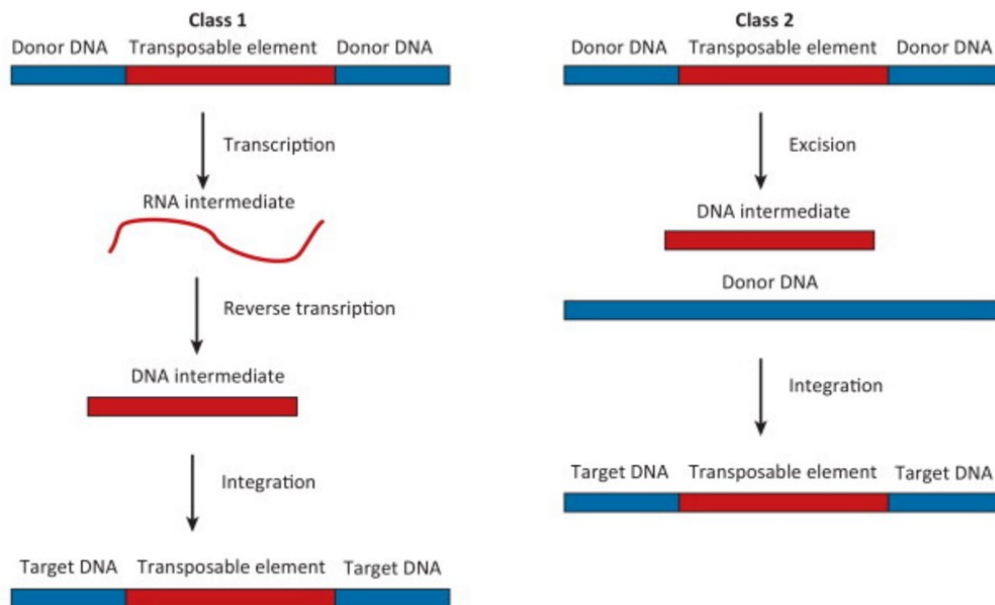


Figure 1: Transposable elements classification [7].

2.1.1 *Tc1/mariner superfamily*

The most extensive family in nature is the Tc1/mariner that is widely distributed within different taxa; only ten elements are naturally active and four Tc1/mariner transposons were reconstructed from inactive elements, such as Sleeping Beauty from salmonid-type fishes [5], Himar1 from the Horn Fly (*Hematobia irritans*) [10], Frog Prince from the frog *Rana pipiens* [11] and Hsmar1, incorporated into the SETMAR gene, from *Homo sapiens* [12]. The Tc1/mariner elements are length 1-5 Kb and the transposase protein is composed by 282-345 amino acids which are flanked by two Terminal Inverted Repeats (TIRs). Within this superfamily, the transposase protein's sequence shows lots of differences even if all of them maintain the two characteristic domains: the motif that recognize and bind the TIRs (helix-turn-helix, HTH), the catalytic motif (three amino acids, DDD, for mariner-like elements or DDE for the Tc1-like elements) and the indispensable motif that is responsible for transposase transport through the nuclear membrane (Nuclear Localization Signal, NLS) [13].

2.1.2 *Sleeping Beauty*

An ancient transposon element was brought back to life in 1997 from fish genomes and called Sleeping Beauty (SB), in analogy of the Grimm brothers' fairy tale. It is a member of the Tc1/mariner superfamily, which is the most widespread DNA transposons in nature. Because of the accumulation of mutations in vertebrates these elements appear to be transcriptionally inactive [5]. The Sleeping Beauty structure is quite simple, and it consists in two-components: a gene-of-interest cloned between the terminal inverted repeats (IRs) of SB, which binds the transposase polypeptide, that is the enzymatic factor of transposition. SB transposase through a conservative cut-and-paste mechanism, excises the transposable element from its original location and then integrate it into a new location [6]. The two elements could be provided in *trans form* if are in two different elements or in *cis form* if the transposase and the transgene are located in the same construct (Figure 2), alternatively the enzymatic element could be provided as an mRNA or a protein [8].

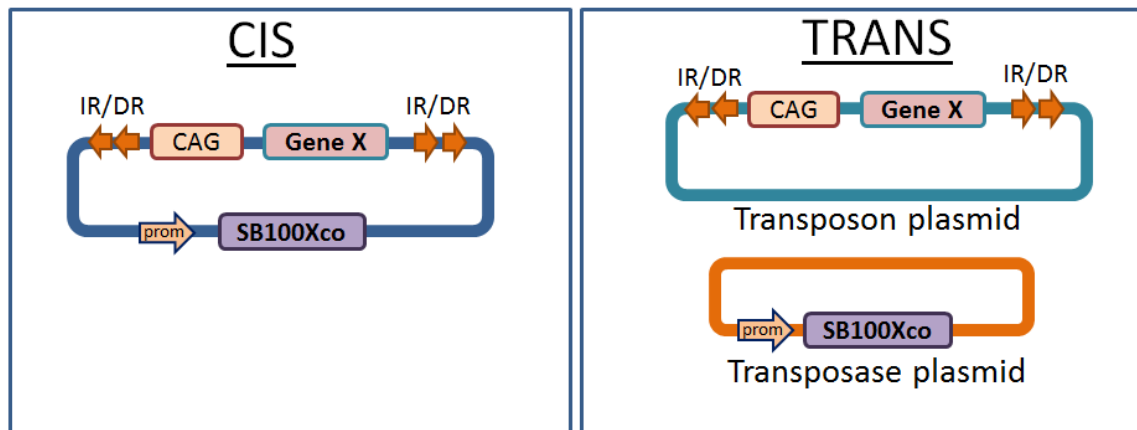


Figure 2: Schematics of Cis and Trans Sleeping Beauty plasmids.

2.1.2.1 Transposase

The transposase's structure is highly conserved in all Tc1/mariner superfamily. Simplifying, the structure (Figure 3) is composed by different domains: the DNA-binding domain that is formed by two helix-turn-helix (HTH) motifs; the nuclear localization signal (NLS) flanked by phosphorylation target sites casein kinase II; these sites are very important because their phosphorylation regulate the transposition. The presence of the NLS sequence promotes the crossing of the nuclear membrane using the receptor-mediated transport machinery of the host cells [14]. The major domain is the catalytic one, which is responsible for the cleavage and joining reactions of the transposition event. Inside its C-terminal there is a well-conserved triad of amino acids known as the aspartate-aspartate-glutamate (DDE) which plays an essential role on the coordination of two cations necessary for the activity, indeed one of them stabilizes the transition state of the penta-coordinated phosphate and the other one, like a general base, deprotonizes the nucleophile during transesterification and strand transfer [15].

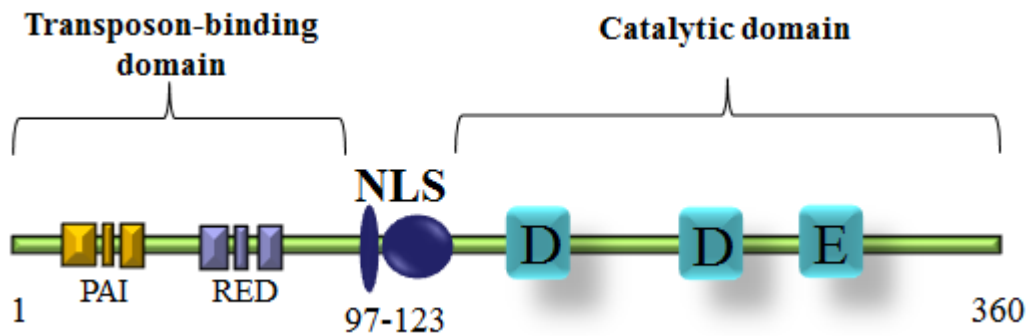


Figure 3: Schematic domain representation of SB transposase enzyme [16].

After the transposase discovery, researchers have done different amino acids modifications in order to generate transposase variants with no change in activity, reduced activity or a modest increase of transposition activity. The majority of the mutations have a neutral or negative effect on transposition activity. The mutations into the evolutionary conserved domains create an inactive transposase. The most active version is the SB100X that shows a 100-fold hyperactivity if compared to the originally resurrected transposase. The hyperactivity of SB100X could be explained by a particular combination of mutations that affect its folding features [17, 18].

2.1.2.2 Transposon

The transposon vector contains the genetic element that has to be mobilized. The Inverted Terminal Repeats (IRs) are the distinctive part of the transposon ends, and they are composed of two functional parts: the 2 to 3 terminal base pair of the ends are the recombinationally active sequences involved in the cleavage and the strand transfer reactions; the other part is located in the IRs and it guarantees the sequence-specific positioning of the transposase on the transposon ends. The IRs length is 200 to 250 bp and each of them contains a pair of transposase-binding sites (short direct repeats DRs, 15 to 20 bp) [19]. IR/DR is the organization of IRs that is present in numerous elements inside the Tc1 transposon family. Within the IR/DR group the spacing of about 200 bp between the outer and the inner DRs is highly preserved in all elements. The four DRs differ in length; indeed the outers are longer by two base pairs. In addition the four IRs show some differences, such as the left IR contains a sequence motif called “half-DR” (HDR). Moreover some experiments show that constructs modified with two right IRs have low

mobility, demonstrating that the left and the right have two different functions. Furthermore the multiple binding sites of the IR/DR elements control the timing and the specificity of the transposition reaction.[20]

2.1.2.3 Cut and Paste mechanism

The “cut and paste” (Figure 4) mechanism could be divided in four major steps: the binding of the transposase to its sites within the transposon IRs; formation of a synaptic complex; the excision from the donor site and the reintegration at a target site. Several studies have demonstrated that each transposition step is regulated by the host, indeed the regulation of SB transposition is mediated by transposon and host-encoded factors [21, 23].

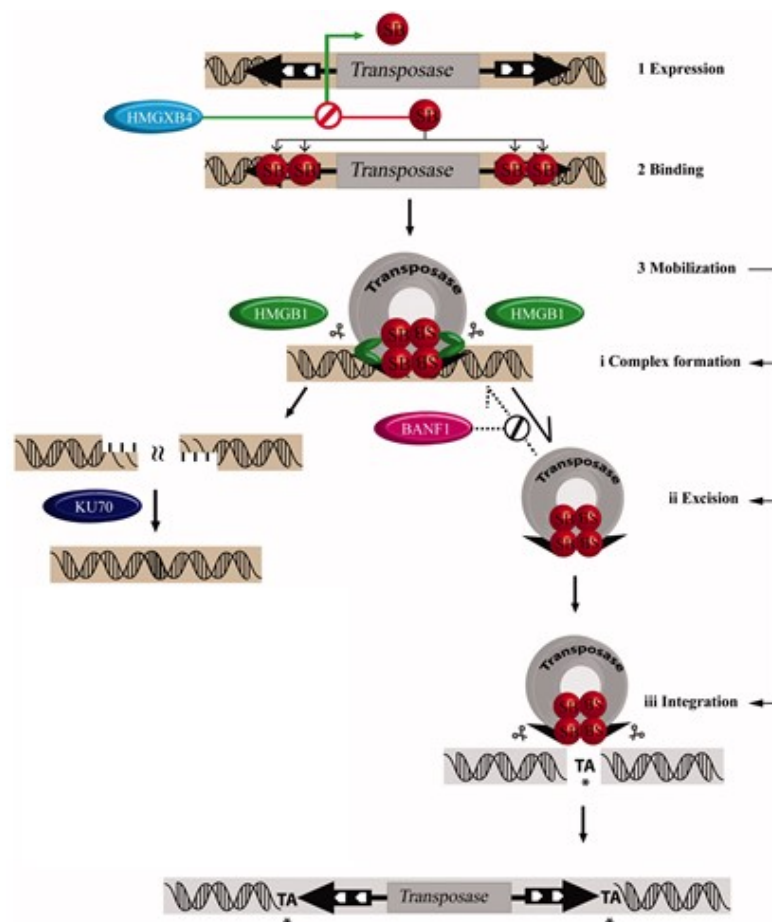


Figure 4: Schematic representation of the cut-and-paste mechanism with some of the host factors which assist the transposition [22].

The early step is the formation of a nucleoprotein complex, in which the two ends of the elements are paired and held together by transposase subunits. The fundamental factors are

the four transposase binding sites, so the complete IRs; the transpositional enhancer HDR motif (a part of the left IR, it is important, but not essential) and tetramerization-competent transposase [24]. For efficient SB transposition in mammalian cells is required the high mobility group protein HMGB1, that is a non-histone, nuclear protein associated with eukaryotic chromatin and has the ability to bend the DNA [26]. In vivo studies suggested a ternary formation between the SB, the HMGB1 and the transposon DNA. It is supposed that HMGB1 promote the communication between the DNA motifs with the transposon. In fact HMGB1 is considered an important element for the formation and the stability of the synaptic complexes during the transposition, controlling the catalytic step [27].

The exposure of the 3'-OH groups of the transposon ends is the most important element for the excision of the donor site. Each cleavages is a transposon-catalyzed, Mg^{++} -dependent hydrolysis of phosphodiester bonds of DNA backbone [28]. In contrast to the other excision mechanism that involved a hairpin intermediate at the donor site, the mariner and the sleeping beauty transposases cleave at the transposon ends the two DNA strands by hydrolysis reactions. During the excision process the transposase leaves on the donor transposon three-nucleotide-long 3'-overhangs that are processed by the cellular DNA repair machinery creating on the transposon donor site a typical "footprint". The NHEJ pathway is involved on the "footprint" generation and, for example, the molecules involved are Ku70 and DNA-PKcs [29] (Figure 5). In relation to that, a Kolacsek study suggested that there is a strong correlation between the excision step of DNA and the cell type. Moreover they have also demonstrated that high excision activity is not necessarily associated with the increasing of copy numbers, so the excision of DNA transposons is not always follows by integration. For example, working with the hyperactive variant (SB100X), the significant aspect that should be change to manipulate the copy numbers is the amount of the transposon instead of the transposase [30].

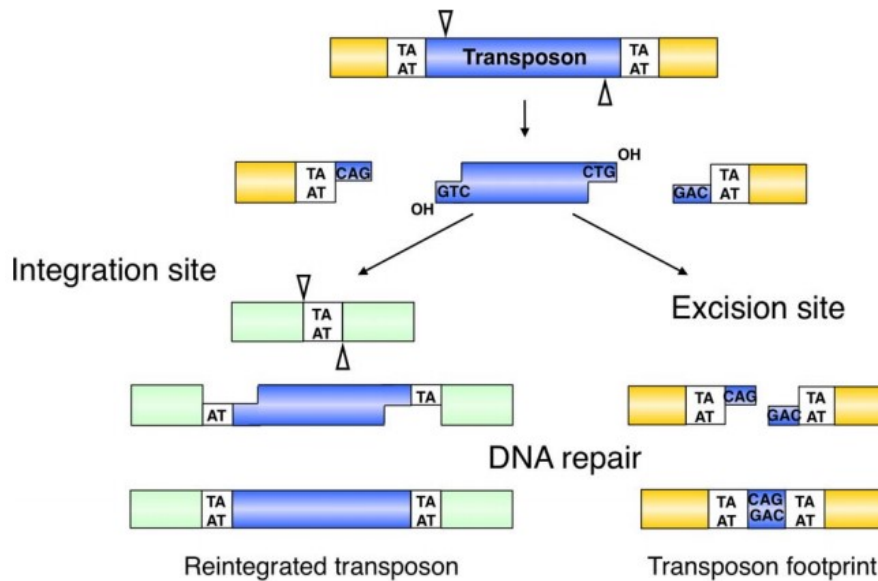


Figure 5: Schematic representation of the "cut and paste" events. Left: the integration of the gene of interest. Right: the break donor site is repaired by the host DNA repair machinery (NHEJ pathway) and a small footprint is left behind at the site of excision [24].

The second step of the transposition reaction is the transesterification of the exposed 3'-OH transposon tip to the target DNA molecule. Also in this process is involved the DNA repair mechanism that generate the typical duplication of the flanking element beside the target site (target site duplication, TSD). Given that SB transposition take place at TA dinucleotides, the integrated elements are always flanked by TA TDs. Despite the other transposons, at the DNA sequence level the SB shows a target selection, for example the bendability and the hydrogen bonding potential inside a palindromic AT-repeat consensus sequence [31]. For this reason studying the physical properties of a sequence it's possible to predict the insertion sites [32]. In contrast with the specificity at the sequence level, at genomic level the integration is quite random and most of the insertions are located in introns [33, 34, 35]. The drawback of the sleeping beauty transposition is the auto-integration in which the excised transposon molecule could reinsert into its own genome. This disruptive event is proportionally correlated with the increasing size of the transposon, because larger transposons show more potential target site [36].

In conclusion, the SB integration could be considered precise and fairly random, this is safer than retrovirus, HIV, or AAV integration events which have the tendency to integrate

into genes, especially for the AAV where the integration mechanism is also associated with a large deletion and chromosomal rearrangements (Table 1).

Genetic material	DNA
Delivering capacity	~ 10 kb
Tropism	Somatic, embryonic, germinal cells, dividing/nondividing cells(?)
Immunogenic potential	The transposase is not toxic, even at high concentrations; no dramatic immune response to repeated administration
Integration sites	Fairly random integration, reduced insertion into other repetitive elements, no rearrangements at the integration sites, no signs of proliferative transformation
Integrated DNA	The gene integrates in a single-copy form; the gene remains intact, no rearrangements
Vector	Can be combined with nonviral or with viral approaches; plasmid-based technology with integrating feature
Safety	SB is less likely to integrate into genes than HIV- or AAV-based vectors; no interference with endogenous transposons

Table 1: Main features of Sleeping Beauty system [9].

2.1.3 *Sleeping Beauty applications*

Thanks to their low immunogenicity, low risk of insertional mutagenesis and the ability to integrate in stable way the gene of interest (GOI) inside the cellular genome for a long-term expression, the transposon elements become the suitable tool for gene therapy [37]. Sleeping beauty was the first transposon element able to transfer gene in vertebrate cells with high efficiency becoming an interesting alternative to virus-based applications that are genotoxic and provoke immune response [38]. Evidence of the sleeping beauty potential as gene therapy tool, was demonstrated the first time in 2000 when researchers transfected a mouse model of hemophilia B with human blood coagulation factor IX [39]. Since then, a lot of preclinical studies was performed using the sleeping beauty system in different diseases models, for example to deliver coagulation factors [40, 41, 42], insulin [43], lysosomal enzymes [44] or to treat different types of cancer [45, 46, 47, 48,49]. In the 2008 in the U.S.A. started the first human trial, in which they re-infused modified T cells in patients affected by CD19+ B-lymphoid malignancies [50]. Other clinical trials developed methods combining the gene therapy with the immune therapy demonstrating the stability and the safety of this therapeutic approach [51, 52, 53].

2.2 Blood brain barrier

The brain is surrounded by a thick blood vessels network that operate as a biological filter between the blood stream and the cerebral parenchyma. Its main purpose is to allow or not the molecular transfer from the blood to the cerebral parenchyma and the cerebrospinal fluid (CSF) in order to protect the nervous tissue. The blood brain barrier (BBB) guarantee the efficiency of the synaptic transmission maintaining the ionic environment stability and safeguarding the low gradient of excitatory neurotransmitters. Moreover it avoids the penetration of toxic molecules, such as metabolites and neurotoxins [54].

The BBB is composed by complex system of capillary endothelial cells which are surrounded and supported by other cell types, such as astrocytes (cells that link the BBB with the neurons), pericytes (that occupied the perivascular space and they maintained the vascular tone, stability, repair and angiogenesis and they modulate the astrocytes function), neurons and mast cells (Figure 6) [55]. The cerebral capillaries show different characteristics compared to the peripheral ones, because the cells form a continuum endothelium without the fenestrations and with a lower number of pinocytic cells. The peculiarity of this endothelium is the presence of the tight junctions that block the free diffusion of several molecules, indeed only the lipophilic molecules (oxygen, carbon dioxide, ethanol and steroid hormones), low molecular weight substances (< 500 Da) and molecules that use the receptor-mediated transport are able to cross the BBB [56]. Two components are critical in the tight junctions formation, the occludins which are proteins (60-65 KD) that regulated the tightness binding zona occludens protein-1 (ZO-1); and the claudin proteins that contributed to the BBB's restriction of small ions.

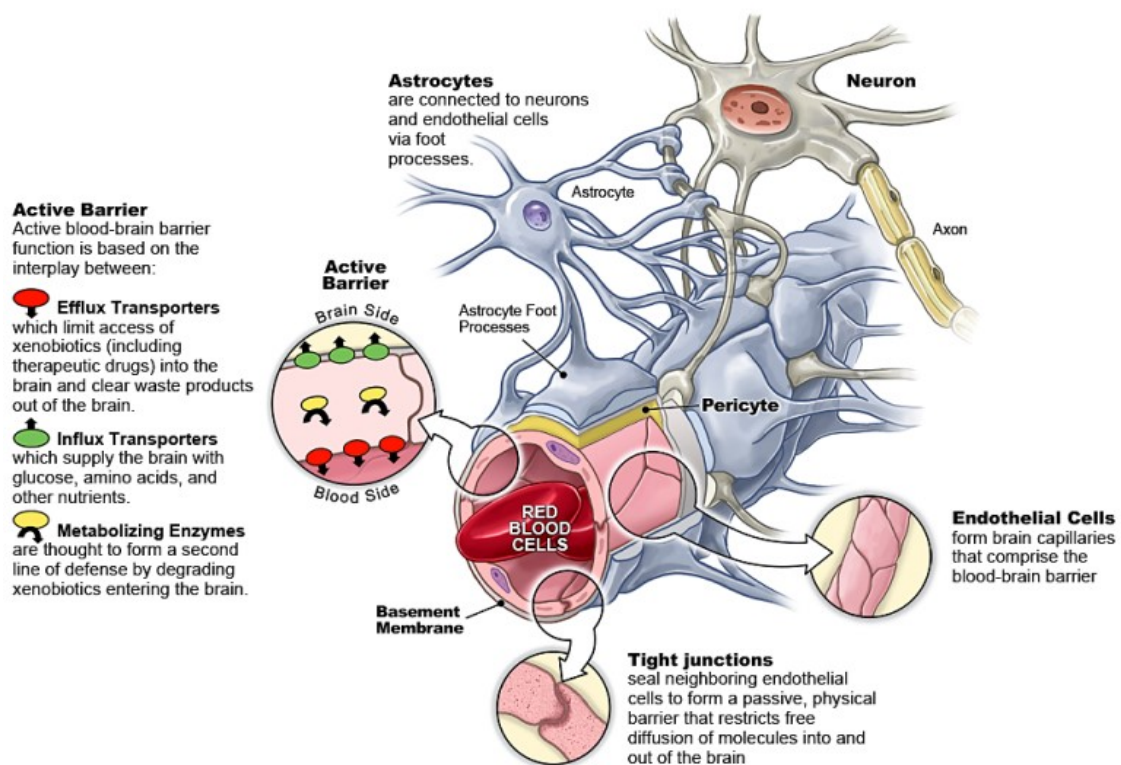


Figure 6: The Blood Brain Barrier [57].

2.2.1 Mechanism to cross the blood brain barrier

The influx and the efflux through the BBB is highly regulated (Figure 7), only the water soluble and the lipid soluble agents are able to cross the endothelium via the paracellular aqueous pathway and the trans-cellular through the lipid plasma membrane, respectively. For the other substances there are three pathways. The carrier mediated transport (CMT) is one of the transport used by the nutrients such as glucose, lactose and neutral amino acids which take advantage of membrane proteins located on the surface of the BBB, sometimes this molecular transfer is against electrical, chemical or electrochemical gradient (active transport). The highest expressed proteins is the glucose transporter (GLUT1) involved in the transport of essential polar molecule D-glucose, others are LAT 1 (Large neutral amino acid transporter), CAT 1 and CAT 3 (Cationic L-amino acid transporters) involved in the amino acids transport; CNT2 transporters involved in nucleosides transfer[87, 58, 59]. The receptor-mediated transport (RMT) is involved on the mechanism that allow large molecules to cross the BBB, for example insulin and transferrin. This type of transport is highly specific, indeed each receptor bind its specific ligand causing a vesicle formation,

and then both of them are internalized into the endothelium. In the presence of CNS disease the receptors expression change, so it is important to keep that in mind during nanoparticles design [60, 61]. The most commonly receptors involved in RMT are: the most well characterized TfR (transferrin receptor) that mediates the transcytosis of transferrin-bound iron through the brain capillary endothelial cell in humans [62]; insulin receptor that its distribution is altered in diabetes and obesity, so its use might disturb the insulin metabolism, so it should be used with caution [63]; the multi-functional and multi-ligand lipoprotein receptors (LDLR, LRP-1 and LRP-2) that bind the amyloid beta precursor protein (APP), apolipoprotein E (ApoE) and alpha-2-macroglobulin (α 2M) [64, 65]; diphtheria toxin (DTR) or known as the precursor of heparin-binding epidermal growth factor (HB-EGF) that do not have endogenous ligand and seems to be involved in inflammatory processes [66, 67]. The less specific route of transport is the absorptive-mediated transport (AMT) which is based on electrostatic interaction between positive charges and negative ones of the endothelial cell membrane [68, 69]

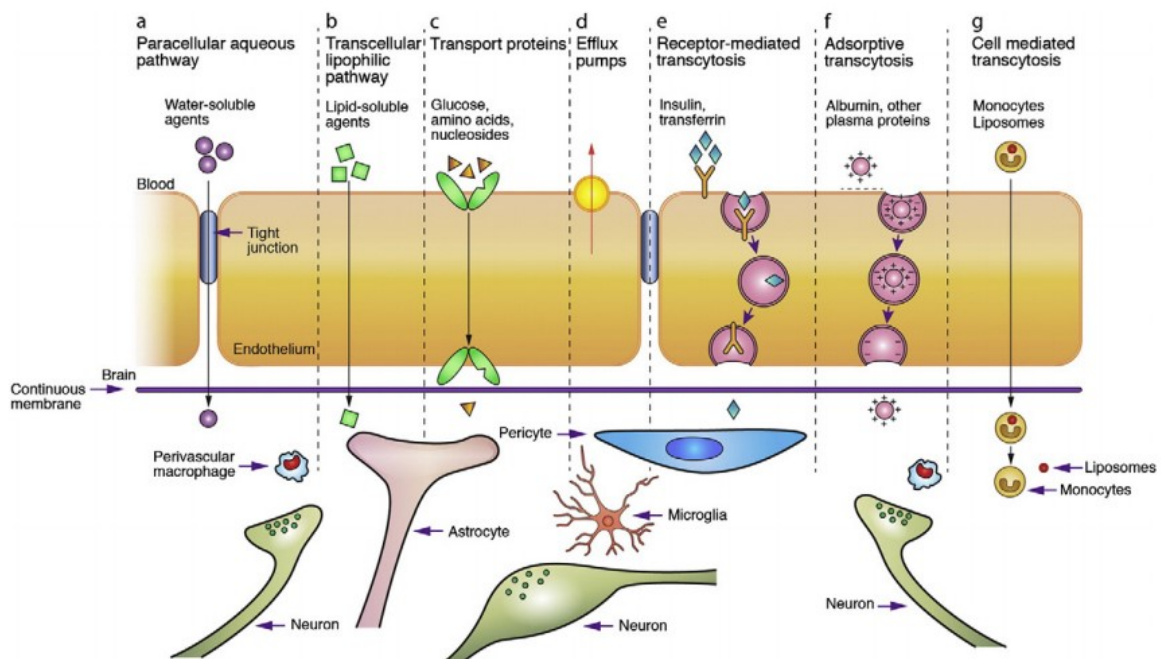


Figure 7: Transport routes across the blood brain barrier [70, 61].

2.2.2 Strategy of drugs delivery

Because of the peculiar anatomic BBB conformation, it is difficult for drugs to cross it. For this reason it is important to consider the chemical and physical properties of the drugs

(pKa, molecular weight, liposolubility, etc.) and their binding to plasmatic proteins. There are two categories of therapeutic delivery: the invasive and non-invasive approaches [65, 72].

An invasive approach is the temporary disruption of the BBB. The oldest method is the hyperosmolar disruption [73, 74, 75], where an osmotic shock shrinks the endothelial cells increasing the permeability. Several substances have been used for the osmotic disruption, but the most commonly used is the mannitol. The main problem of this method is that the increasing permeability do not operate in a selective manner, causing toxicity throughout the Central Nervous System [65]. Recently, another technique has been used as invasive methods, the ultrasound-mediated drug delivery using small (1-10 μm diameter) microbubbles that mechanically disrupt the tight junctions [76, 77]. This technique has shown major advantages to deliver therapeutic agents such as PEG-coated gold nanoparticles, small interfering RNA and stem cells [78]. The same effect could be achieved using vasoactive molecules, one example is the bradykinin that can selectively increase the capillary permeability of the brain tumor and not in the healthy tissue [79].

The alternative is the use of non-invasive strategies. Several molecules are able to cross the blood brain barrier using the passive diffusion due to their small molecular size (less than 500 Da), the high lipophilicity and lack of ionization at physiological pH [80]. Others approaches are inspired by other transport mechanisms, for example carrier mediated and receptor mediated transports.

In recent years, nanomedicine has contributed to develop new strategies to cross the BBB delivering larger amount of therapeutic agents and reducing their toxicity [81]. The nanotechnology has allowed to functionalize the nanoparticles in order to optimize the drug loading and release kinetics, avoiding the plasma protein agglutination and their clearance through the reticuloendothelial system (RES) [82]. Nanocarriers are the new frontier of non-invasive method, because they improve drug delivery and increase solubility and drug protection [83]. The main types of nanocarriers are liposomes, polymeric nanoparticles, magnetic and solid lipid nanoparticles. Liposomes are small vesicles formed by one or more phospholipid bilayers showing low toxicity and the ability to deliver both hydrophilic and hydrophobic compounds. Liposomes are commonly cationic and PEGylated, that are able to cross the BBB through passive diffusion or

phagocytosis, thanks to their small size and their ability to bind the negative charge of the endothelium [84]. The presence of PEG on the surface is important because it impedes the clearance by the RES system [86]. Moreover the liposomes could be bound to a ligand in order to induce the receptor-mediated endocytosis. Liposomes have reduced toxicity, but show low encapsulation efficiency and poor storage stability [85]. Thanks to their biodegradability the polymeric nanoparticles are extensively used to deliver drugs into the CNS. They could be made of different polymers, such as poly lactic acid (PLA), poly ϵ -caprolactone (PCL), poly aspartic acid, poly butylcyanoacrylate (PBCA), poly glycolic acid (PGA), poly D,L-lactide-co-glycolide (PLGA) and poly amino acids. Today the widely used polymers are PLA, PGA and PLGA because of their high biodegradability: being broken down into lactic acid and glycolic acid that are recycled into the Krebs Cycle [87]. Recently the chitosan (CS) has been considered as an interesting alternative, being abundant in nature, biodegradable and biocompatible polysaccharide [88]. An interesting alternative to liposomes and polymeric nanoparticles are the solid lipid nanoparticles (SLNs): that are stable, biodegradable in physiological conditions and with high drug loading capacity [89]. In recent years interest grew toward magnetic nanoparticles (superparamagnetic iron oxide nanoparticles, or SPIONS) for their potential as a theragnostic tools [90].

2.2.3 Synthetic opioid peptide g7

One of the most efficient approach to cross the BBB is to exploit the receptors expressed on it, such as the endocytic mechanism used by the β -endorphins and the opioids. Three opioid receptors were identified: mu, μ , are localized in hippocampus and thalamus; delta, δ is localized predominately in the striatum, limbic system, and cerebral cortex and kappa, κ , is one of the most abundant and ubiquitous in the CNS ($\kappa 1$ and $\kappa 2$) [91].

Taking advantage from this mechanism, the synthetic opioid peptide MMP-2200 (H₂N–l-Tyr-d-Thr-Gly-l-Phe-l-Leu-l-Ser–O– β -D-lactose–CONH₂) was able to cross the BBB [92], but it was chemically modified in order to eliminate the opioid effect. In fact the Tyr was substituted with the Phe and was obtained H₂N–Gly-l-Phe-d-Thr-Gly-l-Phe-l-Leu–L-Ser–O– β -D-glucose–CONH₂ (g7 glycopeptide) [93]. Moreover to increase the BBB penetration in the C terminus the lactose residue was replaced with a glucose molecule

[94]. Several experiments demonstrated that the nanoparticles coated with g7 are able to cross the BBB after different routes of administration in vivo [95, 96], indeed it was possible to claim that this kind of nanoparticles cross the BBB at high rate in less than ten minutes reaching a high concentration in the grey matter. Furthermore the g7-NPs show a cellular tropism, and the concept for which the cellular uptake depends on specific cellular mechanisms was confirmed by their accumulation inside the neurons, interneurons and microglial cells, while were rarely found in astroglial cells [97]. The transport across the membrane occurs through the clathrin pathway that completes inside the lysosomes. Recently, was demonstrated the ability of the g7-NPs to deliver enzymes (high molecular weight molecules) in the animal model of lysosomal storage disorders (Mucopolysaccharidosis type I and II, MPS I and MPS II) [107, 108].

2.3 Alternative routes of administration

In recent years the knowledge on drug transport across tissues has increased. In particular, considering diseases affecting the CNS, several alternative routes of administration were investigated. The most interesting approaches, which avoid the BBB, are the intra-ventricular and intranasal drug delivery.

2.3.1 Ependymal barrier

An important route of administration for several therapeutic agents could be the direct injection into the cerebral ventricles.

The functional units in the ventricular system are single-layered cuboidal epithelial cells called the ependymal cells. The ependyma constitute a ciliated epithelium that derives from the neuroepithelium and is located at the interface between the brain parenchyma and ventricles in the central nervous system (CNS). The ependyma constitute barriers lining the ventricular lumen in the mature CNS, and performs important functions related to the development, morphogenesis, and physiology of the brain [98]. The ependymal cells have cilia, which influence the direction of the cerebrospinal fluid (CSF) bringing nutrients and neurotransmitters. The ependymal cells lining the ventricles are loosely joined together by special intercellular adhesion sites called desmosomes, which enable the cells to form a nearly continuous epithelial sheet over the surface of the ventricles and spinal canal. Because the junctions between the ependymal cells are loose, CSF is able to diffuse from

the ventricles into the central nervous system. Another cellular type is the tanycytes that don't have cilia and play an important role in the transport of the hormones [99].

Several works have demonstrated the presence of adult neural stem cells in the subventricular zone (SVZ) [100]. Both *in vitro* and *in vivo*, it was observed that a subpopulation of ependymal cells CD133+ have the classical neural stem cell features which give rise stem/progenitor cells expressing Nestin, LeX or GFAP after brain injury. Moreover in adult ependymal the Notch signaling is active, that mean the neural stem cells are maintained in an undifferentiated quiescent state [101].

The administration of the drug directly into the CSF, can decrease problems associated with intravenous delivery, such as systemic toxicity, metabolism of the drug in serum, and opsonization by serum proteins.

However, this mode of delivery also implicates problems. Despite the improvement in drug concentration and half-life in the CSF, the distribution through the CFS is very slow. On the other hand, intra-cerebroventricular technique is invasive, and carries both risks of infection and a tendency to increase intracranial pressure through fluid injection [103]. Nevertheless, evidence from several animal LSD models with CNS manifestations suggests that gene therapy approaches with the transduction of cells lining the ventricles give raise to persisting levels of lysosomal enzymes in CFS, demonstrating a potential for clinical use [102]. Moreover the neural stem cells localized in the sub-ventricular zone could be transduced with the vector and, after differentiation, migrate in the brain.

2.3.2 Intranasal drug delivery

In the last twenty years, the nasal mucosa shows several interesting advantages for the treatment of different disease which affect the CNS (Parkinson's, schizophrenia, epilepsy, and Alzheimer's). Intranasal delivery bypasses blood brain barrier (BBB) and circumvents systemic extraction of drugs, targeting therapeutics to the brain via olfactory, rostral migratory stream (RMS) and trigeminal pathways [104]. This route is a non-invasive approach, which avoid systemic side effects.

The nasal cavity is divided in two symmetrical halves by the septum. Each halves is composed by four areas:

- I. Nasal vestibule; stratified squamous and keratinized epithelium with sebaceous glands. It has hairs called vibrissae, which filter the inhaled particles. Here the drugs and molecules absorption is difficult.
- II. Atrium; the anterior section is made by stratified squamous epithelium, while the posterior area is made by pseudostratified columnar cells presenting microvilli.
- III. Respiratory region; is the largest part of the nasal cavity responsible for humidification and temperature regulation of inhaled air. The nasal respiratory mucosa is considered the most important area for the systemic diffusion of the drug delivered by this route of administration. It is composed by the epithelium, basement membrane and lamina propria. The nasal respiratory epithelium consists of pseudostratified columnar epithelial cells, goblet cells, basal cells and mucous and serous glands. Under the epithelium there are high permeable capillaries, nerves, glands and immune cells.
- IV. Olfactory region; pseudostratified epithelium which contained olfactory receptor cells. Its neuroepithelium is the only part of the CNS that is directly exposed to the external environment.[105]

Despite the promising advantages, the intranasal administration has some limitations which could be overcome in future research. For example, the dimension of the drugs influence their absorption and delivery; therapeutic agents could be damaged by enzymes inside the nasal cavity; nasal congestion and allergies should interfere and the nasal mucosa might be damaged by the administration [106].

2.4 Nanoparticles

The history of nanoparticles dates back to the Mesopotamia in the 9th century where the silver and copper nanoparticles were used for decorations [109]; then in the Middle Age was widely used in Europe to stain glass of the gothic cathedrals, indeed the different color of stained glass is due to size and shape of silver and gold nanoparticles [110]. The modern nanotechnology was born in the twentieth century when the technologies became more sophisticated and let to be closer to the nano-scale. Moreover in that times the progress in pharmaceuticals focused its attention on the retarded and controlled drugs release [111]. The

first nanoparticle for drug delivery and vaccines was made in '70s by Speiser and coworkers [112].

The issue on using the transposon system is that the naked DNA is not able to cross the biological barrier and enter into the cellular nucleus and it has also to be protect from nucleases degradation. The other problem is to find the right formulation able to protect the plasmid and at the same time release it inside the cell without cellular toxicity. About this, the nanoparticles could help to overcome these problems.

In recent years the research has developed various nanostructures composed with different materials, such as lipids (liposomes), polymers (nanoparticles; NPs) or metals as drug delivery systems, especially designed for intravenous administration. Many of them, especially the NPs, are characterized by their physicochemical properties, such as a small size has to be coupled with high surface-to-volume (S/V) ratios and the possibility to bind on the surface other (bio)materials [113]. Comparing nanoparticles with the traditional therapies it is clear that nanoparticles show some advantages, like the protection and stabilization of the active molecules from degradation, the chance to control the active molecules release and the ability to catch up the target site. Due to these characteristics, nanoparticles are able to improve the pharmacokinetic profile decreasing the circulating drugs doses avoiding systemic side effects [114].

2.4.1 Polymeric nanoparticles

Over the last years polymeric nanoparticles obtained a particular importance on the fields of drug and DNA delivery into the brain [115]. Polymeric NPs are nanosized carriers (1-1000 nm) that could be made of natural or synthetic polymers. The most useful properties are the aqueous solubility or the possibility to be solubilized with less number of chemical modifications, the long-term stability in biological environments, the ability to control the therapeutic molecules release, biodegradability and the enhanced permeability through the tissues. Moreover the main advantage is that biodegradable polymers are broken down into biologically acceptable molecules that are metabolized by physiological metabolic pathway (Table 2) [85]. A wide different type of polymers are used; they could be hydrophilic, hydrophobic or hybrid amphiphilic copolymers and they are also produced by different technique, such as precipitation of polymers via emulsion/solvent evaporation, poly-condensation of monomers in aqueous emulsion or by simple self-assembly of

copolymers [118]. Based on the type of polymer and type of preparation method, the therapeutic element could be dissolved, entrapped, encapsulated or attached to a nanoparticle; and for these reasons they could take different shapes (Figure 8), for example nanospheres, nanoparticles or nanocapsules. Nanocapsules are similar to the liposomes or vesicles where the drug is surrounded by a polymer membrane that form a shell, while in the nanospheres the polymer forms a matrix in which the drug is dispersed. Recently the biodegradable polymer nanoparticles have resulted attractive as a carriers of DNA in gene therapy. The therapeutic molecules are left through different processes: solubilization, diffusion through the polymeric matrix, erosion or degradation of the polymer and swelling of the polymer [119]. Lots of various synthetic and semisynthetic polymers were developed, even if the natural polymers (polymers made of protein such as albumin and collagen, or made of polysaccharides such as chitosan and alginates) maintain a certain popularity. Currently, the most popular degradable material used for medical applications are polylactides (PLA), polyglucolides (PGA), poly lactide-co-glycolides (PLGA), polyanhydrides, polyorthoesters, polycyanoacrylates and polycaprolactone [85]. Comparing the natural with the synthetic polymers, the last one are more homogeneous in composition and have higher level of purity. Moreover the degradation kinetic is well known and the drug release period is prolonged from days to several weeks [120].

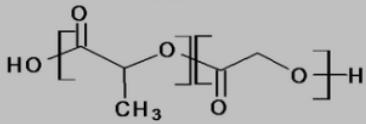
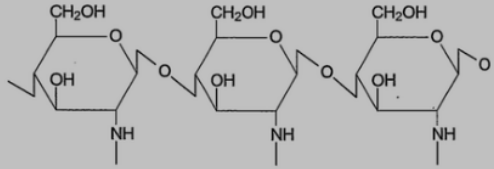
SYNTHESIS	POLYMER	DEGRADATION
<ul style="list-style-type: none"> •LACTIC ACID •GLYCOLIC ACID <p>Polycondensation</p>	<p>PLGA</p> 	<p>HYDROLYSIS Following Krebs Cycle – CO₂ + H₂O</p> <p>OXIDATION - Cleavage of polymer chain following ROS ; formation of new chain ends</p> <p>ENZYMATIC - Surface erosion and loss of material from polymer surface</p>
<ul style="list-style-type: none"> •CHITIN <p>Deacetylation</p>	<p>CHITOSAN</p> 	<p>ENZYMATIC-</p> <ul style="list-style-type: none"> 2x Glucozamine 2x Glucosamine 6- phosphate 2x Fructose-6-phosphate <p>↓ Glycolysis</p>

Table 2: Synthesis and degradation of most important polymers used in formation of nanoparticles [116].

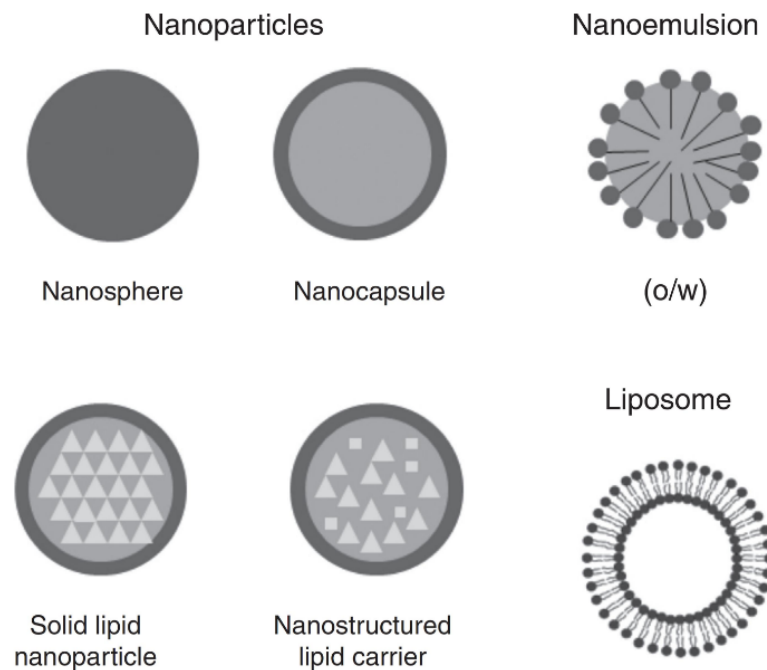


Figure 8: Different structure of nano-systems [117].

Unfortunately polymeric nanoparticles show some drawbacks and the most negative one is expressed in vivo after intravenous injection, where the nanoparticles are rapidly up-taken by the reticuloendothelial system (RES) and distributed into the liver, the spleen and the bone marrow. The RES is a complex of phagocytic cells that originate from the bone marrow and are present in the whole body with an higher concentration in the liver (Kupffer cells), spleen and bone marrow. The nanoparticles are up-taken by RES because, after the injection, the NPs interact with blood plasma proteins and then with the membranes of macrophages (opsonization) that proceed with clearance [121, 122]. The clearance by the RES depends on size, surface charge and surface properties. It is well known that nanoparticles size determine their fate, and if the size is less than 10 nm they are rapidly removed by the renal clearance, while if the size is greater than 200 nm NPs are filtrated by the spleen and removed by the reticuloendothelial cells. Moreover the hydrophobic surface and negative charges promote the protein absorption causing the activation of the complement system [123]. To overcome this problem the NPs could be modified to extend the brain retention coating or linking them with PEGs; in fact the PEGylation improves the pharmacokinetic reducing the opsonization, the phagocytosis and the clearance by the liver [123, 124]. Another approach is based on the binding with surfactants, for example the polysorbate 80 (Tween 80) [125] or with the conjugation with

specific ligands (antibodies, proteins, peptides) taking advantage from the receptor-mediated transcytosis or endocytosis [126].

2.4.1.1 PLGA

The synthetic polymers PLA and PLGA, due to their biodegradability, have been approved by the FDA and the European Medicine Agency for parenteral administration in humans. Especially the PLGA prove to be useful for the encapsulation of different types of drugs, because the end-carboxylic groups is free to react for covalent linkages useful for the NPs functionalization. PLGA has been widely studied and several formulation protocols are described [127]. Other characteristics are its degree of crystallinity and its glass transition temperature, these features could be manipulated changing the molecular weight and the ratio between the two monomers (lactic and glycolic acid). For example a low ratio of the hydrophobic lactic acid and low molecular weights allow the water penetration affecting the drug release profile [128, 129].

There are different protocols PLGA NPs formulation: nanoprecipitation, simple emulsion and evaporation technique are used to encapsulate hydrophobic molecules, double emulsion and solvent evaporation is used to encapsulate hydrophilic compounds and proteins [130, 131]. These protocols have advantages, but have also limits such as the use of organic solvent and some processes that could damage the drug (for example the sonication and ultra-centrifugation); to avoid this drawback could be used the nanoprecipitation technique that does not use external supply of energy and does not undermine the drug stability. The therapeutic elements could be released following different profile: the solubility of the drug in water, the desorption, diffusion through the matrix and erosion or degradation [132].

The principal degradation pathway of the PLGA is the hydrolysis of the ester bonds resulting on formation of oligomers and lactic acid/glycolic acid monomers, which are recycled to Krebs Cycle and eliminated as carbon dioxide and water. It has been hypothesize that the process is divided in three steps: in the first phase there is a molecular weight loss, in the second appeared the degradation's products (oligomers and monomers) and at the end there is the complete degradation [133]. This degradation process cause an

acidification of the cellular environment that could be dangerous if the NPs are loaded with pH sensitive molecules such as enzymes and proteins [134, 135].

At cellular level the first contact between the NPS and the cell membrane is often a non-specific hydrophobic or electrostatic interaction and after the internalization the intracellular trafficking is not well known. The primary aim of the NPS is to protect the therapeutic element and release it in the right intracellular compartment, for example the cytosol for the proteins and siRNA and the nucleus for the DNA [136]. Lot of parameters influence the cellular uptake and the intracellular trafficking; in fact for a good NPs design should be considered the size, the charge, the shape etc. of the NPs and the different internalization mechanisms which are present in the different cell types. The endocytic pathway is the general route for the NPs internalization, in which the endosomes develop into lysosomes where the pH 4.5 could inactivate several types of therapeutic agents [137]. Destabilizing the endo-lysosomes organelles the PLGA NPS are able to escape from the lysosomes and they have the capacity to accumulate in the cytosol [138].

2.4.1.2 PLGA nanoparticles and plasmid DNA

PLGA NPs could be useful to protect the plasmid DNA from the nuclease degradation and to increase its stability, even if there are difficulties to entrap the hydrophilic DNA inside the hydrophobic PLGA. Several methods have been developed (spray-drying, oil-in water solvent evaporation), but each of them could damage the DNA. To overcome this problem during NPs preparation have to be considered various parameters [139].

The first parameter is the selection of the appropriate molecular weight and the ratio between the two polymers, for example nanoparticles with high percentage of hydrophobic LA have reduced capability to bind and release the DNA due to reduced hydrolysis. Moreover high molecular weight has been associated with an high encapsulation efficiencies [140]. Another important aspect is the type and the rate of DNA that is encapsulated, indeed it is more difficult to integrate and release the supercoiled. In addition the encapsulation efficiency is influenced by the increasing amount of the DNA, even if it increase the DNA stability [141]. Other parameters are [139]:

- I. the surfactants that could influence the surface characteristics;

- II. the pH that should damage the DNA;
- III. the excipients that could protect the DNA facilitating its uptake and its expression (for example the PEI is used to increase the delivery);
- IV. the PEGylation that increase the loading efficiency.

Moreover the preparation method could influence the physic-chemical characteristics of the NPs. The technique most commonly used is the double-emulsion solvent-evaporation method (three phases: initial water solution with the DNA, intermediate organic phase with the polymer, water solution containing an emulsion) that allow to control the PLGA particles size, even if during the formulation the DNA could be nicked, mainly by the sonication [142]. To reduce the mechanical force, it is possible to use the spontaneous emulsification solvent diffusion (SESD) that allow to obtain small particles [143]. A modification of this method is the DNA-organic phase self-emulsification (DOPSM) in which cationic lipids are mixed with DNA in the organic phase and then is mixed with the PLGA forming spherical particles that are 1 or 2 μ in size [144]. Alternatively it is possible to use the cryo-preparation of the double emulsion method to preserve the plasmid DNA, even if the particles have diversity in shape and size.

2.4.1.3 Polysaccharide nanoparticles

Polysaccharides are the long carbohydrates molecules of monosaccharides linked together by glucosidic bonds. They could be recovered from various resources, such as plant (pectin), algal (alginate) and animal (chitosan, chondroitin) [145]. Polysaccharides are stable, safe, non-toxic, hydrophilic and biodegradable biomaterials, that makes them suitable for applications in food, biomedical and environment fields [146]. Moreover they are very abundant in nature and their processing is low cost. The majority of the natural polysaccharides have several hydrophilic groups that make them soluble in water and promote non-covalent bonds with biological tissues and mucosal membrane. Moreover this characteristic allows to modify it chemically, for example binding drugs and targeting agents. Polysaccharides are the most promising materials adopted for nanoparticles preparations. The polysaccharides, used to produce nanoparticles, are divided in groups in base on their native charges: cationic (chitosan), anionic (alginate, heparin, hyaluronic acid) and nonionic (pullulan, dextran). There are various preparations mechanism, such as

chemical crosslinking, physical crosslinking, polyion complex and self-assembling [150]. The cross-linking could be chemical or physical. The physical crosslinking is based on ionic interactions between charged polysaccharides and ionic crosslinkers. Several studies demonstrate the successful on using these types of nanoparticles both *in vitro* and *in vivo* [147, 148, 149].

2.4.1.4 Chitosan

Chitosan is a polysaccharide widely used for the manufacture of nanoparticles, especially in the gene therapy application, indeed it has been used as non-viral delivery system since 1995 [151]. Chitosan is a derivative from the partial deacetylation of the chitin, one of the most abundant polysaccharide in nature that is extracted from exoskeleton of crustacean, insects, fungi; and food industry waste (Figure 9). It is composed of randomly distributed $\beta(1-4)$ - linked D-glucosamine and N-acetylglucosamine units. The amine groups make the chitosan a pH responsive polymer, in addition due to the amine groups positive charges it is possible to form polyplexes by electrostatic interactions with the negatively charged phosphate groups of DNA. Thanks to this property and its biocompatibility, biodegradability and non-toxicity, the chitosan is the most suitable cationic polysaccharide for gene therapy; in fact in the last decade several works have published papers on using chitosan complexed to plasmid DNA or miRNA, in particular for the treatment of different types of cancer [152]. However its biomedical application is complicated by its insolubility in water and in organic solvents.

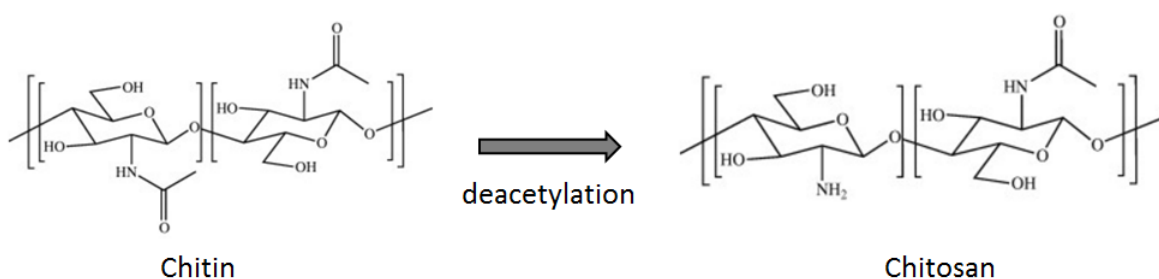


Figure 9: Schematic representation of chitin and chitosan polymer.

At cellular level the chitosan polyplexes, if they are not bonded with specific targeting ligand, they interact with the cell membrane through unspecific electrostatic interactions and, depending on their size, they go into the cell by endocytic pathways (phagocytosis,

macropinocytosis, clathrin-mediated endocytosis (CME), caveolae-mediated endocytosis (CvME) and clathrin- and caveolin- independent endocytosis). However the endocytosis is influenced by several factors, such as the size, the molecular weight etc. and also by the cell types (Figure 10) [153]. Once the polyplexes are inside the cell they have to escape from the endosome to avoid the degradation in the lysosomes. Several endolysosomal escape pathways are possible (such as “proton sponge”, membrane destabilization), even if it seems relevant in this processes the low molecular weight. The last membrane that the polyplexes have to cross is the nuclear membrane. To do that is possible to exploit nuclear pore complex if the particles are smaller than 10 nm, or they could incorporate the nuclear localization signal [154]. *In vitro* experiments have demonstrated that the chitosan MW and DA influenced all the steps involved in the transfection efficiency, such as the cellular up-take, intracellular trafficking and polymer decondensation [155]. Inside the cells the therapeutic agents could be released by diffusion, erosion and degradation. Currently, the mechanism of degradation is unclear. Anyway, several works have established that the polymer is degraded by chemical and enzymatic degradation (α -amylase and lysozyme); in fact chitosan could be degraded by enzymes able to hydrolyze glucosamine–glucosamine, glucosamine–Nacetyl-glucosamine and N-acetyl-glucosamine–N-acetylglucosamine linkages. *In vivo*, chitosan is degraded by several proteases; such as t chitinases which lead to the formation of non-toxic oligosaccharides of variable length. These oligosaccharides could be incorporated in metabolic pathways or could be excreted [156]. The two main organs involved in the chitosan degradation are the liver and the kidney.

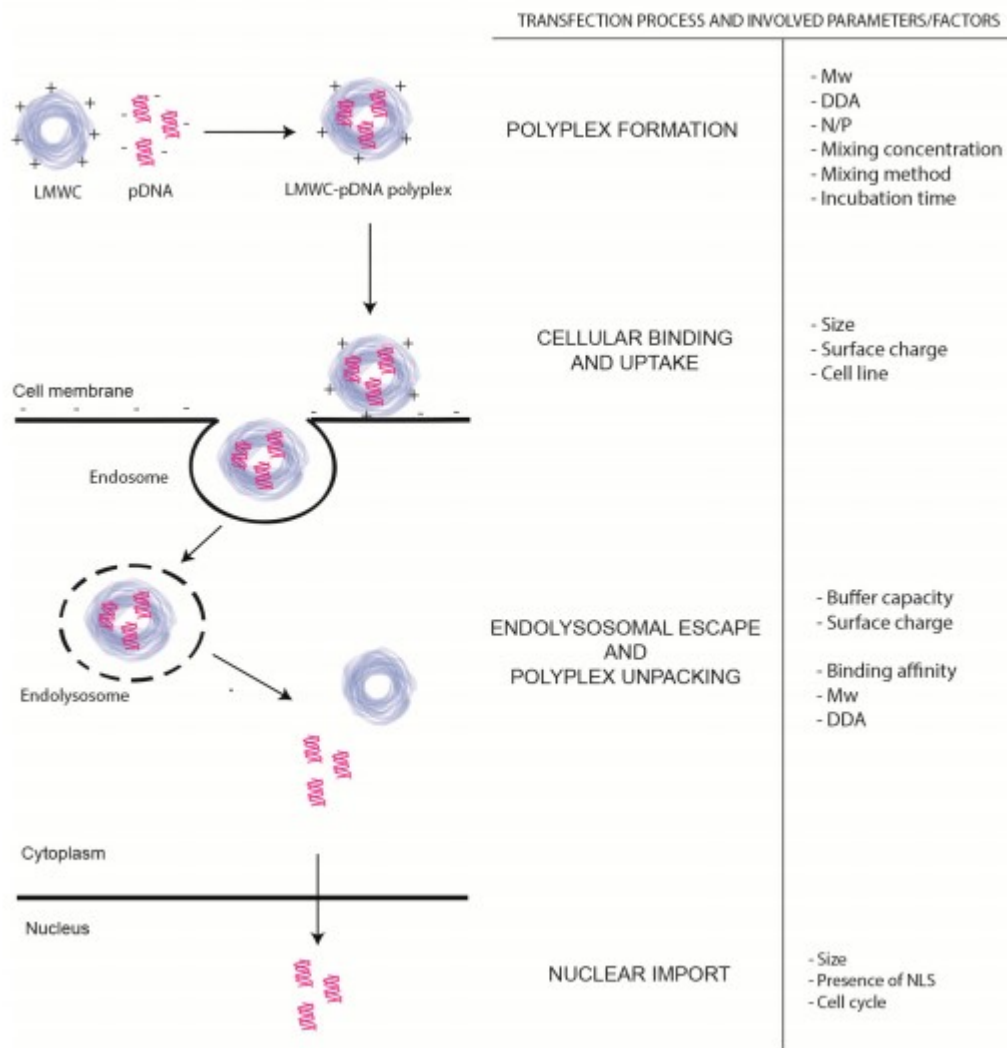


Figure 10: The transfection process and the parameters/factors that influence each step [157].

2.4.1.5 Chitosan and plasmid DNA

Several manufacturing processes were established, Chitosan may be simply complexed with nucleic acid by direct mixing of the positively charged Chitosan with negatively charged DNA, the binding occurs through electrostatic interactions. Through this easily method it is possible to obtain Chitosan nanoplexes.

Several parameters of this technique could influence the plasmid integrity and the transfection efficiency and final plasmid DNA expression, for example the incubation time and the energy applied on the mixing. Despite there are different opinions about the

incubation time, the optimal incubation time to obtain the right formation of the polyplexes avoiding the formation of aggregates is between 15-30 minutes. Others parameters are:

- I. the ratio between the chitosan and the plasmid DNA, generally the nanoplexes are produced using an excess of the polysaccharide;
- II. the pH of the solution that could influence the size of the complexes.

Moreover, other physic-chemical factors could affect the transfection efficiency, regardless the methods used. The most important are the molecular weight (MW), because it regulate the particle size, the binding affinity with the DNA, the cellular uptake and the dissociation to release the DNA; for this reason it is important the right balance between the plasmid and the polysaccharide. For example chitosan with the molecular weight more than 150 KDa (high molecular weight chitosans, HMWC) is able to protect very highly the DNA, but inside the cell the release is reduced; while if the chitosan have the molecular weight less than 150 KDa (low molecular weight chitosans, LMWC) releases easily the DNA cargo [158]. The second important factor is the deacetylation (DDA) that is the percentage of deacetylated primary amine groups in the chitosan molecule backbone, namely the number of potential interactions with nucleic acids. The DDA percentage reduction causes weaker electrostatic interactions, which provoke an easier DNA release and degradation [159]. The two parameters are strictly linked to each other, in fact it seems to be an appropriate DDA for each molecular weight. For the biomedical application the low molecular weight chitosans seems to be the optimal choice due to its high solubility at physiological pH [160].

Otherwise different techniques were set up in order to obtain more stable chitosan nanoparticles such as emulsion cross-linking, ionic gelation, spray drying and so on.

The most popular method to obtain stable and biocompatible nanoparticles is the ionotropic gelation of chitosan by the addition of TPP (sodium tripolyphosphate) where the chitosan amino groups interact with anionic groups of tripolyphosphate. This small negative ion is suitable for medical application because at physiological pH it contains three negative charges and it is no toxic [167]. Moreover the TPP is able to create five ionic cross-linking points with cationic groups of chitosan that make it the best cross-

linking agent for chitosan nanoparticles preparation. Nanoparticles parameters could be influenced by different factors:

- I. the size is effected by the chitosan/plasmid ratio, in fact increasing plasmid concentration the diameter of nanoparticles increase [170];
- II. the surface charges is influenced by the pH, chitosan/TPP ratio and chitosan/plasmid ratio.

Each parameters and the method of nanoparticles preparation affect the storage stability, loading, release performance and the interaction of the particles with different biological tissues where they are introduced. In order to obtain the best nanoparticles with the most suitable parameters, it is important to control the method of preparation [171].

In order to prepare nanoparticles capable of endosomal escape with reduce toxicity, prolonged circulation and able to protect the nanoparticles from the serum proteins, the chitosan could be coated with poly(ethylene glycol) (PEG), dextrans, poly(N-vinyl pyrrolidone), poly(glycerol methacrylate) and glycosaminoglycans, such as heparin or hyaluronic acid (HA). Hyaluronic acid is useful when is required degradability and biocompatibility [167]. It was demonstrated that the chitosan nanoparticles coated with hyaluronic acid have an interesting potential as a gene delivery system with a reduced toxicity [172, 173].

2.5 Globoid Cells Leukodystrophy (or Krabbe's Disease)

Lysosomal storage diseases (LSDs) are caused by defects on lysosomal enzyme that compromise cell viability and cell integrity due to the accumulation or storage of non-catabolized products.

Krabbe's disease was described the first time in 1916 by the Danish neurologist Knud Haraldsen Krabbe who found the presence of globoid cell in the brain [181, 182]. The presence of multinuclear (globoid) macrophages is the major histopathological change in white matter, linked with extensive demyelination and gliosis (Figure 11).

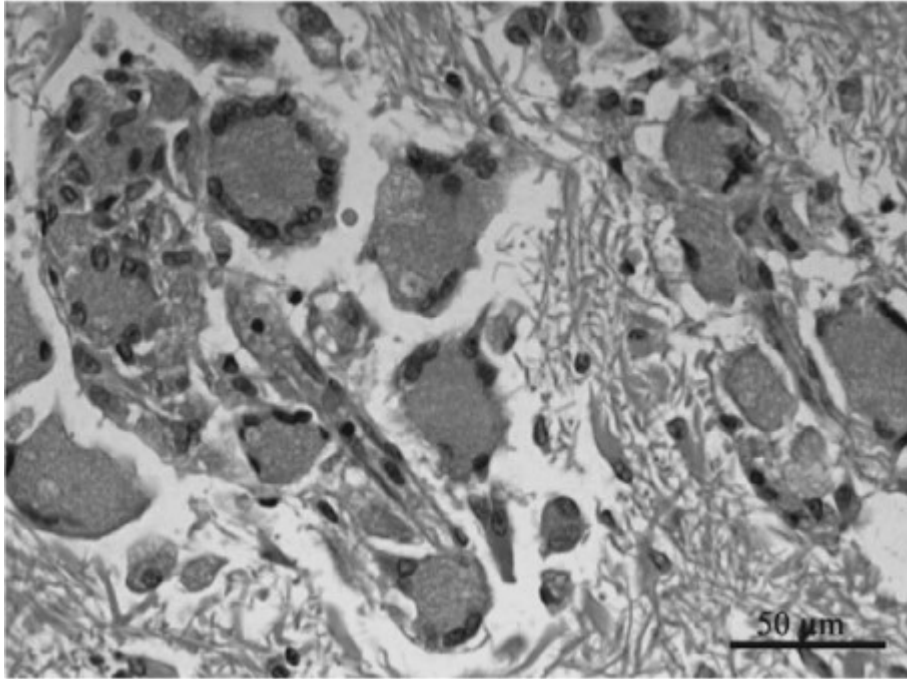


Figure 11: Typical histology of the white matter of a patient with infantile Krabbe's disease. It's present a nearly complete loss of myelin and oligodendrocytes, which are replaced by severe astrocytic gliosis and lots of multinucleated macrophages (globoid cells) [183].

Krabbe's disease or globoid cell leukodystrophy (GLD) is an LSD that affects both central and peripheral nervous system (CNS and PNS) in several species, including humans, rhesus, dogs, mice and sheep [184, 185, 186 187]. It is a rare autosomal recessive disorder in which extensive demyelination is accompanied by rapid and fatal neurodegeneration. GLD is caused by mutations in the β -galactocerebrosidase gene that codifies for the lysosomal enzyme galactocerebrosidase (GALC) that is essential for the catabolism of glycolipids, important component of myelin (galactocerebroside). The human *GALC* gene is located on chromosome 14 (14q24.3-34.1) and consists of 60652 bp. The organization of the human gene was studied in 1995 and it is composed of 17 exons and 16 introns [189]. The mouse *GALC* gene is located on chromosome 12 and consist of 3723 bp. The cDNA is composed by 2278 nucleotides and it codifies for a protein of 668 amino acids [190]. The mouse protein has the 83% of homology with the human aminoacidics sequence [191].

The GALC protein is produced and glycosylated in the endoplasmic reticulum (ER) and trans-Golgi network (TGN), where it is post-translationally modified by N-linked glycosylation at four sites [192]. The precursor protein is approximately 80 to 85 kDa, the active form is composed of two subunits, a 50 to 52 kDa and a 30 kDa mature forms [193]. This process is obtained by the action of proteases probably localized inside the lysosomes.

GLD severity and progression are variable and the age of onset can vary from the first few weeks of life (early infantile) through late-infantile, juvenile and adult clinical presentation (late-onset) [188].

2.5.1 Pathogenic Mechanisms

Currently, researchers consider that GALC deficit results in the impaired degradation of two lipids: the primary substrate Gal-cer and the second one psychosine [182]. The Gal-cer is the most important glycosphingolipid in the brain tissue. These lipids are the major constituents of oligodendrocytes in CNS and of Schwann cells in the PNS [194]. The Gal-cer synthesis takes place on the luminal surface of the reticulum. The amount of galactosylceramide in an immature brain is very low because its biosynthesis is more active when there is a rapid myelin turnover, so during the 18 months in humans and 15-25 days in rodents [195]. During myelin turnover, Gal-cer is broken down into galactose and ceramide by GALC and these products are re-used in a separate remyelination pathway. In Krabbe's disease the Gal-cer doesn't break down and free Gal-cer is able to draw infiltration of macrophages into the brain [196, 197]. Inside the brain the macrophages phagocytize Gal-cer and are transformed in multinucleated globoid cells. Anyway there is no proof that Gal-cer is toxic, indeed loss of myelin-forming cells is not attributed to Gal-cer. The other lipid involved in the pathogenic process is the galactosylsphingosine or psychosine (psy). Its biosynthesis is not completely clear. In normal brain the concentration of psychosine is very low, while in the Krabbe affected brain it is highly accumulated into the oligodendrocytes [198; 182]. At cellular level has been demonstrated that psychosine accumulates in the CNS and PNS lipid rafts of GLD patients, and causes the membrane perturbation. In addition, psychosine induces dysfunction of several cellular pathways [199].

2.5.2 Therapy

To date the treatments for LSDs are transplantation of hematopoietic stem cell transplant (HSCT) or bone marrow cell transplantation (BMT), the gene therapy (GT) and the enzyme replacement therapy (ERT) (Figure 12). These therapies have been tested both alone and in combination. Notably the HSCT or BMT have to be initiated before the onset of symptoms, for this reason an early diagnosis is crucial. Another cell-mediated therapy could be the injection of the neuronal stem cell (NCS) transduced with a recombinant GALC-encoding viral vector directly into the brain. Twitcher mice treated with these modified cells have shown an increase on their life span; but the control Twitcher mice treated with non-transduced cells show the similar increase in life span. This might be because the GALC overexpression in brain is not as critical or there are unspecific aspects of the disease that limit the effectiveness of GALC overexpression [200]. The ERT consists in a periodic enzyme administration in order to reduce and prevent the substrate accumulation, cause of the clinical phenotype. This approach shows some drawback obtain, such as the frequency of enzyme intravenous administration necessary to maintain a functional amount of Galc enzyme, the development of antibodies a-GALC and the poor crossing of the blood brain barrier (BBB) in an active form [201]. Substrate reduction therapy uses small molecule compounds to inhibit the synthesis of galactosylated lipids, including psychosine. The most promising treatment strategy is the gene therapy. The aim of this approach was from the beginning to modify the pathological cellular genome using virus-based approach (Adeno associated virus, AAV; retrovirus, RV; lentivirus, LV) or non-viral approach. The serotype AAVrh10 of the adeno-associated viruses (AAVs) is able to cross the blood brain barrier. Its capsid protein shows a high neural tropism. It was demonstrated in the mouse model of GLD, Twitcher mouse (see 2.5.3), an increased GALC activity after a single injection of AAVrh10 containing the mouse GALC cDNA. As a result these mice displayed normal functioning for an extended period. In addition, they showed that the time window for treatment could be larger than believed before [202]. Safety issues related to immune response of the adenoviral vectors and the possibility of insertional mutagenesis of viral vectors led researchers to develop non-viral approaches to treat LSDs [203]. The ideal vector should have a high translation efficiency, to guarantee a good protein production, to be able to incorporate DNAs fragments, not to be pathogenic, not to be immunogenic and, finally it should be easy to produce. To date, among the non-

viral vector approaches the transposon systems are the most appealing vectors because the integrated gene has stable expression and they are less immunogenic and less toxic than viral vectors [204, 205, 206].

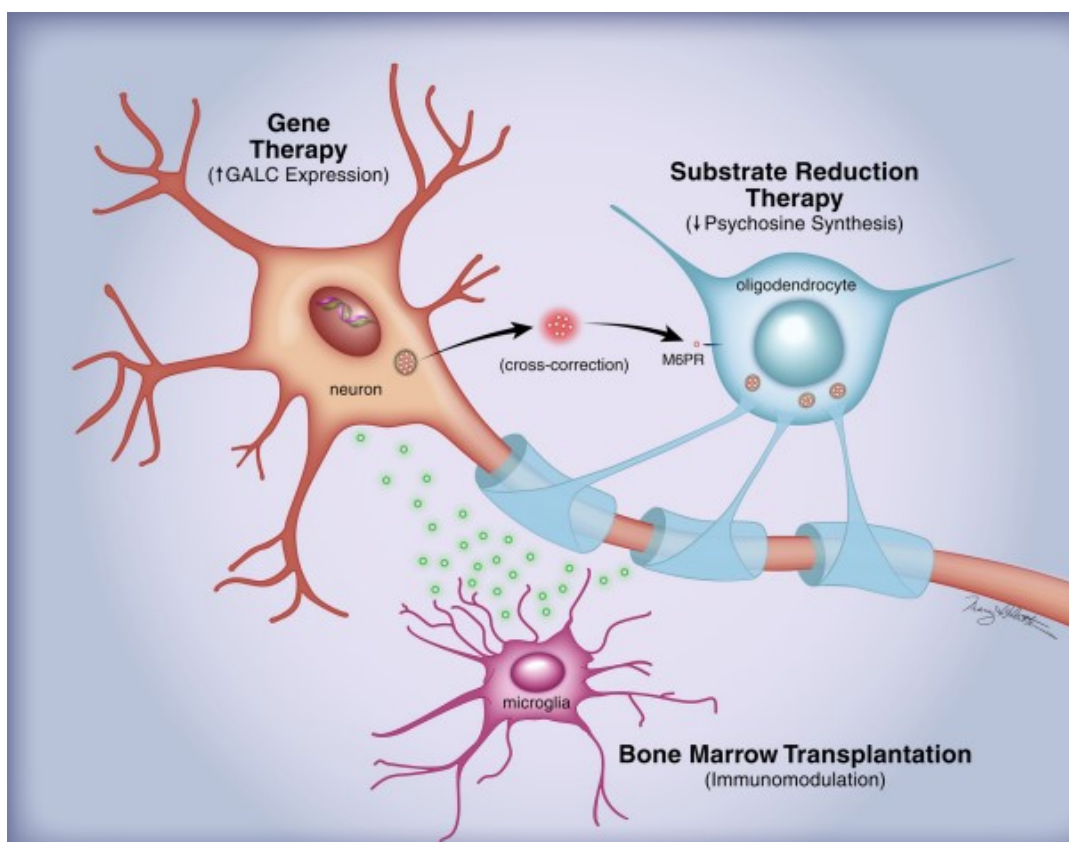


Figure 12: The triple- treatment strategy targets the primary and the two second consequences of GALC deficiency [207].

2.5.3 Animal Models

There are different animal models of Krabbe's disease that mimic the human pathology: dog, mouse and rhesus monkey.

The Twitcher mouse was obtained by Dr. Jackson in the 1976. These mice show a leukodystrophy characterized by the ataxia (twitching) and globoid cells in the PNS and CNS. Twitcher mice are considered both as a Krabbe model and a model of congenital demyelination, indeed these mice are very useful both for therapy studies and to study the myelination and demyelination processes [208]. 20 days after birth, Twitcher mice show the ataxia and weakness of the hind paws and approximately after 40 days it is possible to find the psychosine accumulation inside the brain, the spinal cord and peripheral nerves.

In 1960 was described the first time the canine GLD [209]. In contrast to the Twitcher mice in which the signs of the disease are uniform, the canine model is more variable. In GLD canine model the first signs appear between one and three months, and between eight and nine months the dogs become moribund. Similar to the Twitcher mice and human, the affected dogs have high level of psychosine, and a decrease myelination and accumulation of globoid cells [210].

Non-human primate model are often necessary before the therapy translation in clinic. The utility of this model is limited by the low reproduction rate of rhesus and the expensive maintenance cost [211].

3 Objective

The aim of this dissertation is to assess the efficacy of a novel gene therapy approach in the mouse model of Globoid cell leukodystrophy (GLD) or Krabbe's Disease, a disorder due to the deficiency of the lysosomal enzyme Galactocerebrosidase (GALC). It will be based on polymeric nanoparticles loaded with a transposon system called "Sleeping Beauty" which is able to transfer gene sequences through a cut and paste mechanism avoiding the onset of mutations. Moreover the nanoparticles will be coated with a short synthetic opioid peptide (g7) that is able to cross the blood brain barrier and enter into the central nervous system.

First aim is to establish *in vivo* the ability of the opioid peptide bound to PLGA nanoparticles to cross the blood brain barrier through the optical imaging experiments. This ligand will be bound on the surface of the chitosan nanoparticles. Next the "Sleeping Beauty" will be encapsulated inside the chitosan nanoparticles that seems to be the suitable material to bind nucleic acids.

At the end we will evaluate *in vitro* the Sleeping Beauty system efficiency through the analyses of the transposon copy number, the mRNA expression and the enzymatic activity using the traditional and polymeric approaches.

4 Materials and Methods

4.1 Plasmids

The *pcGlobin2-SB100Xco* (transposase) and the *pT2HB-CAG-Luc2* (transposon) plasmids (Figure 13) were kindly provided by Drs. Zsuzsanna Izsvák (Max Delbück Center for Molecular Medicine, Berlin, Germany).

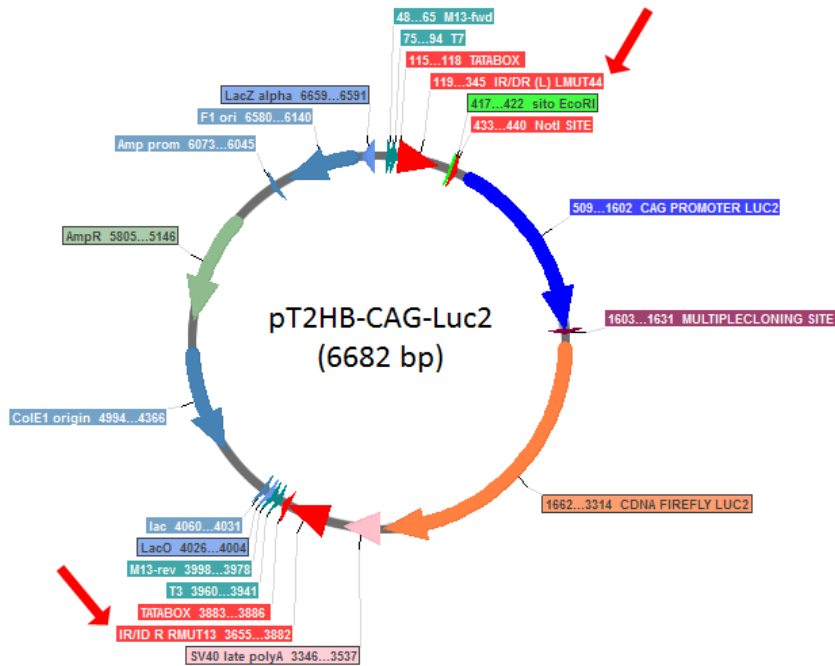


Figure 13: Schematic representation of the *pT2HB-CAG-Luc2* transposon. The red arrows are the two sequences recognized by the transposase enzyme.

As first thing, the *pT2HB-CAG-Luc2* plasmid was modified in order to insert the Renilla luciferase and the neomycin resistance sequences. In order to obtain this new plasmid, it was adopted a strategy that allows to create a multiple cloning sites (MCS, Addgene) in relevant position for the cloning strategy. As donor of the sequence that codify for a Renilla luciferase/neomycin fusion protein has been chosen the commercial *pmirGlo* vector (Promega). About twenty nucleotides were annealed (5'-ATCCGCCGGAATTCCGGCCAT-3'; 3'-GGCGGCCTTAAGGCCGGTAGC-5') to obtain a double strand sequence containing the EcoRI restriction site which is necessary to clone the Renilla luciferase/neomycin fusion sequence inside the original *pT2HB-CAG-Luc2*. The *pmirGlo* vector was properly cut using the enzymes BamHI and ClaI in order to

insert the short sequence containing the useful EcoRI restriction site downstream the Renilla luciferase/neomycin fusion sequence (Figure 14).

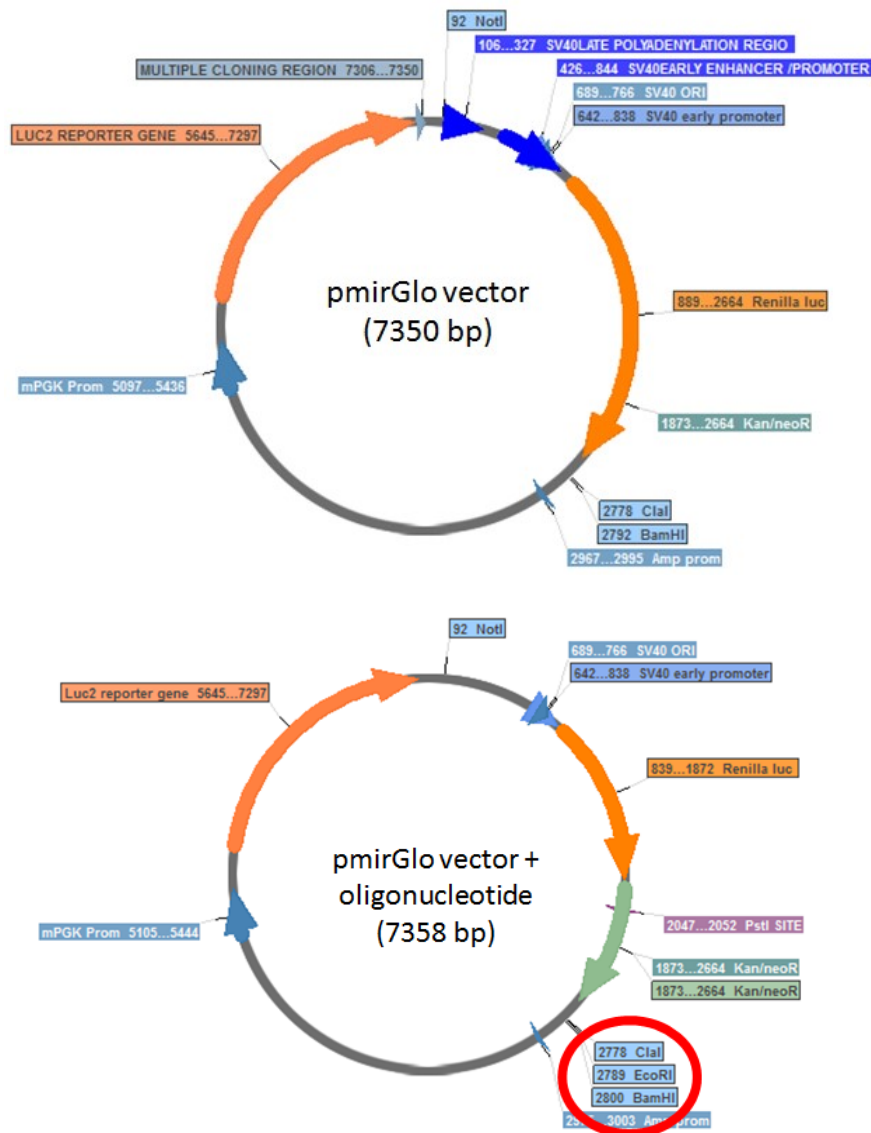


Figure 14: Schematic representation of the *pmirGlo* vectors. Top: original sequence of the commercial vector; bottom: *pmirGlo* sequence after the modification with the oligonucleotide containing the EcoRI restriction enzymatic site (red circle).

Afterwards, due to the presence of these new cut sites, all the interesting elements have been cloned inside the original transposon using the EcoRI and NotI restriction enzymes. This process allowed us to obtain a transposon with the Firefly luciferase and the Renilla luciferase/neomycin fusion protein with their own promoter. All the aforementioned sequences have been inserted between the two regions recognized by the transposase

(inverted terminal repeat sequences, IR/DR (L) e IR/DR (R)). We obtained a new transposon called *pT2HB-CAG-Luc2-Ren/neo* (9361 bp) (Figure 15).

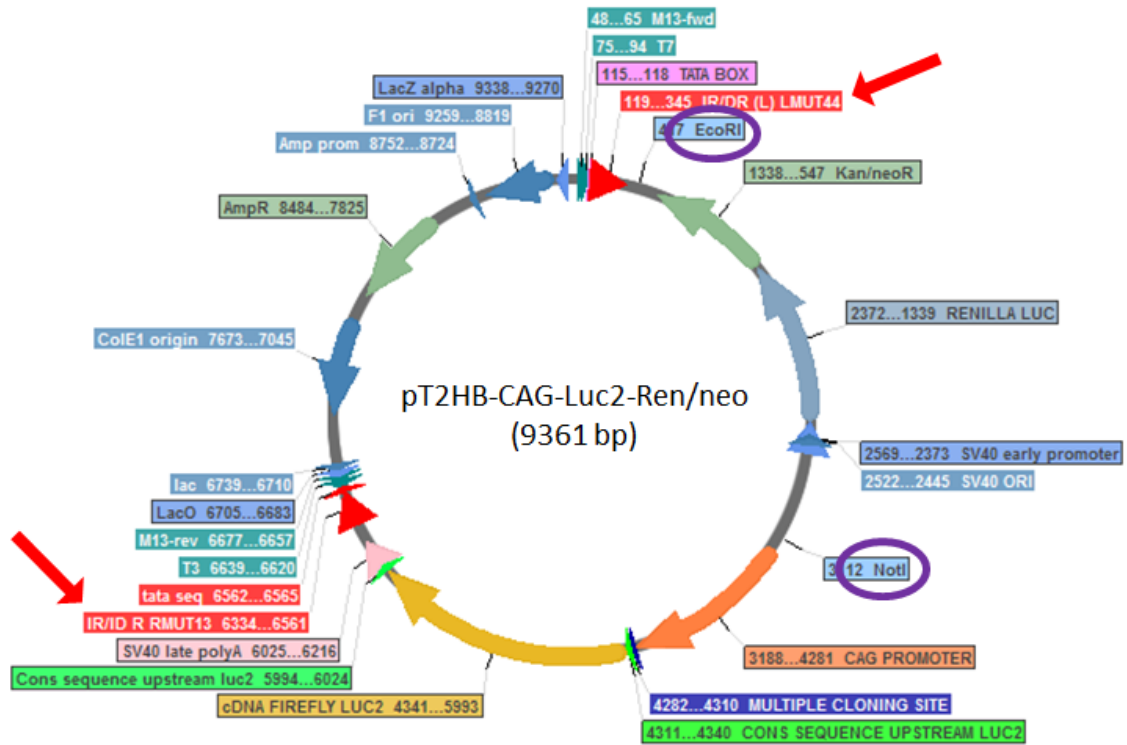


Figure 15: Schematic representation of *pT2HB-CAG-Luc2-Ren/neo* transposon. The purple circles are the restriction enzyme used for the cloning strategy; the red arrows are the regions recognized by the transposase enzyme (IR/DRs).

For the second modification the Firefly Luciferase sequence was replaced with the murine GALC coding sequence that was obtained from in-house Lentiviral vector. We designed the primers in order to have at the two extremities the sequences of restriction enzymes (*Bgl*II and *Fse*I) useful for our cloning strategy (Forward_ *Bgl*II-5'-GGAAGATCTTCCGTCATGACCGCCGCC-3'; Reverse_ *Fse*I-5'-GATGGCCGCCTGTGGACTAGCGAGCA-3'; Ta=64°C). The cDNA GALC sequence was amplified from the donor vector using the AccuPrime DNA Polymerase (Invitrogen) following the manufacturer's protocol. At the end we obtained a new transposon called *pT2HB-CAG-mGALC-Ren/neo* (9663 bp) (Figure 16).

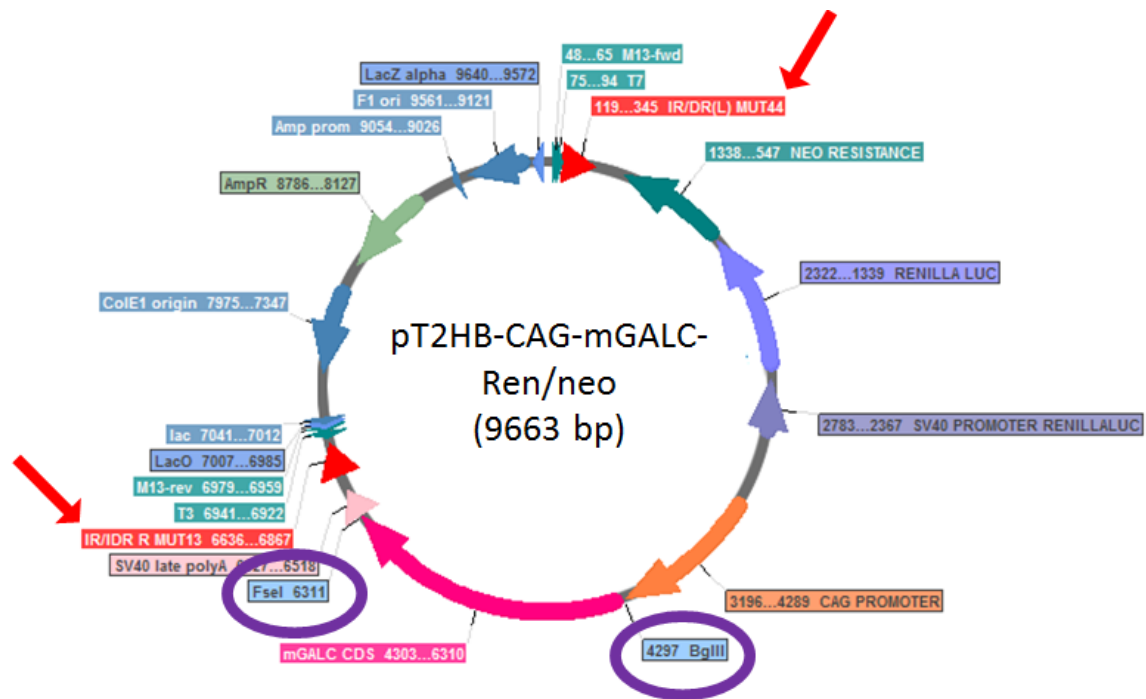


Figure 16: Schematic representation of the final transposon plasmid: the purple circles are the restriction enzymes used to clone the mGALC sequence instead of the Firefly luciferase sequence; the red arrows are the site recognized by the transposase enzyme (IR/DRs).

The pCRII- β -Globin plasmid, as standard for the real time PCR experiments, was created employing the commercial kit TA Cloning Kit Dual Promoter (Invitrogen) following the manufacturer's protocol.

T4 DNA ligase and restriction enzymes were purchased from New England Biolabs and for the reaction set up has been followed the manufacture's protocol. One shot TOP10 Electrocomp E.coli were commercially provided from Invitrogen. QIA quick gel extraction kit and Hispeed Plasmid Midi kit were purchased from the Qiagen (Valencia, CA). Sanger sequencing allowed us to check the right transposon constructions.

4.2 Plasmids sequencing

The Sanger sequencing reactions were carried out with BigDye Terminator v. 3.1 mix (Applied Biosystems), buffer 10X (Applied Biosystems), Betaine 5M (Sigma Aldrich), 4 pM of primer, and 200 ng of plasmid template in a final reaction volume of 10 μ l. Cycle conditions were an initial denaturation at 96° for 3', then 30 cycles of 96° for 30", (ta) annealing temperature for 15", 60° for 4'. Excess dye terminators were removed using

BigDye® XTerminator™ Purification Kit (Applied Biosystems). Samples were electrophoresed on an Applied Biosystems 3500DX Genetic Analyzer CE-IVD instrument, using 50 cm capillary arrays and POP-7 polymer. Data were analyzed using SeqScape version 2.7 of Sequencing Analysis.

4.3 Cell culture

For in vitro experiments were used different type of cells.

For the preliminary studies were used the HELA cell line and the CHO cell line. The HELA line is an immortal cell line derived from human cervical cancer cells and they grow in the high glucose formulation of DMEM (with 4500 mg/L glucose, L-glutamine (0.292 g/L), sodium bicarbonate (3.7 g/L) without sodium pyruvate) supplemented with 10% fetal bovine serum. The CHO is an epithelial cell line derived from the ovary of Chinese hamster and that grows in serum-free CHO medium (CHO-S-SFM II, Gibco).

The SVG cell line is an immortalized human fetal astrocyte cell line, that synthesizes a replication-proficient SV40 T-Ag. The cells grow in the high glucose formulation of DMEM (with 4500 mg/L glucose, L-glutamine (0.292 g/L), sodium bicarbonate (3.7 g/L) without sodium pyruvate) supplemented with 10% fetal bovine serum.

The primary cell culture of Human Fibroblast were obtained from foreskin. The cells grow in the RPMI 1640 medium (with 300 mg/L L-glutamine, 2000 mg/L glucose, sodium bicarbonate (2000 mg/L) and without sodium pyruvate) supplemented with 15% fetal bovine serum.

The primary cell cultures of Human Fibroblast presenting the Krabbe disease (ML) grow in the RPMI 1640 medium (with 300 mg/L L-glutamine, 2000 mg/L glucose, sodium bicarbonate (2000 mg/L) and without sodium pyruvate) supplemented with 15% fetal bovine serum.

The Human Oligodendrocytic (Glial) (MO3.13) Cell Line is an immortal human-human hybrid cell line that express phenotypic characteristics of primary oligodendrocytes. The cells were provided by Dr. Marco Cecchini (CNR-Istituto Nanoscienze, Pisa). The cells grow in the high glucose formulation of DMEM (with 4500 mg/L glucose, L-glutamine

(0.584 g/L), sodium bicarbonate (3.7 g/L) without sodium pyruvate) supplemented with 10% fetal bovine serum.

Human Glioma cell line A172 (ECACC, UK) were maintained in humidified atmosphere (5% CO₂) in RPMI-1640 medium supplemented with 10% fetal bovine serum, 2 mM l-glutamine, 100 U/ml penicillin and 100 µg/ml streptomycin.

Before every in vitro experiments, the culture cell medium of each cell line was tested for the absence of mycoplasma through a specific PCR (F_GPO 5'-GGGAGCAAACAGGATTAGATACCCT-3', R_MGSO 5'-TGCACCATCTGACACTCTGTAAACCTC-3'; Ta=55°C).

4.4 Cell transfection

All the cells were transfected with the nucleofector Amaxa (LONZA). In order to stabilize the best nucleofector Amaxa protocol that allows a good transfection efficiency and a good cell viability, each cells type were transfected with the commercial vector pmaxGFP™. The cells were resuspended with 100 µl of Ingenio Electroporation Solution (Mirus) and to the solution were added 2µg or 1µg of transposon plasmid and 500 ng or 250 ng of pcGlobinSB100Xco transposase in a 4:1 or 2:1 ratio. The mix solution was transferred into a certified cuvette that was inserted inside the Nucleofector Cuvette holder. 500 µl of culture medium was added to the cuvette and the cells were gently transferred into the culture dish. The clones selection was performed using the 800µg/µl of G-418 Sulphate Geneticin Solution 50 mg/ml (EuroClone).

4.5 Luciferase assay

To investigate the luciferase expression we used the commercial kit "dual-luciferase reporter assay" (Promega); this kit allows to retrieve, at the same time, the expression of the two enzymes (Firefly Luciferase and Renilla Luciferasi) in order to normalize the data of the Firefly expression based on the data obtained from the Renilla luminescence. The test was performed after 24 hours from the transfection and after the neomycin selection. The cells, which were obtained from ¼ of one well of six-well plate (~7,5x10⁴ cells), were treated with Passive Lysis Buffer 1X and 4 µl were added into the cuvette with 20 µl of the reagent LARII that allows to read the Firefly Luciferase with the TD-20/20 Luminometer (Turner Designs). After the reading, inside the same cuvette, 20 µl of the

reagent Stop&Glo 1X were added to the reaction mix. This reagent permits to read the Renilla Luciferase fluorescence.

4.6 DNA extraction

The cell DNA was extracted with the QIAMP kit (QIAGEN) following the manufacture's protocol and with the classical phenol-chloroform method [160]. The pellet was dried at room temperature and then was resuspended with 50 µl of sterile water. The DNA concentration was measured with the NanoDrop-1000 (Thermo Scientific).

4.7 RNA extraction and RT

For the RNA extraction was used the commercial kit EuroGold total RNA (EuroClone) from $\sim 0,3 \times 10^6$ cells and the RNA was eluted with 50 µl of RNasefree water pre-warmed at 70°C. At the end the RNA concentration was measured with the NanoDrop-1000 (Thermo Scientific). 1 µg of total RNA was retro-transcribed with the GoScript Reverse Transcription System (Promega) following the manufacture's protocol.

4.8 Real Time PCR

The quantitative real-time PCR reactions were achieved on 7900HT Fast Real-Time system (Applied Biosystems) in order to investigate different aspects after the transfection experiments. The singleplex reaction was run in duplicate with a final volume of 20 µl using SyberGreen chemistry (primer concentration of 10 µM). Cycle conditions were an initial denaturation at 95° for 10", then 40 cycles of 95° for 15", ta° for 15", 60° for 1' and the final melting curve.

4.8.1 Absolute Real-Time quantification

After 48 hours from the transfection experiments the plasmid DNA was isolated from the cells through the phenol-chloroform method. 25 ng and 5 ng of total DNA were analyzed in absolute real time PCR, that was carried out with Power Syber Green (Life Technology). To set up this experiment we designed two different pair of primers, one able to recognize at the same time the episomal and the excision plasmids (F_PCR2 5'-GGTATCAGCTCACTCAAAGG-3', R_PCR2 5'-CTTTTACGGTTCCTGGCCT-3'; Ta=50°C) and the other one able to anneal only on the episomal plasmid (F_PCR4 5'-GGCGATTAAGTTGGGTAAC-3', R_PCR4 5'-AACTGTATAGGGATCCGAGC3';

Ta=53°C). In order to normalize data, the same samples were amplified with the β -globin primers (β -GLOBIN_R 5'-CAACTTCATCCACGTTCCACC-3', β -GLOBIN_F 5'-ACACAACACTGTGTTCACTAGC-3'; Ta=55°C). After 48 hours it is possible to establish the relative excision activity.

Average copy number of transgenic cell populations were measured from transfected and selected cells. 50 ng and 5 ng of genomic DNA were analyzed in absolute real time PCR (SyberGreen method). To set up this experiment were used primers that annealed on the sequence recognized by the Transposase (F_IRDR_R 5'-ACCCACTGGGAATGTGATGA-3', R_IRDR_F 5'-CCTGTCTTAGGTCAGTTAGG-3'; Ta= 55°C). In order to normalize data, the same samples were amplified with the β -globin primers (β -GLOBIN_R 5'-CAACTTCATCCACGTTCCACC-3', β -GLOBIN_R 5'-ACACAACACTGTGTTCACTAGC-3'; Ta=55 °C).

The absolute quantification was achieved by a serial dilutions of two plasmids (*pT2HB-CAG-mGALC-Ren/neo* and *pCRII- β -Globin* plasmids) which contained inside the specific sequences amplified by the primers. The standard curve was created using a range between 300000 and 30 copies. The following formula has been applied to establish the right correlation between the plasmid copy number and the ng to put into the reaction. The mass of a single plasmid molecule was calculated applying the formula:

$$\text{Plasmid length (bp)} \times 1,096\text{e-}21 \text{ g/bp} = \text{mass (g)}$$

Subsequently the plasmid mass was multiply by the copy number of interest to obtain the mass of plasmid DNA needed in each reaction.

4.8.2 Relative Real-Time quantification

The relative gene expression was measured amplifying a serial dilution of cDNA (100 ng, 25 ng, 6,25 ng) using the primer that recognise the GALC's mRNA (K12_F_RT 5'-TAGGAGCTCACTATCCTGGA-3', K12_R_RT 5'-AGGCTGTTGGAGTCGCATAT-3'). The β -Actin house-keeping gene (F_ β -Actin 5'-TAAGGAGCTGTGCTACG-3'; R_ β -Actin 5'-GCTCATTGCCAATGGTGATG-3') amplification allows to normalize the data. Cycle conditions were an initial denaturation at 95° for 10', then 40 cycles of 95° for 15'', 58° for 15'', 60° for 1' and the final melting curve. The raw data were analyzed using the $\Delta\Delta\text{Ct}$ method.

4.9 Protein extraction and quantification

For the protein extraction the cells were harvested from a well of a six-well plate ($\sim 0,3 \times 10^6$ cells) and it was resuspended with 200 μl of M-PER Mammalian Protein Extraction reagent (Thermo Scientific) and mixed for 5 minutes at room temperature. Then it was centrifuged for 10 minutes at 14000xg at 4°C. After this step the surfactant was collected into a new clean tube and preserved on ice. The samples obtained from this procedures were quantified through Lowry's method or BCA protein assay. The protein quantification was performed with LAMBDA 40 UV/VIS Spectrometer (PerkinElmer instruments) [161].

4.10 Enzymatic assay

The protein's extracts were diluted 1:6 and 1:18 with NaP buffer pH6 and used for the enzymatic assay. The fluorogenic substrate 4-methylumbelliferyl- β -D-galactoside was purchased from Sigma Life Science and dissolved in Citrate buffer, pH3.4. The enzymatic assay was performed mixing 40 μl of substrate with 20 μl of samples' dilutions and incubated 30 minutes at 37°C in darkness. This allows to measure the total activity of β -GAL plus GALC. In order to measure only the GALC activity, it was added to the mix reaction 3 μl of AgNO_3 3mM. After 30 minutes of incubation, the reactions were stopped with 290 μl of 0.4 M Glycine/NaOH, pH10.4. The reactions were performed in black 96-well plate and the fluorescence of released 4-methylumbelliferyl was measured on Glomax Multi Detection System instrument (Promega) and UV optical kit (excitation at 360 nm and emission of 450 nm). The raw data were analyzed with the formula: $(\text{IF} \times \text{dilution} \times \text{total assay volume}) / (\text{slope} \times \text{time} \times \text{sample}) = \text{mU/ml}$. This value is multiply by the total amount of protein. The enzymatic activity was expressed as nanomoles of substrate hydrolyzed per minute and normalized from milligram of protein.

4.11 Plasmid labeling

In order to follow the plasmid encapsulation processes, each plasmids was labeled with Label IT Tracker following the manufacturer's protocol. Briefly, 5 μg of plasmid DNA was mixed with 2,5 μl of Label (ratio 1:0.5; weight: volume), 5 μl of Buffer A 10X in a final volume of 50 μl . The labeling reaction was incubated at 37°C for one hour. The labeled plasmid DNA was separated from the unattached label by ethanol precipitation

using 1/10 volume of NaCl 5M, two volumes of ice cold 100% ethanol and incubated for one hour (or overnight) at -20°C. After a centrifugation for 40 minutes at 14000g at 4°C, the supernatant was eliminated and the pellet was washed with 70% ethanol and centrifuged for 30 minute at 14000g at 4°C. Then it was reconstituted with 10 µl of sterile water.

4.12 Cell labeling and fixation

After the transfection, the cells were placed on a coverslip and after the appropriate time they were labeled with 5µg/ml of *Wheat Germ Agglutinin Conjugates* (WGAC 488-LifeTechnologies) diluted in culture medium to dye plasmatic membrane for 10 minutes at 37°C. The labeling solution was removed and the cells were washed twice with PBS solution. Then the cells were fixed with PFA 4% (SigmaAldrich powder 95%) for 20 minutes at 37°C and washed for three times. To mount cells on a slide, the Vectashield Hardset (Vector laboratories Inc. Burlingame, CA) was dispensed onto the specimen; in this way the DAPI coloured the cellular nuclei. To analyze the slides we have used the inverted microscope Axioplan 2 and the object 40X (ZEISS Oberkochen German), the images were acquired with Axiocam MRc and modified with the corresponding program.

4.13 Cell viability assay

In order to evaluate a range of nanoparticles toxicity, the MTT assay has been performed. These is a colorimetric assay for evaluating cell metabolic activity. The NAD(P)H-dependent cellular oxidoreductase enzymes reflect the number of viable cells because these enzymes are able to reduce the tetrazolium dye MTT 3-(4,5-dimethylthiazol-2-yl)-2,5-diphenyltetrazolium bromide (SIGMA-ALDRICH) to its insoluble formazan, which has a purple color. 24 hours before the experiment the cells were plated in a 96-wells plate (~1,25x10⁴ cells). 12 wells were used as controls. After 24 hours, the cells should be attached to the well and it was possible to change the cell medium with the medium with the appropriate nanoparticles concentration. The plate was incubated at 37°C, 5% of CO₂ for the established period of time. After the treatment time it was possible to add the MTT reagent diluted 1:10 inside each well (the filtrated stock solution is 5 mg/ml PBS). The 96-wells plate was incubated for 4 hours and then was added 100 µl of isopropanol, in this way the sale was resuspended. Each well is read at wave length of 570nm using Glomax Multi Detection System (Promega).

4.14 Animals

Balb/c mice of approximately 20 g and 6 weeks of age were obtained from Harlan Laboratories (San Pietro al Natisone, Udine, Italy) and maintained under pathogenfree conditions and on low-fluorescence diet [162]. All the experimental procedures were performed according to the guidelines of the European (86/609/EEC) and the Italian (D.L.116/92 and subsequent addenda) law.

4.15 The g7 opioid peptide bound to PLGA nanoparticles

4.15.1 *The g7-PLGA nanoparticles preparation and characterization*

The g7 peptide bound to PLGA NPs were provided by Prof. Tosi [94] in order to evaluate the ability of this peptide to cross the BBB. NPs preparation has been performed in different phases. First of all the PLGA polymer was bound with the DY 675 (C44H53N4O5SCI; Mol. Wt. 785.45; Dyomics; Jena, Germany) to obtain DY-PLGA, and then the g7 was conjugated in according to the already described protocol [174]. The nanoparticles DY-g7-PLGA were obtained in accordance with the nanoprecipitation procedure. To evaluate the morphology of DY-g7-NPs was performed a scanning electron microscope (SEM) (XL-40 Philips, Eindhoven, The Netherlands). The samples were coated under argon atmosphere with a 10-nm gold palladium thickness (Emitech K550 Supper Coated, Emitech LTD, UK). Photon correlation spectroscopy (PCS) and laser Doppler anemometry have been used to analyze the DY-g7-NPs size (in distilled water) and zeta potential (z-p) using a Zetasizer Nano ZS (Malvern, UK; Laser 4 mW He-Ne, 633nm, Laser attenuator Automatic, transmission 100% to 0.0003%, Detector Avalanche photodiode, Q.E>50% at 633nm, t = 25 C). The results were normalized with respect to a polystyrene standard solution.

4.15.2 *In vivo imaging*

To performed in vivo imaging the PLGA NPs were conjugated with dye 675 that emit at seven hundred nm. These NPs have been injected into the tail vein of Balb/C mice and then the images were acquired with Pre-clinical optical imaging system eXplore Optix (ART Advances Research Technologies Inc). The 12 mice were divided in two groups, the control group was injected with 100µl of nanoparticles without the peptide g7 and the other one was treated with 1 ml of nanoparticles functionalized with the peptide g7 (8 mg).

During the experiments the mouse was anesthetized with a gaseous anaesthesia and placed in the holder that is an heated plate. The plate is automatically transferred into the laser chamber, where there is a pulsed laser, exciting the region previously selected and inducing a fluorescence emission which is detected by a specific detector. A prescan image was acquired before labeled probe administration. Fluorescence emission was collected at 700nm. At the end of the imaging analysis, the mouse was allowed to recover from the anaesthesia. To evaluate the ability to cross the BBB the two groups of mice were analysed after ten minutes (t=0) and two hours (t=2h) from the injection.

4.16 Chitosan

4.16.1 Chitosan/plasmid DNA nanoplexes preparation

In order to obtain chitosan nanoplexes has been used polydisperse polysaccharide with average molecular weight of 50 KDa, with 87% of deacetylation degree, in form of hydrochloride salt at pH5 (NOVOZYME). The chitosan has solubilized with MilliQ water, filtered using a 0,22 μm filter and then has been obtain a solution CHIT1 with a concentration of 10 mg/ml. The stock solution has been diluted in order to obtain CHIT2 (0,1 mg/ml), CHIT3 (0,5 mg/ml) and CHIT4 (2,5 mg/ml). The suitable amount of chitosan has been added to the vector to obtain three different solution with different ratio between chitosan and DNA (maintaining constant the amount of DNA). The concentration of chitosan used for the preparations was suitable to have the constant final volume of complexation. Then the solutions were lightly stirred for 30 minutes, froze and dried. Before the in vitro experiments each preparations were resuspended with sterile water (Figure 17).

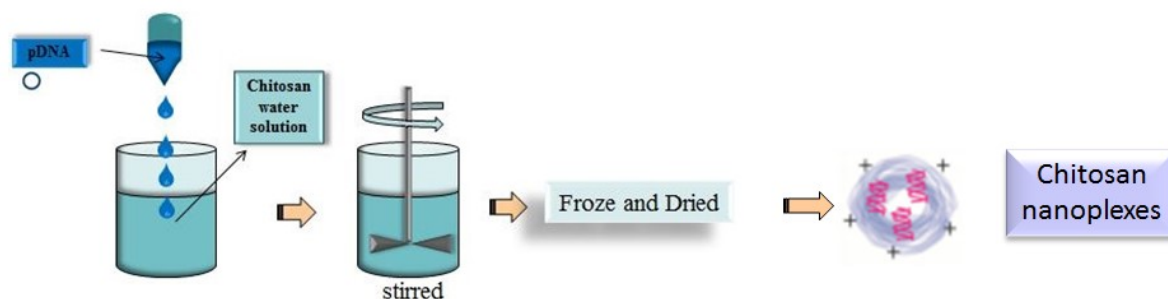


Figure 17: Schematic representation of the chitosan nanoplexes preparation.

4.16.2 Gel retardation assay

The efficiency of the complexation between the chitosan and the plasmid DNA was evaluated through the gel retardation assay using 1% agarose gel. 200 ng of each chitosan polyplexes preparations were loaded onto the gel with 2 μ l of loading dye. In the same gel was loaded the same amount of the naked plasmid. The plasmid retardation has been visualized under UV transillumination.

The stability of the chitosan-plasmid DNA nanoplexes was evaluated using the gel retardation assay after the samples were kept at -20°C for 2-3 weeks.

4.16.3 Cellular uptake

For the purpose of evaluating the uptake of the chitosan/DNA complex, $0,3 \times 10^6$ MO3.13 cells were plated on a well of 6-wells plate and were tested different conditions:

1. C1: 1 μ g of pT2HB-CAG-mGALC-Ren/neo+Rhodamine (~200ng of chitosan)
2. C2: 1 μ g of pT2HB-CAG-mGALC-Ren/neo+Rhodamine (~1 μ g of chitosan)
3. C3: 1 μ g of pT2HB-CAG-mGALC-Ren/neo+Rhodamine (~5 μ g of chitosan)
4. D1: 250 ng of pcGlobin2-SB100Xco+Fluoresceine (~50 ng of chitosan)
5. D2: 250 ng of pcGlobin2-SB100Xco+Fluoresceine (~250 ng of chitosan)
6. D3: 250 ng of pcGlobin2-SB100Xco+Fluoresceine (~1,25 μ g of chitosan)
7. C1+D1: (1 μ g of pT2HB-CAG-mGALC-Ren/neo+Rhodamine) + (250 ng of pcGlobin2-SB100Xco+Fluoresceine) (~250 ng of chitosan)
8. C2+D2: (1 μ g of pT2HB-CAG-mGALC-Ren/neo+Rhodamine) + (250 ng of pcGlobin2-SB100Xco+Fluoresceine) (~1,250 μ g of chitosan)
9. C3+D3: (1 μ g of pT2HB-CAG-mGALC-Ren/neo+Rhodamine) + (250 ng of pcGlobin2-SB100Xco+Fluoresceine) (~6,250 μ g of chitosan)

The cells were incubated for two and six hours at 37 °C, then they were labeled with Alexa Fluor 350 WGA, fixed with PFA 4% and mounted on slide.

4.16.4 Chitosan/TPP-hyaluronic acid nanoparticles preparation

Plasmid DNA loaded nanoparticles were synthesized by the ionotropic gelation technique between positively charged chitosan and negatively charged TPP as previously reported in literature [175] (Figure 18). Chitosan was dissolved in HCl (4.6 mM) at concentration of 2 mg/ml (w/w) and the pH was adjusted to 4.9 by the addition of appropriate volumes of NaOH. Then, a 0.5% (w/w) solution of the anionic crosslinker, pentasodium triphosphate (TPP), was prepared in water. All the solutions were filtered with a 0.22 μm filter to remove traces of solid particles. In order to promote the encapsulation of nucleic acid, the *pcGlobin2-SB100Xco-Fluorescein* (2 $\mu\text{g}/\mu\text{l}$) was added to the TPP solution to assure that no interaction would occur between negatively charged DNA and positively charged chitosan. Then, the complexes were obtained at different N/P ratio, adding dropwise the required amount of TPP solution/plasmid DNA to 4 mL of chitosan solution under magnetic stirring (300 \pm 50 rpm) for 30 min. N/P ratio was defined as the molar ratio of the positive amino group of chitosan and the negative DNA phosphate group. The formulated nanoparticles were then pelleted by centrifugation at 17,000 g for 30 min. Chitosan/PcGlobinSB100Xco-2-Fluorescein nanoparticles were dispersed in a 100 mM acetic acid/acetate buffer (pH 5) and slowly added to an equal amount of hyaluronic acid (MW < 10 kDa) in acetate buffer and stirred for 30 min.

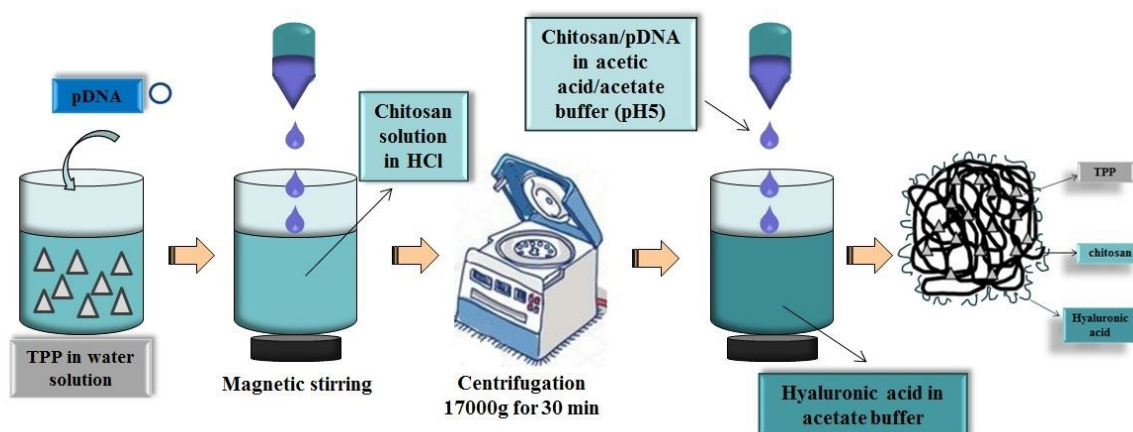


Figure 18: Schematic representation of the ionotropic gelation technique.

4.16.5 Chitosan/TPP-hyaluronic acid nanoparticles characterization

Nanoparticles size and zeta potential were determined by dynamic light scattering (DLS) using Zetasizer Nano ZS instrument (Malvern Instruments, Worcestershire, UK). To determine the hydrodynamic diameter by DLS, nanoparticles were diluted in milliQ ultrapure water as a dispersant medium, followed by 30 min incubation at room temperature prior to analysis. Size measurements were performed in automatic mode with a scattered light detection angle of 173°. The reported particle size was obtained as an intensity distribution by cumulative analysis performed in the zetasizer software (version 6.20). All the measurements were performed in triplicate. The zeta potential values (mV) were calculated from the electrophoretic mobility using the Smoluchowsky relationship. The experiments were performed in triplicate and an average of 100 measurements was acquired individually for each sample.

4.16.6 Chitosan/TPP-hyaluronic acid nanoparticles encapsulation efficiency

The encapsulation efficiency (EE) of the pDNA inside the nanoparticles was determined after isolation by centrifugation (10 000g, 30min, 25°C) and recovery of the supernatant. The amount of unbounded pDNA was determined by UV–vis analysis (Shimadzu UV–vis 1700 spectrophotometer), as reported by [176]. The encapsulation efficiency was calculated as follows:

$$EE(\%) = \frac{\text{Amount Total pDNA} - \text{Amount of pDNA}_{\text{supernatant}}}{\text{Amount of Total pDNA}} \times 100.$$

4.16.7 Chitosan/TPP-hyaluronic acid nanoparticles up-take efficiency

Human Glioma A172 (ECACC, UK) cells were seeded at a density of 10^5 cells/cm² onto black 24-well plates. On the second day, the cells were pre-incubated with Hank's buffered salt solution (Hyclone, Italy) for 15 min, and the medium was replaced with the suspension of nanoparticles and incubated for 30, 60, and 120 minutes at 37°C. Then the cells were washed with ice-cold PBS for five times and solubilized in 400 µl 1% Triton X-100. Fluorescence in cell lysates was quantified with a spectrofluorometer (Cytation 5, BioTeck). In addition, cell lysates were subjected to BCA protein assay. The uptake of nanoparticles by A172 cells was expressed as percentage of nanoparticles uptaken per mg cell protein.

4.17 Statistical analysis

The experiment were generally performed in triplicate and the data were reported as the mean \pm standard deviation. The Student's t-test and one-way ANOVA test were performed to establish the significance of the results ($P < 0.05$). The graphics were made using Prism 7 GraphPad software, Inc, USA.

5 Results

5.1 *In vitro* experiments

In vitro preliminary experiments were performed to establish the efficacy of the Sleeping Beauty System using a traditional transfection method. Several types of cells were employed to measure the transposase excision activity, the transposon copy number and the enzymatic activity.

5.1.1 Cell transfection

To perform *in vitro* experiments the cells were co-transfected with the transposon and the transposase using the nucleofector Amaxa (LONZA). First of all, for each different cell line, we established the best nucleofection program testing different protocols suggested by the Lonza company using the commercial vector pmaxGFP™. After 24 hours the transfection efficiency was established verifying the expression of the green fluorescent protein (GFP) (Figure 19).

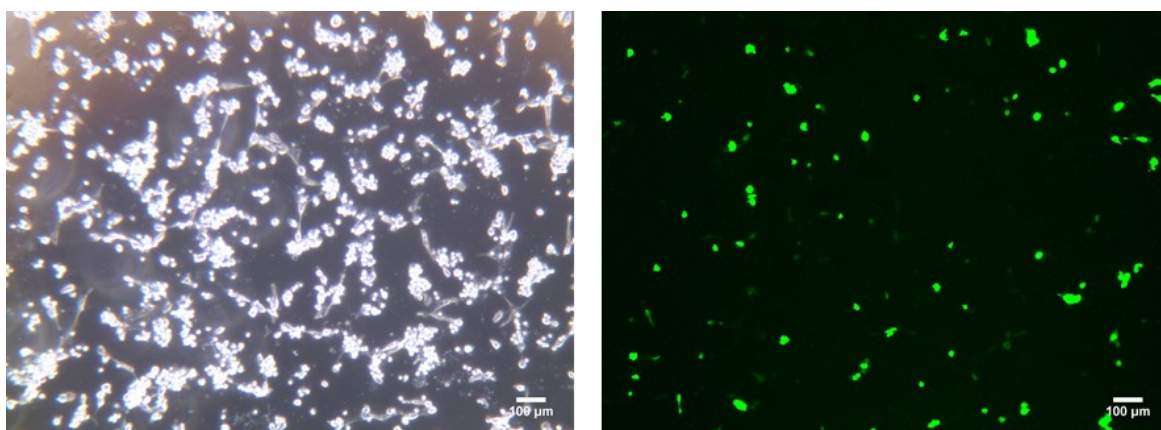


Figure 19: Example of cell transfection with the commercial vector pmaxGFP. Here 2 μ g of vector were used to transfect the MO3.13 using the T-020 program. Scale Bar indicates 100 μ m.

According to the preliminary test we were able to determine the right transfection protocol for each different cell line; the protocols reported in Table 3 are the best compromise between cell viability and transfection efficiency.

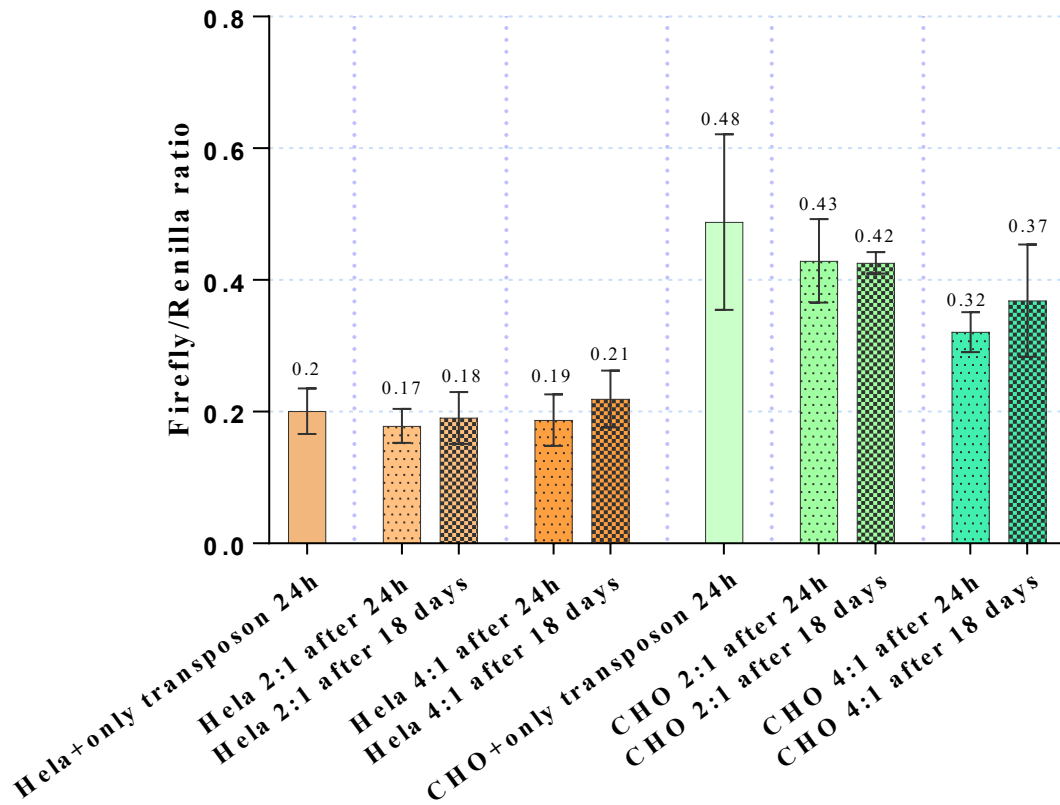
Cells	Nucleofector program	Cell number per reaction
HELA	I-013	2 x 10 ⁶
CHO	U-023	1 x 10 ⁶
Human Fibroblast	U-023	0,5 x 10 ⁶
SVG	D-023	2 x 10 ⁶
MO13.3	T-020	2 x 10 ⁶

Table 3: Transfection conditions.

5.1.2 Luciferase assay

When the new vector was obtained, we wanted to establish the transfection efficiency and the right ratio between the transposon and the transposase to use. For this reason HELA and CHO cell lines were co-transfected with *pT2HB-CAG-Luc2-Ren/neo* transposon and the *pcGlobin-SB100Xco* transposase. Moreover as a control the cell lines were transfected with only the transposon. After 24 hours post transfection the cells were selected adding in culture medium neomycin G-418. The vector has the neomycin resistance sequence so the medium selected the only transfected cells. 18 days later, control cells died and bulk have been obtained. The raw data were analyzed putting in ratio the Firefly Luciferase with the Renilla Luciferase luminescence and the Graphic 1 shows that there is no difference between the relative luminescence value expressed after 24 hours or after 18 days.

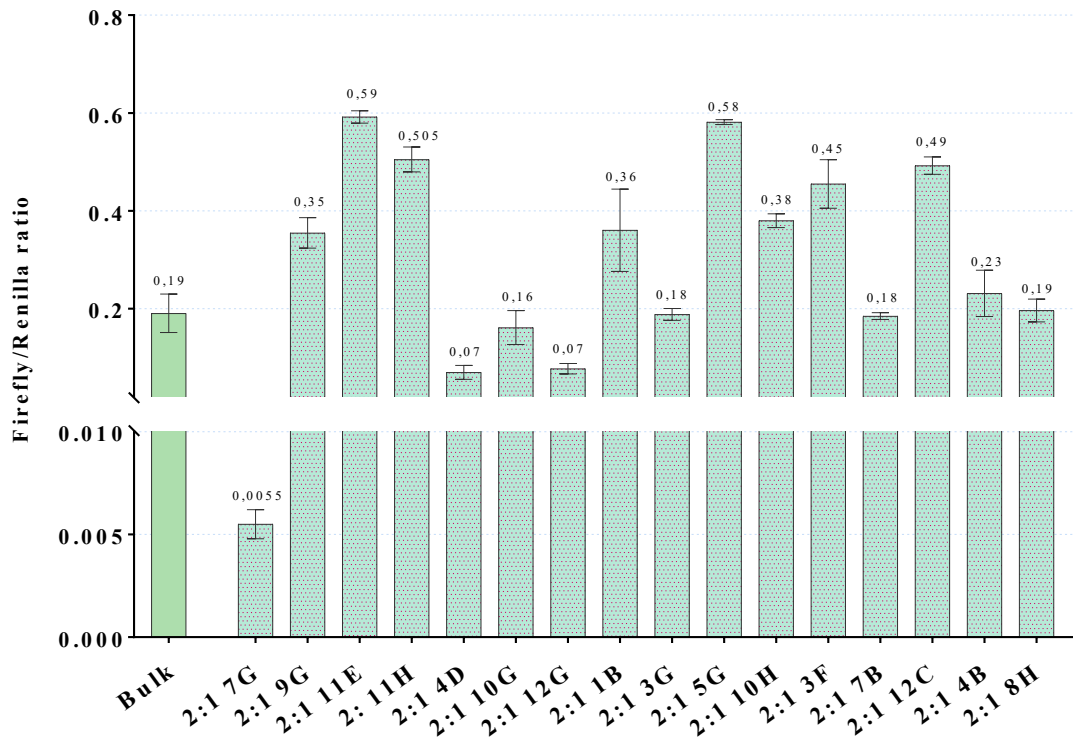
Relative luminescence values



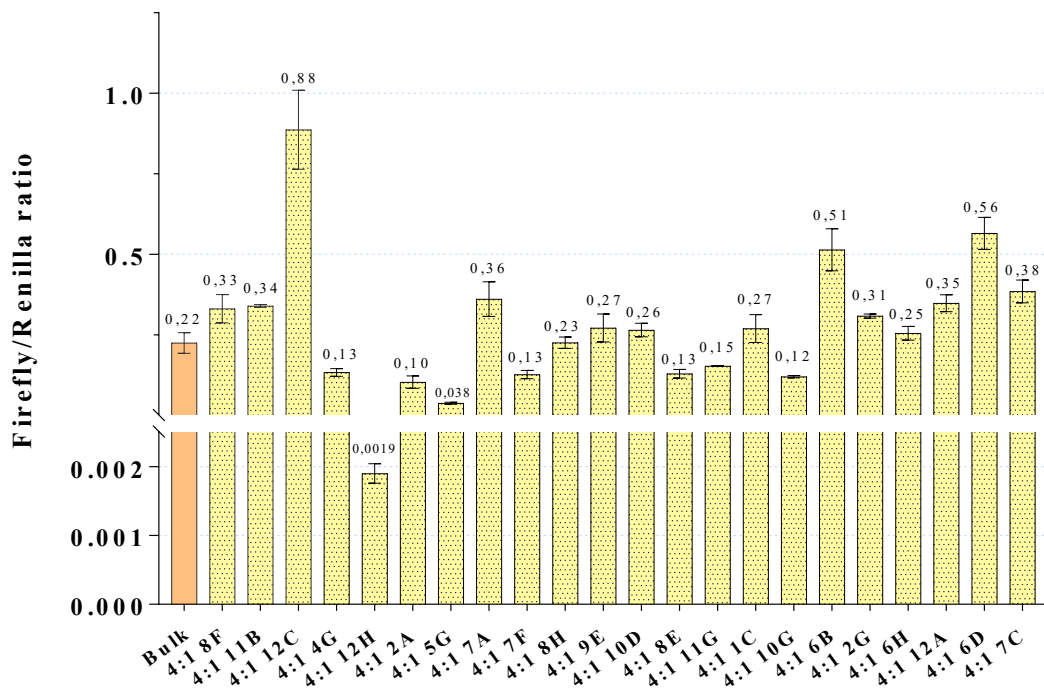
Graphic 1: Relative luminescence values after 24h and after 18 days in the bulk cells.

The vector has the neomycin resistance sequence, so the cells were selected with the neomycin G-418 solution and we obtained several clones. At the end of selection, bulk cells were diluted to isolate clones. Then we analyzed the reporter gene (Firefly luciferase) both in the bulk and in clones (Graphic 2, Graphic 3). Comparing the bulk values, obtained from the two ratio (transposon : transposase), no significant differences in the Firefly luciferase expression have been identified; the relative luminescence values of the clones were similar between the two ratio 2:1 and 4:1, but the cellular viability was higher in the ratio 4:1, in fact it was easier to obtain a greater number of clones.

Luciferase assay: HeLa clones (2:1)

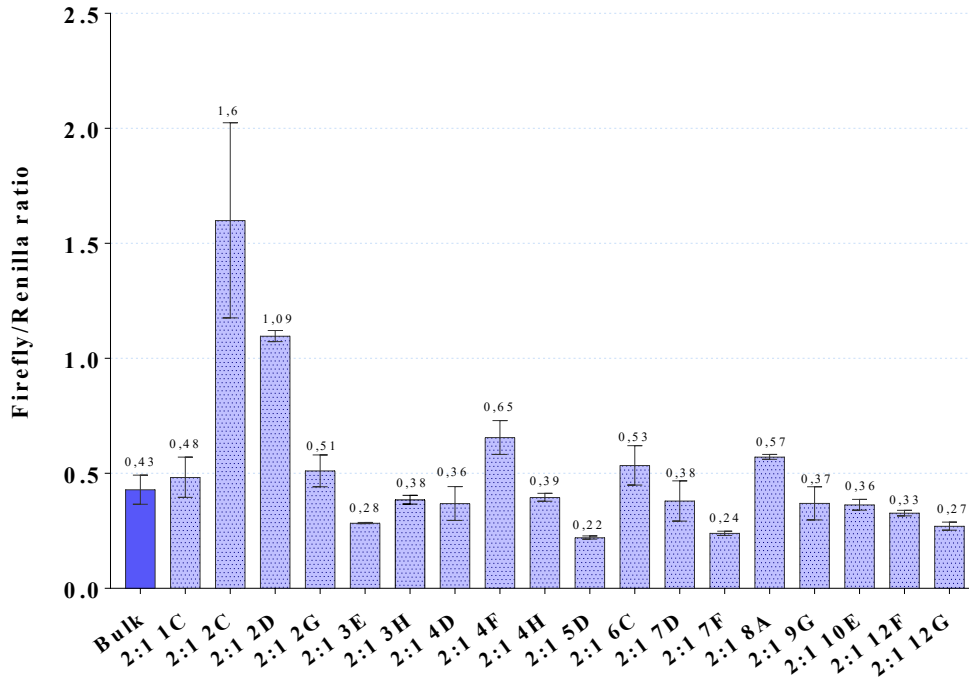


Luciferase assay: HeLa clones (4:1)

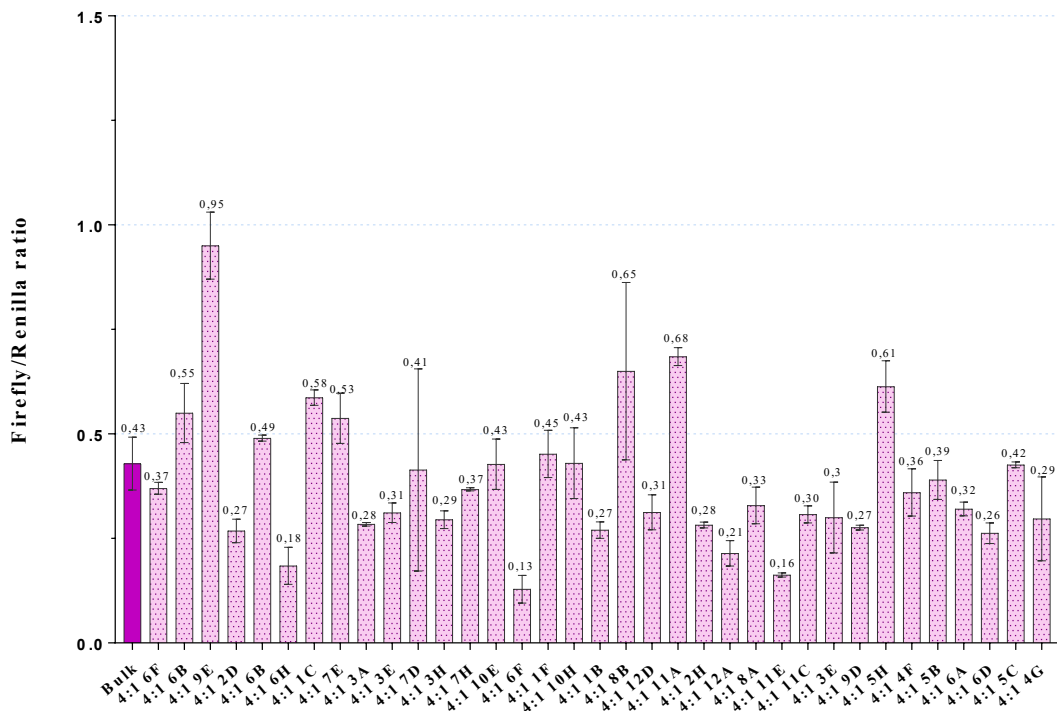


Graphic 2: Relative Luminescence values in HeLa bulks and clones. Top: transfection with transposon and transposase in 2:1 ratio. Bottom: transfection with transposon and transposase in 4:1 ratio.

Luciferase assay: CHO clones (2:1)



Luciferase assay: CHO (4:1)



Graphic 3: Relative Luminescence values in CHO bulks and clones. Top: transfection with transposon and transposase in 2:1 ratio; Bottom: transfection with transposon and transposase in 4:1 ratio.

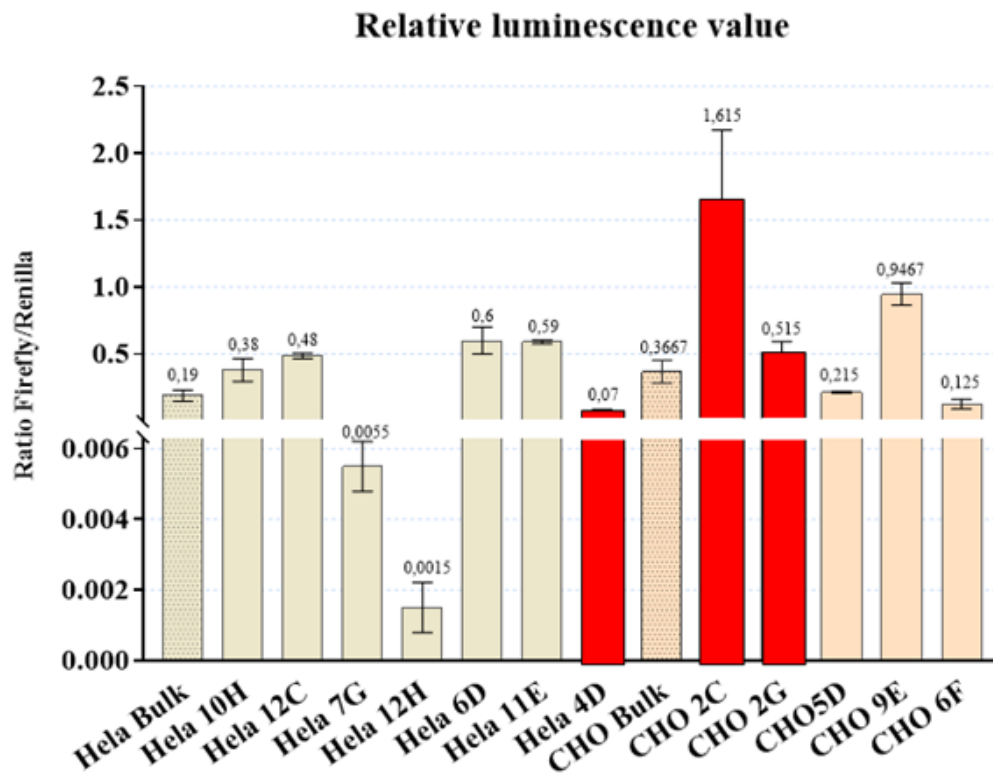
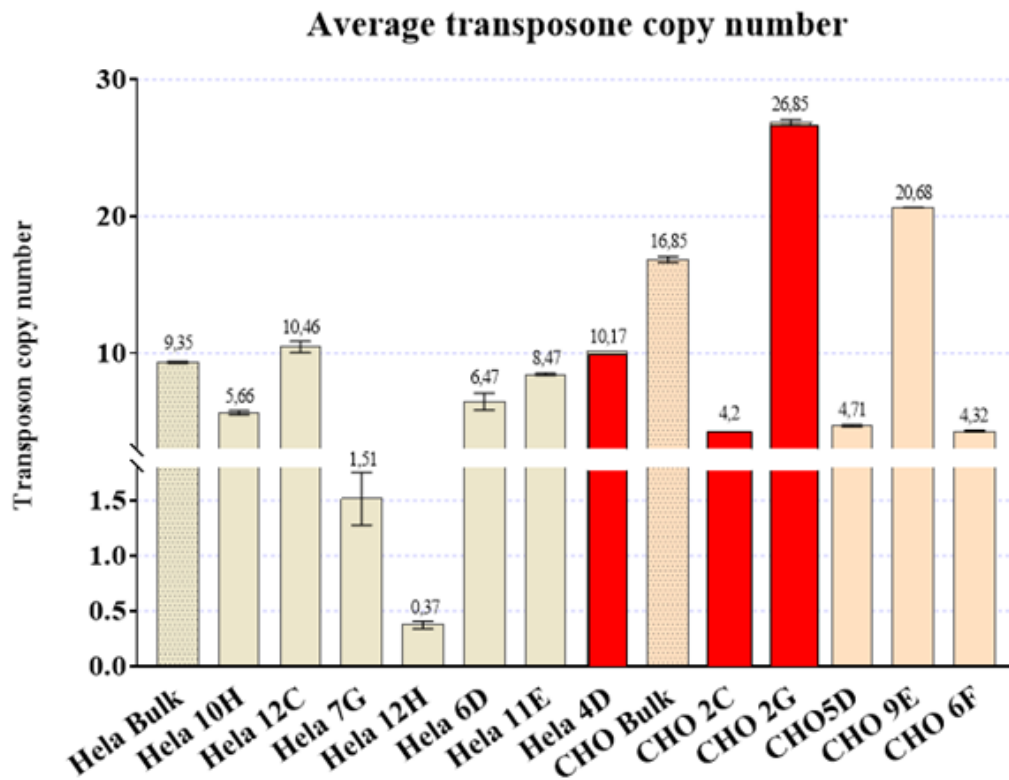
Data suggest that the transgene expression is lasting in time. Comparing the two cell lines it is clear there is a variability, maybe due by the cellular molecules involved on the transposition mechanism. Moreover among the same cell line there is a difference between the clones, in particular some clones had a very high luciferase expression, such as the HeLa 12C clone (0.88) and CHO 2C (1.6), while others had very low expression values, for example HeLa 12H clone (0.0019) and CHO 6F clone (0.13). As it will be demonstrate in the following chapter, the transgene expression is not always correlated with the transposon copy number.

5.1.3 Absolute Quantitative Real time PCR

The absolute quantitative real time PCR was set up to establish the average transposon copy number in bulk and clone cells after the neomycin selection.

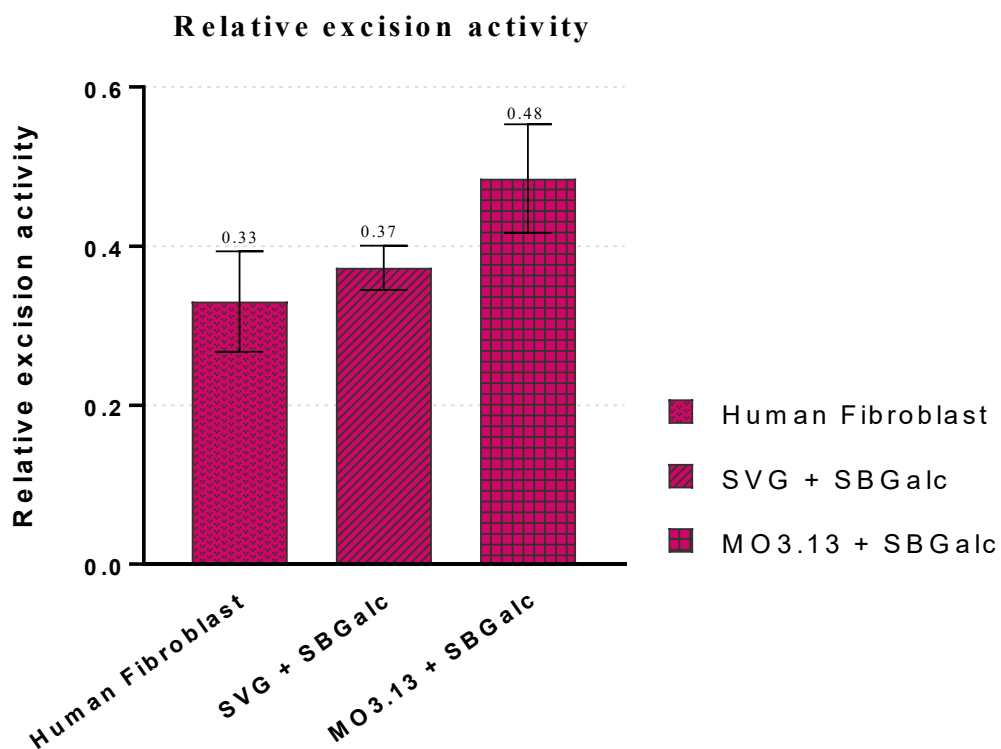
We performed the calibration curve with the serial dilutions of the transposon plasmid using the primers which anneal on the right consensus sequence of transposase (IRDR_R). Another calibration curve was carried out using the dilutions of the plasmid containing the β -Globin sequence that allowed to normalize the data. The first calibration curve of transposon shows an efficiency of 100% and a regression of 0.999. The β -Globin standard curve shows an efficiency of 99,6% and a regression of 0.995.

First of all we tested the DNA extracted from the bulk and three different clones of the HeLa and CHO cell lines. We have chosen the clones with high, mean and low value of Firefly luciferase luminescence in order to establish if there was a correlation between luminescence values and the transposon copy number. The Graphic 4 (Top) shows the transposon copy number in HeLa and CHO cell lines, and it is cleared that the CHO clones had a higher copy number of transgene integrated into the cellular genome, in particular the highest is the CHO 2G clone with approximately 26 copies. Data shows that there is a correlation between integrated copy numbers and relative luminescence values (Graphic 4) for the majority of the samples, except for the three samples colour in red where other elements should play a significant role in the reporter gene expression such as the integration site.



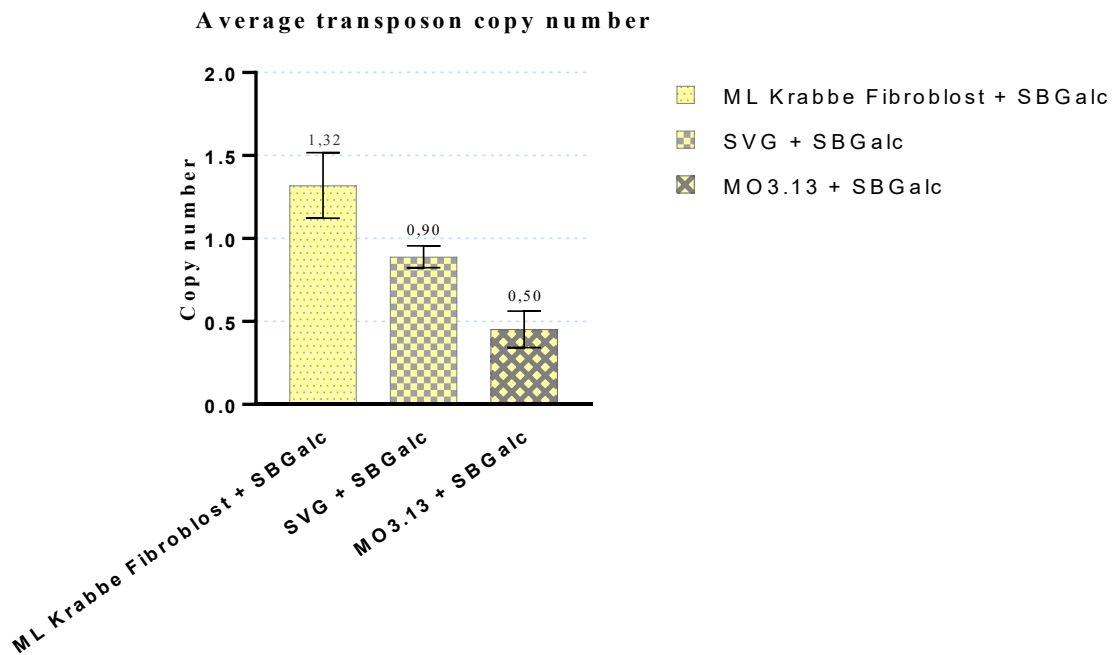
Graphic 4: Top: Transposon copy number in HeLa (grey) and CHO (pink) bulk and clones. Bottom: Relative luminescence values in HeLa (grey) and CHO (pink) bulk and clones.

To determine the efficiency of the “cut and paste” activity of transposase we set up an absolute real time PCR quantification (qPCR) to amplify a plasmid region located both in the episomal plasmids and in the excision circular plasmids (called PCR_2). Another absolute qPCR was performed to amplify the only episomal plasmids (called PCR_4). The efficiency of both reactions were of 98% and a regression of 0.999. Normalizing the data with the β -Globin amplification we measured the copy number of the total amount of plasmids inside the cells (PCR_2) and the copy number of the only episomal plasmids (PCR_4) and with a subtraction we calculated the copy number of the circle excision plasmid. In Graphic 5 is reported the ratio between the excision copy number and the total number of plasmids inside the cells (namely the data took from the PCR2). In this way it was possible to determine the efficiency of transposase activity expressed as percentage of the excision plasmid inside the cell after 48 hours from the transfection, that corresponds to the relative excision activity. Comparing the three cell lines there is no significant differences, even if the highest excision activity is on MO3.13 cell line.



Graphic 5: Relative Excision Activity.

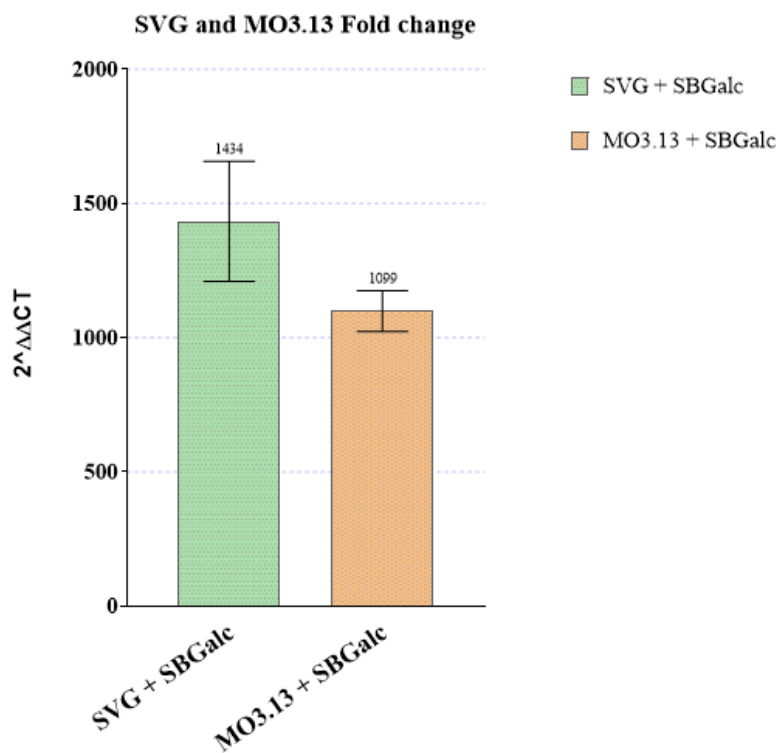
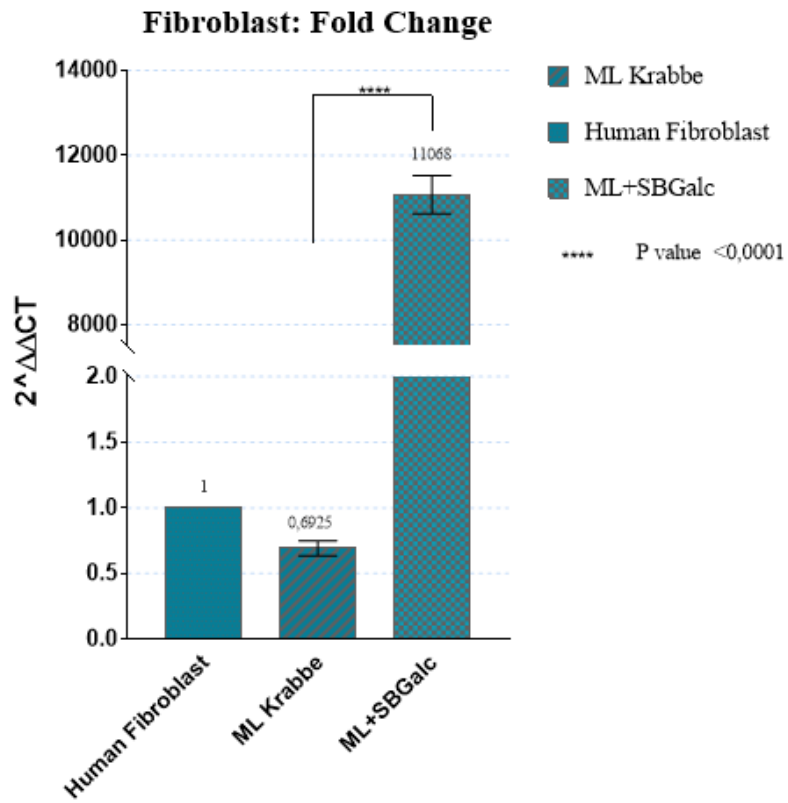
The average transposon copy number was determined in the bulk cells of different cell types (SVG, Krabbe Fibroblast and MO3.13). The data, reported on the Graphic 6, show some differences between the various cell types highlighting that the transposition mechanism is influenced by the cell machinery [165]. On average the transposon copy number is not more than two.



Graphic 6: Average Transposon Copy Number.

5.1.4 Relative quantitative Real Time PCR

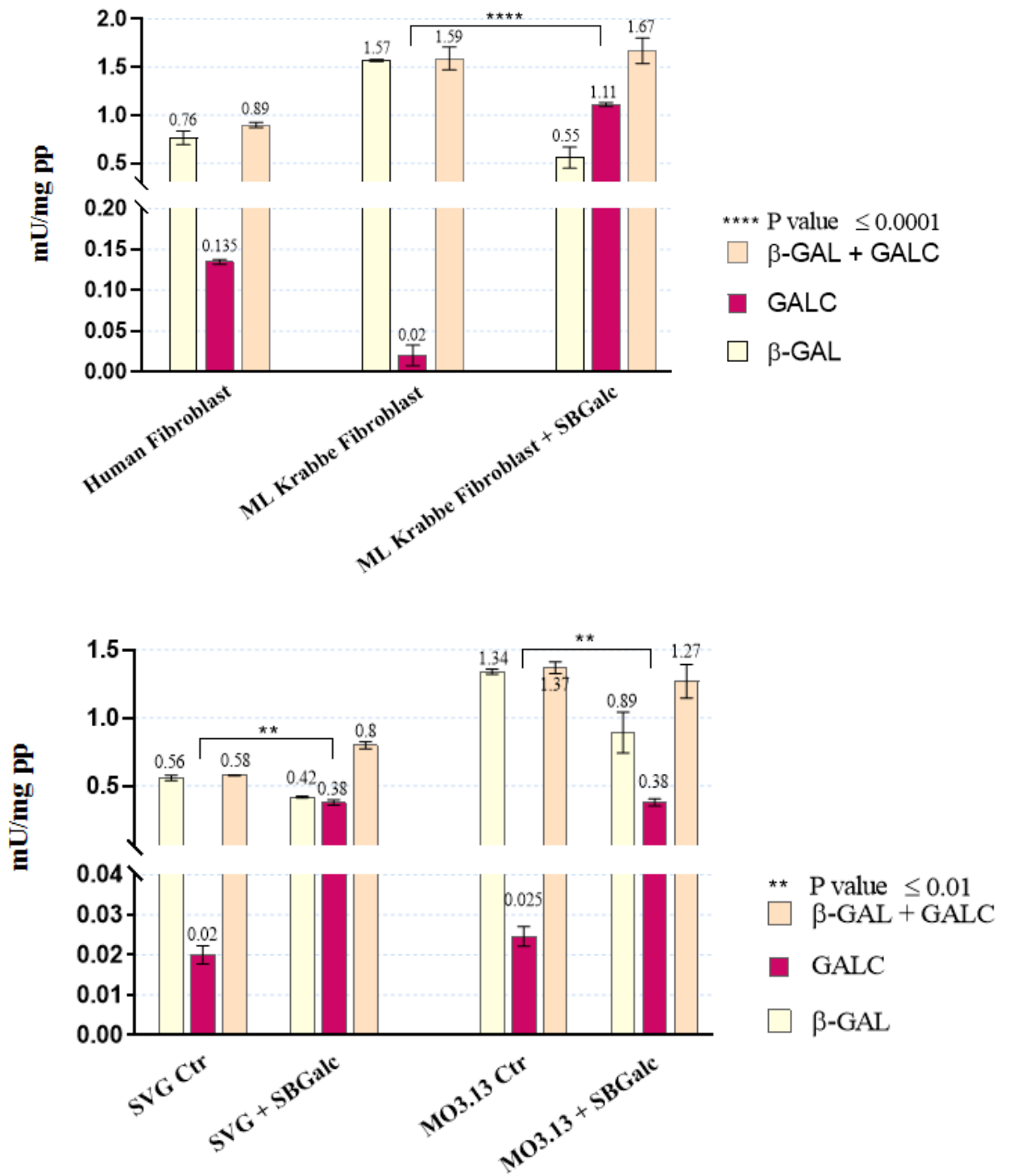
An important aspect essential to determine the *in vitro* gene therapy success, is the relative trans-gene expression. For this reason was performed a relative quantitative Real-Time PCR using a serial dilution of the cDNA of each different bulk cell line. The raw data were analyzed applying the $\Delta\Delta Ct$ method and normalized with the β -Actin gene expression. At the end we obtained the quantity change in the GALC expression (Graphic 7). The treated Krabbe fibroblasts show an highly increase of GALC expression compared to the healthy control; in addition the difference between the same fibroblast before and after the transfection is highly significant with a p-value less than 0.0001. The SVG and MO3.13 cells show an increased expression higher of 1000-fold than untreated same cultures.



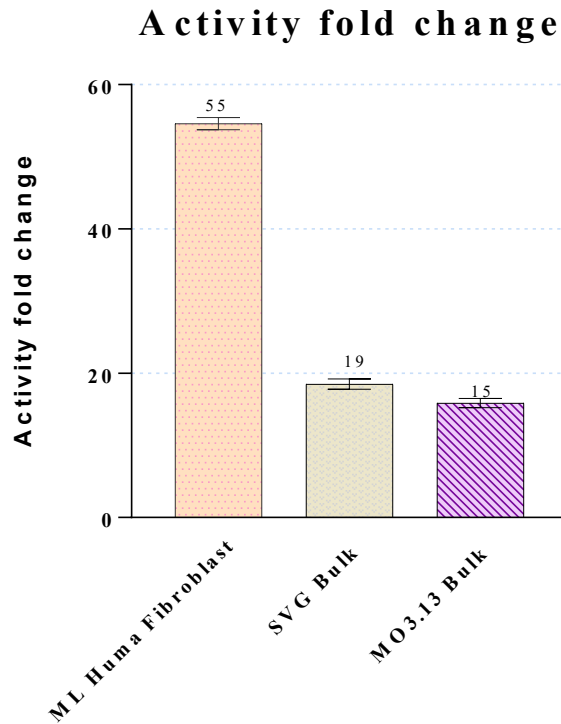
Graphic 7: Relative mRNA amount normalized to the b-actin gene expression.

5.1.5 Enzymatic activity

To evaluate in vitro correction another essential aspect is to determine if translated exogenous protein is active. For this aim we have performed a specific enzymatic assay to measure the GALC activity. The proteins extracted from the bulk cells were used for the enzymatic test and we obtained two graphics that show the activity of the GALC enzyme (Graphic 8). Comparing the GALC activity in Krabbe fibroblasts before and after the transfection with the Sleeping Beauty system, as you would expect, the specific activity increase in the treated fibroblasts; in fact a p-value less than 0.0001 between treated and a untreated fibroblasts means that the difference has highly significance. While for the SVG and MO3.13 the difference between before and after the transfection has a mildly significance with a p-value less than 0.01. The increase in GALC activity is calculated by the ratio of the specific enzyme activity between the treated cells and the untreated control (Graphic 9).



Graphic 8: Specific enzymatic activity in Bulk cells expressed as nanomoles of substrate hydrolyzed per minute and normalized from milligram of protein.



Graphic 9: Increase in GALC activity.

5.2 Plasmid labeling

In order to follow the plasmid encapsulation preparation, each plasmid was covalently bound with a fluorescent tracker. During the preliminary test we labeled the *pcGlobin2-SB100Xco* with the Label IT tracker TM-Rhodamine kit and the *pT2HB-CAG-mGALC-Ren/neo* with the Label IT Tracker Fluorescein kit.

To evaluate the covalent binding, the plasmids were run in an agarose gel (1%) without ethidium bromide staining. The nucleic acid appeared faint under UV illumination because the transilluminator emits at approximately 300 nm, which is not optimal for the fluorescent labels. Later the gel was stained with ethidium bromide to detect a potential gel shift related to unlabeled nucleic acids. Here, Figure 20 reports the example of the plasmid labeled with the Fluorescein tracker. Figure A shows the agarose gel without ethidium bromide staining, while the figure B shows the same gel stained with ethidium bromide; comparing the two gels it is easy to assume that the plasmid is covalently bind with the label.

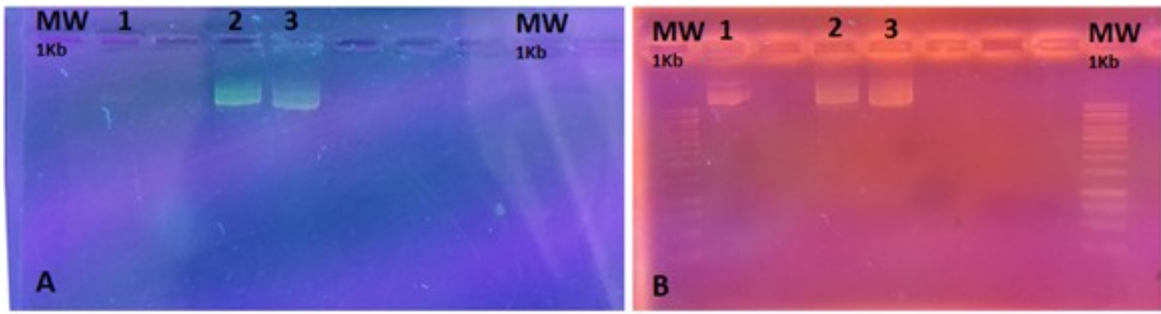


Figure 20: Determination of labeling success. (A) Gel without ethidium bromide. (B) Gel with ethidium bromide staining. 1- plasmid without label; 2 and 3 plasmid labeled with Fluorescein

To verify the presence of labeled DNA *in vitro* the MO3.13 cell line was transfected with 1.5 μg of *pT2HB-CAG-mGALC-Ren/neo* labeled with fluorescein and with 500 ng of *pcGlobin2-SB100Xco* labeled with rhodamine. The fixed cells were analyzed using fluorescent microscopy and the first image showed (Figure 21) the cells transfected with the transposon labeled with fluorescein (green), while the second (Figure 22) is showing the cells with the transposase labeled with rhodamine (red). In blue are displaying the nucleus (DAPI) and the cell membrane (Alexa Fluor 350 WGA).

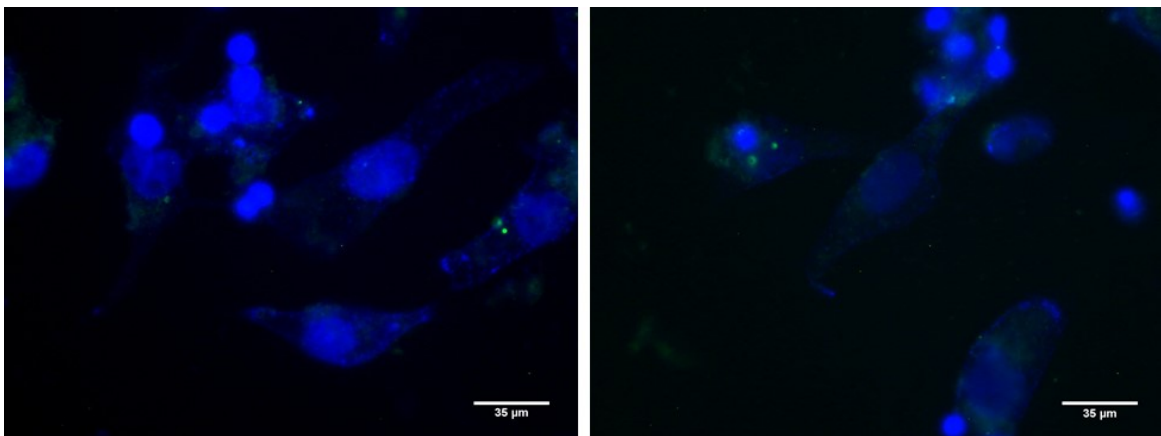


Figure 21: MO3.13 transfected with *pT2HB-CAG-mGALC-Ren/neo* labeled with fluorescein (green), stained with Alexa Fluor350 WGA (membrane, blue) and DAPI(nucleus, blue). Scale Bar indicates 35 μm .

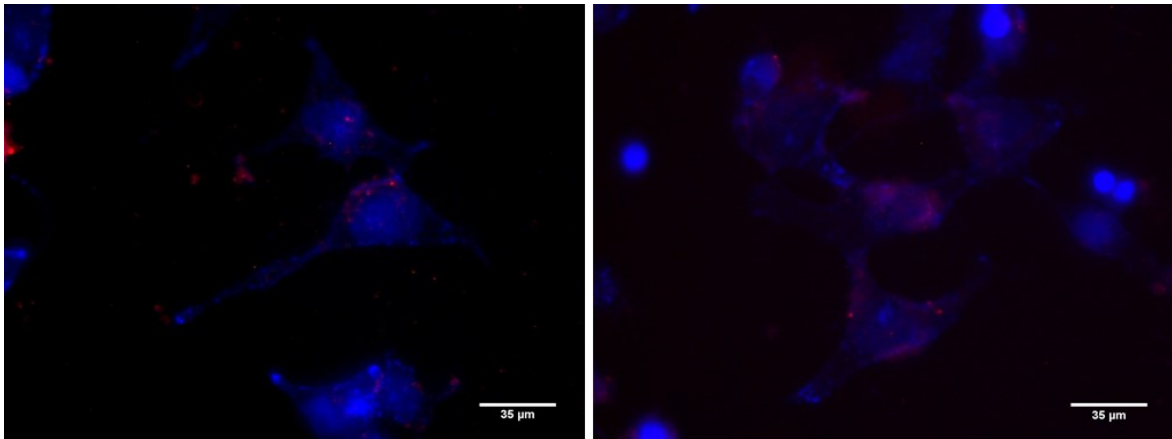


Figure 22: MO3.13 transfected with *pcGlobin2-SB100Xco* labeled with rhodamine (red), stained with Alexa Fluor350 WGA (membrane, blue) and DAPI (nucleus, blue). Scale Bar indicates 35 μ m.

Analyzing these figures, the labeled plasmids have been uptaken by cells and it is possible to follow up their pathway into the cytoplasm. In fact the majority amount of the fluorescence was visible mainly inside the cytoplasm or around the nucleus membrane.

5.3 g7 opioid peptide bound to PLGA nanoparticles

Given that the aim is to transport the two plasmids across the Blood Brain Barrier, it was decided to establish the ability of the g7 peptide, bound to PLGA NPs, to get inside the mice brain. Unfortunately PLGA NPs are not suitable to encapsulate nucleic acids, maybe due to the inability of the hydrophobic PLGA to entrap hydrophilic DNA. PLGA NPs could be chemically modified to make them able to encapsulate nucleic acids, but these modifications change the physical-chemical properties, such as the dimension, the charge, the cellular toxicity and the cellular up-take.

5.3.1 g7-PLGA nanoparticles preparation and characterization

Both g7-NPs and DY-g7-NPS were characterized in their chemical, physical, and morphological features. The mean size of these NPs was close to 200 nm, the surface charge (z-p) was negative in all samples ($-20/25$ mV) with homogeneous distribution (PDI values lower than 0.04). The SEM analysis showed the spherical shape of the NPs (Figure 23). These results clearly indicate that the modification with the g7 and DY did not affect the integrity and the superficial features of the NPs.

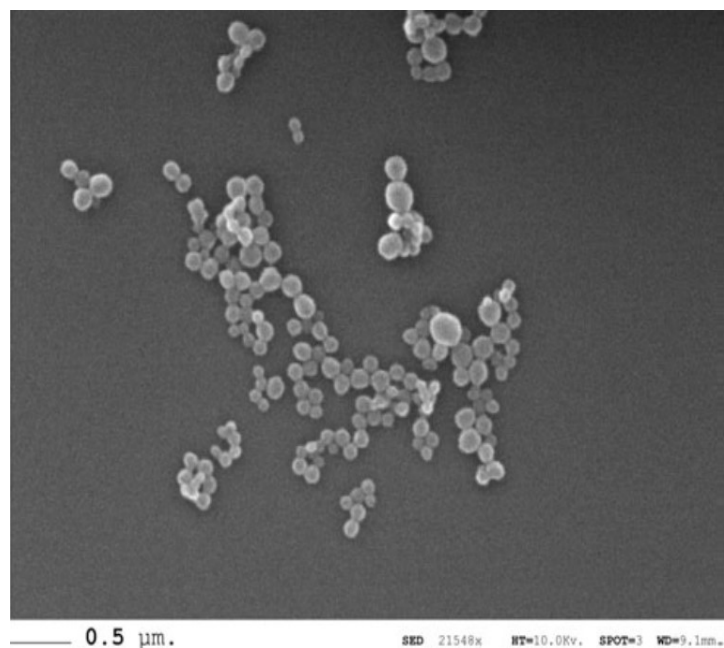


Figure 23: SEM image of DDY-g7-NPs. Scale Bar indicates 0.5μm.

5.3.2 *In vivo* Imaging

The *in vivo* imaging allowed us to detect the bio-distribution of DYg7-NPs in a bulb/C mouse after injection. The targeting of the probe to the brain area was monitored at different time intervals post-injection and normalized. We obtain overlapping images (Figure 24): the real image of the mouse that is viewed by the camera and the fluorescence image shown in a pseudo-colour scale representing the fluorescence intensity.

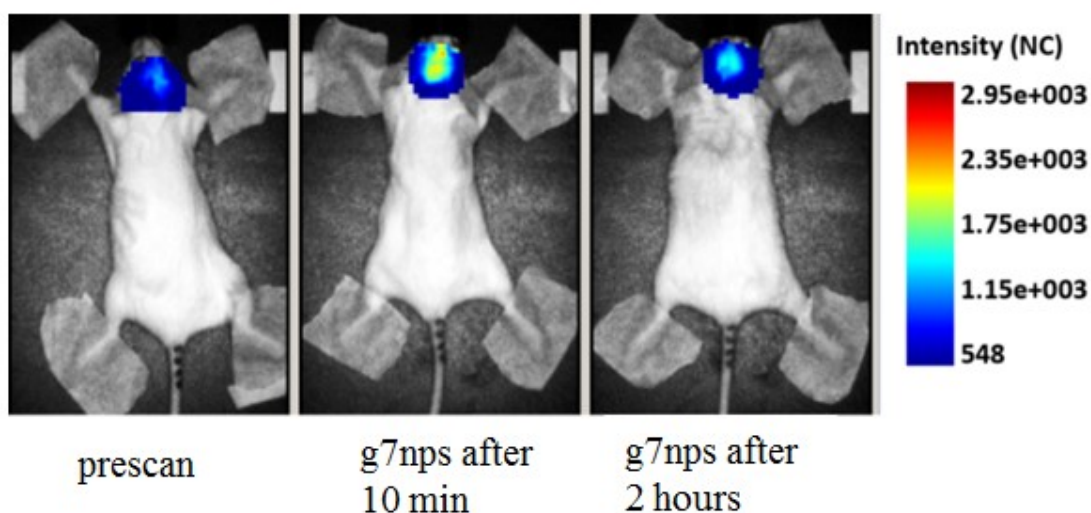
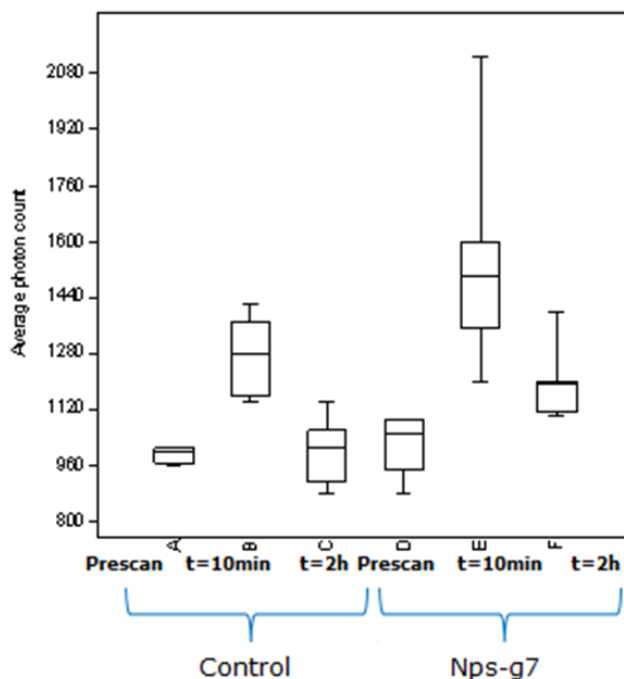


Figure 24: Overlapping image the real image of the mouse that is viewed by the camera and the fluorescence image shown in a pseudo-colour scale representing the fluorescence intensity.

The prescan and after two hours fluorescence values in the control group are overlapping, in fact the p-value is 0.8, while the second group fluorescence values in the prescan and after two hours are significantly different (p value of 0.02) with a fluorescent increment of 12% (Graphic 10).



Graphic 10: Average photon count. A- prescan of the control group; B- control group after 10 minutes from the injection of PLGA NPs without g7; C- control group after 22 hours from the injection of the PLGA NPs without g7; D- prescan of the treated group; E- fluorescence value after 10 minutes from the injection of PLGA NPs with g7; F- fluorescence value after 2 hours from the injection of PLGA NPs with g7.

5.4 Chitosan nanoplexes and Chitosan/TPP-hyaluronic acid nanoparticles

Chitosan polysaccharide has been chosen due to its ability to cross the cell membranes. This biodegradable and biocompatible polysaccharide is able to form nanoplexes with the plasmid DNA due to its cationic feature. As first experiments the simply chitosan nanoplexes were used to understand its ability to entrap the plasmid-DNA and its cellular up-take. Then, established the potential of chitosan as a good approach for the gene therapy, chitosan/TPP-hyaluronic acid nanoparticles were prepared in order to obtain more stable carrier with a higher up-take efficiency. Because of the enormous dimension of the

two plasmids, we started to evaluate the ability to entrap inside the chitosan matrix the smallest *pcGlobin2-SB100Xco* plasmid that is about 7000 bp.

5.4.1 Preparation of chitosan/plasmid DNA nanoplexes

Different preparations were obtained mixing the fixed amount of vectors with different concentrations of chitosan (Table 4).

Preparation name	Vector name	µg of DNA	µg of Chitosan	Ratio Chitosan/DNA
A 1	pT2HB-CAG-mGALC-Ren/neo	38	7,6	1:5
A 2	pT2HB-CAG-mGALC-Ren/neo	38	38	1:1
A 3	pT2HB-CAG-mGALC-Ren/neo	38	190	5:1
B 1	pcGlobin2-SB100Xco	61	12,2	1:5
B 2	pcGlobin2-SB100Xco	61	61	1:1
B 3	pcGlobin2-SB100Xco	61	305	5:1
C 1	pT2HB-CAG-mGALC-Ren/neo+Rhodamine	5	1	1:5
C 2	pT2HB-CAG-mGALC-Ren/neo+Rhodamine	5	5	1:1
C 3	pT2HB-CAG-mGALC-Ren/neo+Rhodamine	5	25	5:1
D 1	pcGlobin2-SB100Xco+Fluoresceine	5	1	1:5
D 2	pcGlobin2-SB100Xco+Fluoresceine	5	5	1:1
D 3	pcGlobin2-SB100Xco+Fluoresceine	5	25	5:1

Table 4: Chitosan preparations.

5.4.2 Gel retardation assay of the chitosan nanoplexes

The agarose gel electrophoresis was used to study the plasmid retardation caused by the polysaccharide. The Figure 25 shows that the migration of the nanoplexes is delayed in respect with the increasing amount of chitosan, so in the less negatively charged complexes. Comparing to the control naked plasmid, chitosan binding causes retarded mobility of the plasmid; in fact nanoplexes forming full complexation were retained within the well. In Figure 26 is shown the gel retardation assay after two weeks of storing at -20°C, and the results demonstrate that the retardation is lightly maintained except for the sample D2 where the plasmid is released.

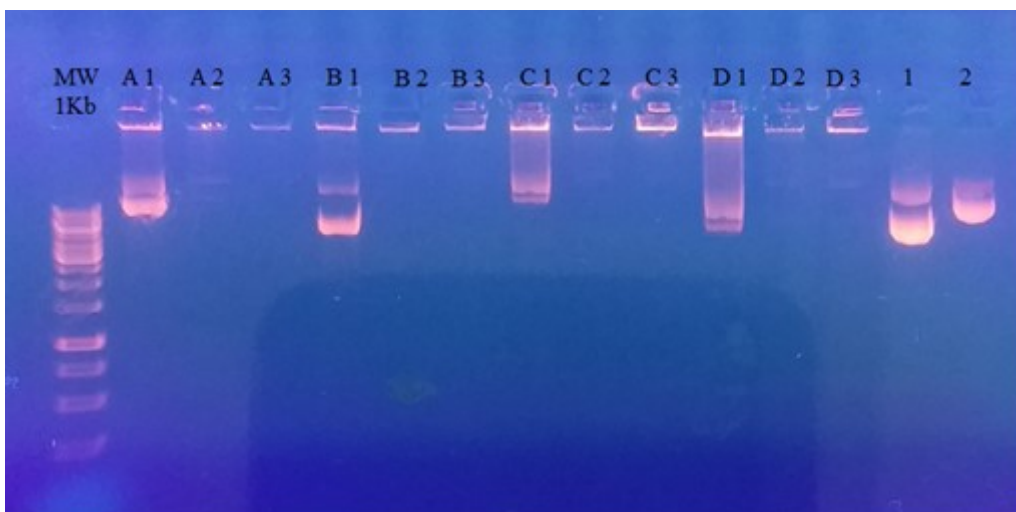


Figure 25: agarose gel electrophoresis retardation assay of the chitosan-plasmid DNA at different chitosan/plasmid ratio. 1- naked plasmid of pT2HB-CAG-mGALC-Ren/neo; 2- naked plasmid of pcGlobin2-SB100Xco.

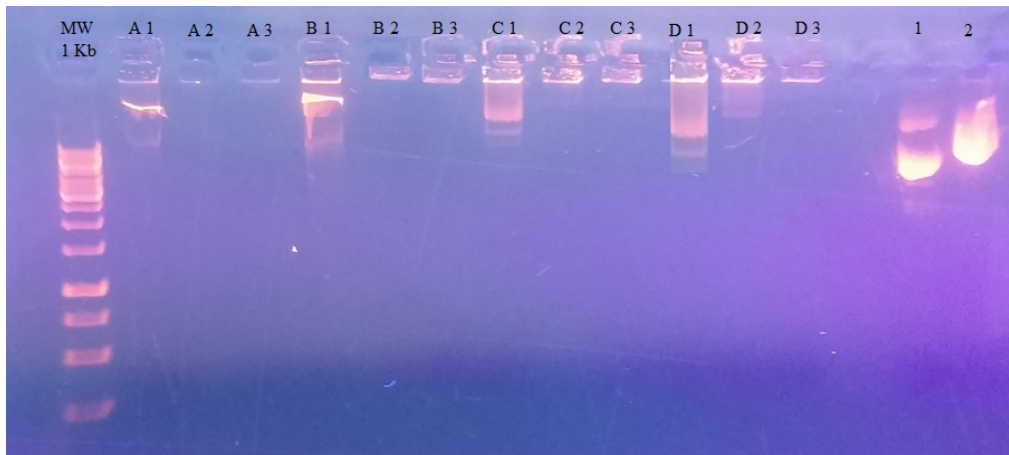


Figure 26: agarose gel electrophoresis retardation assay of the chitosan-plasmid DNA at different chitosan/plasmid ratio after 13 days of storing at -20 °C. 1- naked plasmid of pT2HB-CAG-mGALC-Ren/neo; 2- naked plasmid of pcGlobin2-SB100Xco.

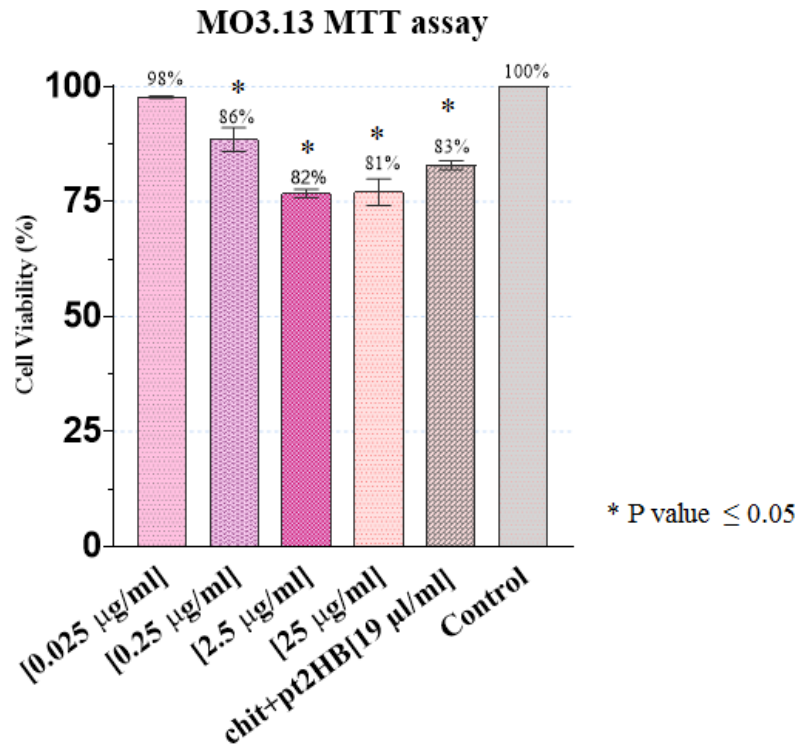
5.4.3 Cell viability of the chitosan nanoplexes

1.2x10⁴ MO3.13 cells were plated on 96-well plate 24 hours before the viability assay. At 70% of confluence the cells were incubated for 2 hours with several concentrations of chitosan preparation (for the test were used the preparations CHIT2, CHIT3, CHIT4 that are made of only chitosan and A1, that is one of the nanoplex). After the incubation time has been performed the MTT assay (see above). Data were collected in triplicate.

The cell viability was calculated using the following formula:

$$\text{Cell viability (\%)} = \left(\frac{\text{Abs sample}}{\text{Abs control}} \right) \times 100$$

The Graphic 11 shows the percentage of cellular viability after 4 hours of incubation with the MTT reagent. Clearly to an increase of chitosan concentration corresponds the decrease of cell viability, even if with a low significance p-value.



Graphic 11: Cell toxicity of chitosan and chitosan-plasmid DNA nanoplex on MO3.13 cell line. The data are represented as the mean ± standard deviation and were analyzed with the Student's t-test.

5.4.4 Cellular uptake of the chitosan nanoplexes

The cellular uptake of the different chitosan preparations was performed using the MO3.13 cell line after two and six hours of incubation. Looking at the different preparations it was clear that the increasing amount of chitosan promotes the cellular uptake. Comparing the preparation C3+D3 incubated for 2 hours and the same preparation incubated for six hours, it was noticeable that after six hours more number of cells showed a co-presence of the two plasmids. The Figure 27 shows a single cell, that after two hours of incubation time, has inside itself the both plasmids, while in Figure 28 are showing two examples of cells where there is co-localization of the two different fluorescent signal, in detail green and red dye that might be inside the nucleus and in the cytoplasm.

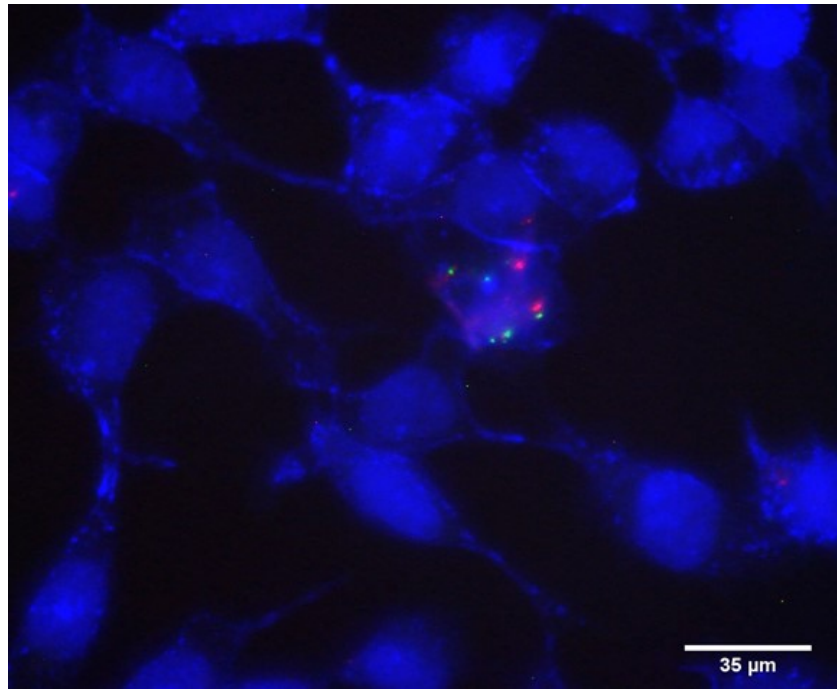


Figure 27: C3+D3: incubation of two hours: MO3.13 cell line treated with the two preparation of chitosan/plasmid DNA. In blue are the nucleus (DAPI) and the cellular membrane (Alexa350), in green *pcGlobin2-SB100Xco plasmid* and in red the *pT2HB-CAG-mGALC-Ren/neo*. Scale Bar indicates 35 μm .

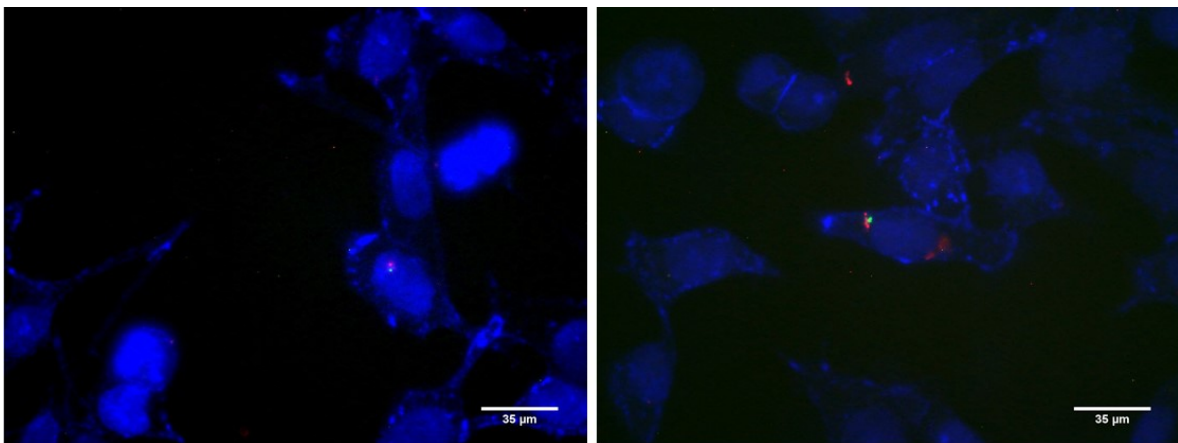


Figure 28: C3+D3 - incubation of six hours: MO3.13 cell line treated with the two preparation of chitosan/plasmid DNA. In blue are the nucleus (DAPI) and the cellular membrane (Alexa350), in green *pcGlobin2-SB100Xco plasmid* and in red the *pT2HB-CAG-mGALC-Ren/neo*. Scale Bar indicates 35 μm .

5.4.5 *Synthesis and characterization of Chitosan/TPP-hyaluronic acid nanoparticles*

pcGlobin2-SB100Xco-Fluorescein loaded nanoparticles were synthesized by the ionotropic gelation technique in presence of TPP, as described in the methodology section.

Particle size is known to affect the interaction and uptake of a nanomaterial at the cellular level. As shown in Figure 29, the size distribution of synthesized nanoparticle was found below 120.1 ± 11.2 nm with a narrow distribution. Determination of zeta potential was carried out to understand the charges as well as particle stability. Zeta potential for *pcGlobin2-SB100Xco*-Fluorescein loaded nanoparticles was found to be 29.7 ± 3.9 mV (Figure 30). Moreover, the encapsulation efficiency of synthesized nanoparticles was 42.3 ± 2.7 %. The nanoparticles formulated exhibit a strong positive charge on their surface, an important feature that not only influences particle–cell membrane interactions but also particle colloidal stability.

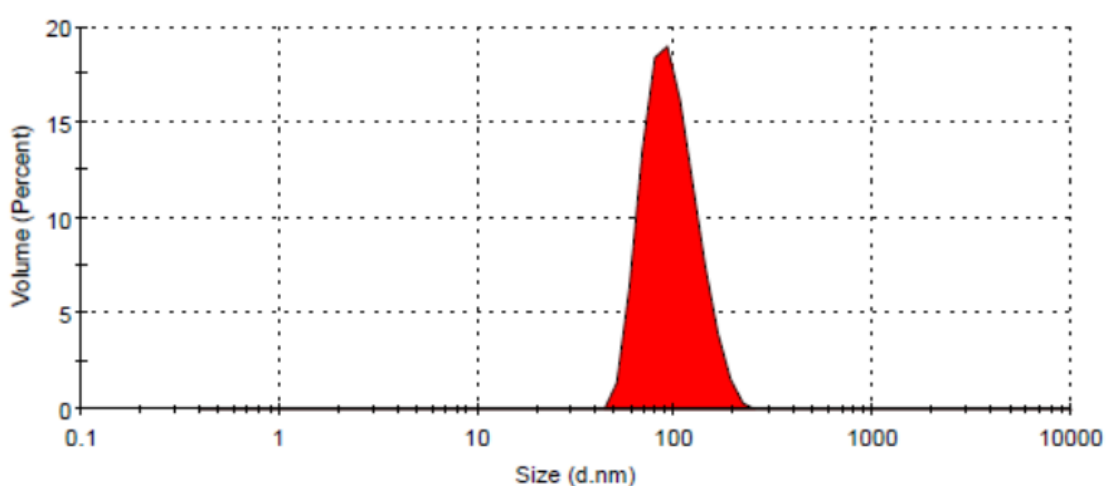


Figure 29: Size distribution of *pcGlobin2-SB100Xco*+Fluorescein loaded nanoparticles (transposase/NPs).

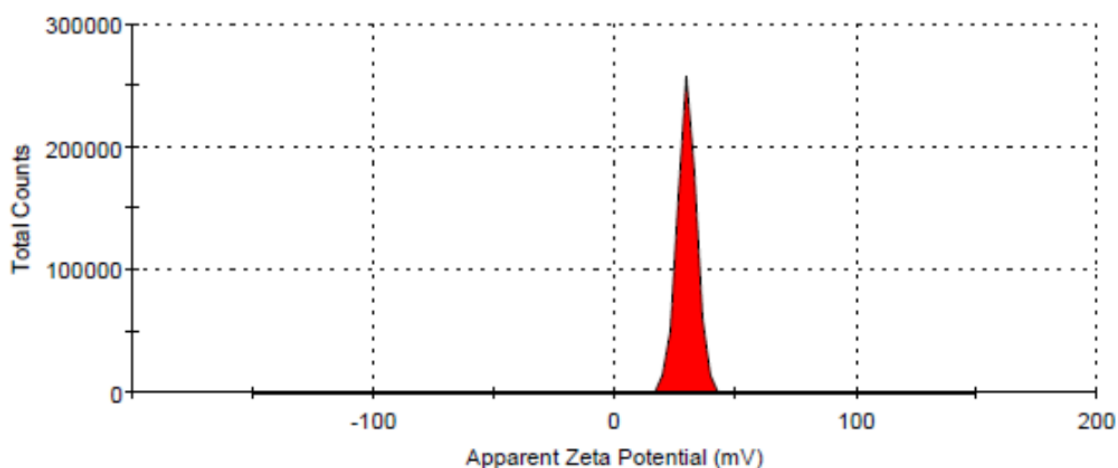


Figure 30: Surface charges of *pcGlobin2-SB100Xco* + Fluorescein loaded nanoparticles as determined by zeta potential.

5.4.6 Cellular uptake of the chitosan/TPP-hyaluronic acid nanoparticles

The cellular uptake of the different chitosan preparations was performed using the A172 cell line after 30 minutes, one hour and two hours and six hours of incubation. The incubation time influence the nanoparticles uptake; in Figure 31 are reported the cellular uptake after two hours of incubation with the *pcGlobin2-SB100Xco+* Fluorescein, in detail the blue colour indicates cellular nucleus (DAPI staining) and the green colour indicates the fluorescence due to the labelled plasmid inside the cells.

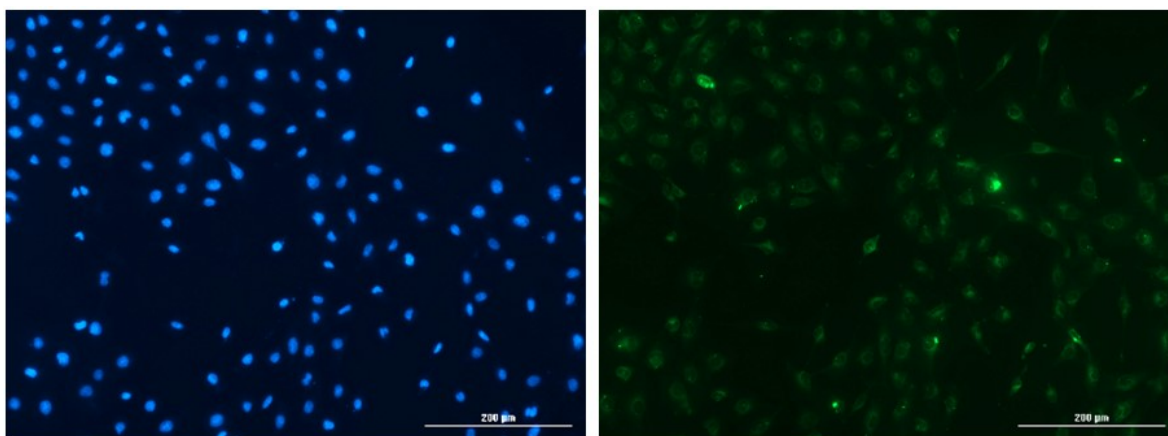
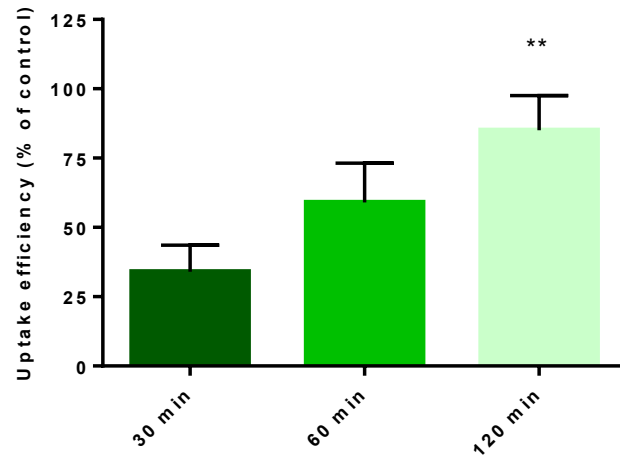


Figure 31: *pcGlobin2-SB100Xco+* Fluorescein/NPs uptake in A172 cells. Left: cells with DAPI staining. Right: green fluorescence. Scale Bar indicates 200 μm .

The relevance of incubation time in nanoparticles uptake was demonstrated measuring the percentage of nanoparticles uptaken per mg cell protein. As reported in Graphic 12 the uptake was seen as early as at 30 min, which increased gradually with the incubation time especially after two hours the uptake is significant.



Graphic 12: A172 uptake quantification of *pcGlobin2-SB100Xco+ Fluorescein* after 30, 60 and 120 minutes. Mean \pm SD, n=3.

6 Discussion

Krabbe's disease or Globoid cell Leukodystrophy is a fatal autosomal recessive lysosomal storage disorder caused by genetic or abnormalities of galactocerebrosidase gene that cause substrates accumulation in macrophages and neural tissue with a progressive loss of myelin [182]. And although the genetic cause of this disease was discovered many years ago, there is still no treatment. Currently the standard of care is the hematopoietic stem cell transplantation, even if it is effective only for slowly disease progression and only when initiated prior to symptom onset. Recently it has been considered more useful in clinical using a multimodality therapies. In recent years the gene therapy has been considered the most interesting approach to correct the GALC deficiency, in particular the virus-mediated (AAV) method is the widely used. Even if a relatively small number of cells can be transduced, this one can overexpress the GALC which can be secreted and correct adjacent cells [202]. In this work we have proposed a non-viral gene therapy approach in order to avoid the side effects caused by the viral methods, such as insertional mutagenesis. This new approach of gene therapy employs a Sleeping Beauty system [5]. It is composed of no viral elements (transposon and transposase) that use a "cut and paste" method that is safer than the viral methods.

Given the involvement of the brain in the Krabbe's Disease, we verify the ability of the synthetic opioid peptide (g7) to convey PLGA NPs inside the CNS [94]. This capability has been confirmed by our *in vivo* experiments. Unfortunately PLGA NPs are not suitable for the DNA binding due to their hydrophobicity. Moreover, one negative aspect of the transposon and the transposase are the plasmids' sizes that make complicated their encapsulation. The PLGA NPs might be modified to make them more suitable for the nucleic acids binding, one of the most used molecule for this aim is the PEI, but this molecule increase the cells toxicity because high-MW PEI destroy membranous structures of cells and organelles, with lysosomal breakdown and mitochondrial damage. Moreover the PEI toxicity effect has negative impact on the cellular up-take [177, 178]. In addition during the preparation processes the DNA is exposed to several shear stress and organic solvents which could inactivate it. Also, most of the time, the nucleic acids are electrostatically bind on the external surface of the NPs causing problems of integrity [179].

In order to encapsulate the plasmids we used chitosan NPs, a cationic polysaccharide. Some *in vitro* experiments have demonstrated the ability of the chitosan to entrap plasmids forming nanoplexes and their ability to enter inside the cells. The issue in using plasmid-chitosan nanoplexes is their low stability in the blood stream, in fact they are usually use for local injection of miRNA to treat cancer [148]. To overcome the stability and poor solubility problems, the chitosan could be used to prepare more stable nanoparticles, such as the chitosan/TPP-hyaluronic acid NPs that we used to entrap the plasmids. From the preliminary *in vitro* experiments we obtained positive results that lead us to believe that chitosan/TPP-hyaluronic acid NPs are good carrier for the nucleic acids targeting. Moreover this type of nanoparticles could be modified in order to achieve the target site as it is reported in several works where the chitosan was modified to direct the carrier to the site of action [180, 212], so it could be linked with the opioid peptide g7 which is able to cross BBB and enter inside CNS.

6.1 Plasmids modifications and *in vitro* transposase efficiency

For the first functional study, we have chosen the vector with the luciferase gene that allows to perform either *in vitro* and *in vivo* experiments, in fact it is possible to measure the luciferase expression in cultured cells and also *in vivo* through the optical imaging technique [164]. Therefore we have required and obtained the Transposon with luciferase gene (*pT2HB-CAG-Luc2*) from Dott. Zsuzsanna Izsvák (Max Delbück Center for Molecular Medicine, Berlin, Germany). To adapt this vector for our study, we modified the transposon inserting the Renilla luciferase and neomycin sequences. The Renilla luciferase bioluminescence has an important role in data normalization process; the ratio between Firefly and Renilla luciferase bioluminescence allows to evaluate the transfection efficiency. In addition, for the *in vitro* analysis, all cells with the transgene integration should be selected; this process it's possible using the neomycin resistance inside the vector sequence. As second modification we amplified the GALC gene from a lentivirus vector and clone it inside the transposon instead of the firefly luciferase sequence. During the cloning process of the transposon we came across some issues related to the identification of enzymatic restriction sites and the length of the cloning fragment. Afterwards, all the interesting elements have been cloned inside the original transposon.

All the interesting sequences have been inserted between the two regions recognized by the transposase (inverted terminal repeat sequences, IR/DR (L) e IR/DR (R)).

During the first part of this study, in order to evaluate the *in vitro* transposase efficiency we obtained and maintained in culture some clones of the two cell lines that we transfected with the two plasmids (the transposon *pT2HB-CAG-Luc2-Ren/neo* and the plasmid that codify for the transposase *pcGlobin-SB100Xco*). We were able to select the clones thanks to the presence of neomycin resistance sequence. First we analyzed the luciferase expression after 24 h in order to establish the best ratio to use between the transposon and the transposase. In accordance with literature, from the data we were able to identify that the cell transfected using the ratio 4:1 had higher level of luciferase expression than the ratio 2:1 (Graphic 1), moreover the cell viability was higher using the ratio 4:1 [213]. Moreover we analyzed the luciferase expression in the two cell lines after 30 days in the selected clones. The data confirm us that the expression is lasting in time, so the sleeping beauty system has an high transposition efficacy. Furthermore, some clones have higher level of luciferase expression than the bulk, indeed the bulk have value that is the average of the clones' values. The Graphic 2 and Graphic 3 report the relative luminescence of some HeLa and CHO clones and they show differences between the two cell lines. Therefore the luciferase expression changes depending on evaluated cell line; this is in accord with literature where is reported that there is a correlation between the transposition efficiency and the cell type [30].

After the expression analyses, we designed the Real-time PCR in order to establish the reporter gene copy number. Progressively, from our data obtained from the bulk and clones' DNA of the two cell lines with high, mean and low luminescence value have established a correlation between luminescence values and the transposon copy number, even if the expression could be influence by several factors.

6.2 Relative excision efficiency

Performing the gene therapy studies using the transposon elements, it is important to establish if the enzymatic element of this system (transposase) is able to work correctly in the model used in the experiments. For this reason some papers set up an approach to determine the excision activity using the absolute quantitative real time using the TaqMan

method [165, 166]. Here we used a different approach based on SyberGreen method and we were able to confirm that there was variation between the different cell line. We found that the major excision activity is in the MO3.13 cell line with an activity approximately of 50%, while the less excision activity is in the primary cell culture of Human Fibroblast with an activity of 33%. This is in accord with literature because during the excision process are involved different cellular machinery, in addition the excision and transposition depends on the size of the transposed element. Moreover the excision activity is not strictly correlated with the copies that are transpose in the cellular genome, and our data confirmed the absence of correlation between the two events (the excision and the transposition) [30].

6.3 Sleeping Beauty system efficacy

Defined that the sleeping beauty system works well in our models and our vectors didn't have any modification that could influence the transposition, we focused on the analysis of the sleeping beauty system efficacy in the cell line that are closing to our final target. We took in exam the SVG cell line (fetal human astrocyte cell line), the human fibroblast and the MO3.13 cell line (human oligodendrocyte cell line). For these cell lines we evaluate the transposon copy number, the mRNA expression and the enzymatic activity after the bulk selection. Referring to the results obtained from the analysis of the cells after the transfection, it was clear a correlation between the transposon copy number, the GALC expression and the enzymatic activity (Graphic 6, Graphic 7, Graphic 8). The transposon copy number is not more than two copies in each cell, this is important when you considered the gene therapy application, because low transgene copy number means a low risk of insertional mutagenesis [30]. Moreover, it is interesting to see the efficacy of this system evaluating the increment on the enzymatic activity (Graphic 9) that is the final goal of the gene therapy, in particular the human Krabbe fibroblasts have an increment of fifty-five fold in GALC activity.

6.4 The ability of g7 opioid peptide to cross the Blood Brain Barrier

The substantial involvement of the Central Nervous System in Krabbe's disease had led us to plan a strategy able to help the NPs to cross the Blood Brain Barrier (BBB). In fact we have evaluated if the synthetic opioid peptide was the right strategy to achieve our goal.

6.4.1 g7 bound to PLGA nanoparticles synthesis and characterization

The characterization of the PLGA NPs features conformed the size, the good homogeneity and the surface charges is compatible with the systemic administration. Moreover the nanoparticles features were not affected by the covalent modification with the g7 peptide.

6.4.2 In vivo imaging

We analyze the bio-distribution of the g7 peptide bound on PLGA-NPs surface, even if this kind of polymer is not suitable to bind and release nucleic acids.

After intravenous injection, the NPs are widely distributed in the animal organs (data not shown), mainly in lungs, liver and spleen. This distribution confirm that the NPs are rapidly up-taken by the reticuloendothelial system (RES) [121, 122].

These data show that the opioid peptide localized inside the central nervous system and also after two hours the fluorescence signal increase of 12% in the mice injected with NPs coated with g7 compared to the mice injected with NPs without g7.

6.5 Chitosan polysaccharide as gene delivery

Chitosan shows several characteristics that makes it suitable as gene delivery system, especially because it is able to form complexes with negatively charged plasmid DNA, RNA, siRNA and miRNA due to its cationic nature [214]. However the chemical modification are required to change its physicochemical and pharmacological properties in order to increase its solubility [215]. At the beginning, it was studied the ability of the simple chitosan nanoplexes to entrap and target the plasmid-DNA inside the cellular model (MO3.13 cell line). So, confirmed the possibility to use this polysaccharide as carrier, it was modified to make it more stable and less toxic. In order to achieve this aim, during the preparation processes was added the crosslinker TPP, which increase the stability of the nanoparticles, and the hyaluronic acid that made this NPs less degradable in blood stream and less toxic [167]. As it is reported in literature, the chitosan/TPP-hyaluronic acid is suitable nanoparticle for the gene therapy because the chitosan is able to create complexes with the negative charges of the DNA. Moreover the chitosan could be functionalized on its surface with molecules in order to target the cargo in a specific site, in particular several

works have already used chitosan nanoparticles functionalized on their surface with antibodies in order to target drugs into solid tumors or into the brain [168, 169]. In fact we want to bind the synthetic opioid peptide (g7) on the chitosan/TPP-hyaluronic acid NPs surface to direct the NPs into the CNS.

6.5.1 Nanoplexes preparation, cellular up-take and cytotoxicity

In this study the nanoplexes formulation has been prepared by simple self-assembled electrostatic complexation by mixing in aqueous solution the low molecular weight chitosan at different ratio of plasmid. The complexation and the stability was controlled evaluating the agarose gel electrophoresis retardation, that demonstrate a relation between the amount of the chitosan and the binding efficiency of the plasmid, in addition this assay highlights that the nanoplexes are quite stable if they are stored in aqueous solution at -20 °C, this is maybe because the high level of DA (87%) make the complex more stable.

In vitro study was performed to control the cellular uptake and the cellular internalization of the nanoplexes. After two and six hours the nanoplexes are taken up, after two hours the internalization was not widely distributed in all cells, in fact only few cells have shown a co-presence of the both plasmid; while after six hours of incubation the fluorescence was widely distributed inside the cells and a major number of cells showed the co-presence of the two fluorescence labels.

Form this preliminary tests, chitosan results to be suitable for biomedical application because it is biocompatible and induce low cytotoxicity [157], in fact our results suggest that cell viability remain high and at higher chitosan concentration the differences with the untreated control is lightly significant.

6.5.2 Chitosan/TPP-hyaluronic acid nanoparticles synthesis and characterization

In agreement with literature, our results confirmed that the ionotropic gelation technique is a good method to obtain chitosan/TPP-hyaluronic acid nanoparticles [175].

One of the most important parameter that influenced the cellular uptake is the nanoparticles size that is also connected with the size of the plasmid. Despite the outstanding dimension of the *pcGlobin2-SB100Xco* plasmid, we were able to entrap it

inside the chitosan/TPP-hyaluronic acid nanoparticles maintaining a small nanoparticles dimension.

During the cellular up-take, another important parameter is the surface charges, especially for the endo-lysosomes escape, in fact recent works claimed that positive charge nanoparticles are able to bind anionic microtubules or molecular motor proteins and move towards the nucleus by the cytoskeletal network [216]. The positive charge of our nanoparticles suggests that they are able to bind the cell membrane and favor the cellular uptake.

Even if the enormous dimension of our plasmids has caused problems in the encapsulation process, we obtained a good encapsulation efficiency of the *pcGlobin2-SB100Xco* plasmid inside the chitosan/TPP hyaluronic acid nanoparticles (42.3 ± 2.7 %).

6.5.3 Chitosan/TPP-hyaluronic acid nanoparticles cellular uptake

In vitro preliminary test has demonstrated that chitosan/TPP hyaluronic acid nanoparticles with the *pcGlobin2-SB100Xco*+Fluorescein are able to enter inside the cells. Of course the uptake increase proportionally with the increasing of incubation time, in fact after one hour the uptake efficiency is more than 50%. Moreover the green fluorescence inside the nucleus demonstrate the ability of the hyaluronic acid to pass the membrane[217]. What is lacking is the evidence that the plasmid is released inside the cells and it is able to produce an active protein.

7 Conclusion

Krabbe's disease is a rare genetic disorder with lack of a definitive and efficient therapy because of the CNS involvement. In fact the big problem is to get to the brain and cross the blood brain barrier, for this reason among the gene therapies the most effective one is the AAV method because the capsid protein shows an high tropism, in particular the serotype AAVrh10 is able to cross the blood brain barrier. The problems related to the use of virus on gene therapy have led us to followed the direction of the non-viral gene therapy, in particular the use of a method called "Sleeping Beauty". The peculiarity of this system is that the transgene is translocated on the cellular genome by a "cut and paste" method that avoid to insert mutations, in addition the fairly random integration guarantees the tendency to integrate inside introns.

During the molecular experiments, we came upon several difficulties during the transposon plasmid modification. The original *pT2HB-CAG-Luc2* (transposon) was modified twice, the first modification was made in order to analyze *in vitro* the reporter gene expression and the second one was made in order to obtain the final plasmid that codified for the cDNA of the GALC gene. Moreover in order to study the efficiency of the Sleeping Beauty System we designed several molecular assays. Two absolute quantitative real time (SyberGreen method) were performed to establish the excision activity after 48 hours from transfection, that allows us to evaluate the efficiency of the transposase in different cell types, and the other one was performed to analyze the transposon copy number to establish the correlation between excision activity, translocation event and gene expression. In order to assay the transgene expression were performed two different analysis, a relative quantitative real time ($\Delta\Delta\text{Ct}$ method) was set up to understand the expression of the GALC mRNA; and a specific enzymatic assay was done to evaluate if there was a real effect at protein level with an increment on the GALC activity. Our data, obtained analyzing different cellular models, show an high efficiency of the SB system and the differences between samples confirmed that every cell types have different molecular mechanisms that interact with the SB system and the transposition mechanism. Moreover we established that the modified transposon (*pT2HB-CAG-mGALC-Ren/neo*) was able to increase the GALC activity in our cellular models.

Because of the main organ involved on Krabbe's disease is the brain and given that the naked plasmid DNA is totally unable to cross the BBB, we tried to target the plasmids through the use of nanoparticles.

To achieve the brain we verify the ability of the g7 peptide to cross the blood brain barrier and our *in vivo* experiments confirmed the ability of the synthetic opioid peptide g7 bound to PLGA NPs to cross the BBB. Unfortunately this type of NPs are not suitable for the encapsulation and release of nucleic acids, for this reason we do not used this polymer as carrier to target our plasmids.

In order to protect the plasmid against degradation we entrapped them inside the matrix of the polysaccharide chitosan. Chitosan is the most widely used polysaccharide for the gene therapy. Our results suggest that the simple chitosan nanoplexes are able to drag plasmid DNA inside the cells, in spite of the big plasmids dimension. Successively more stable chitosan/TPP-hyaluronic acid nanoparticles were prepared to entrap the two plasmids inside the chitosan matrix. Preliminary *in vitro* test suggests that this type of nanoparticles have a big potential as plasmid-DNA delivery.

Next steps will be to encapsulate with an high efficiency the transposon inside the matrix of the chitosan/TPP-hyaluronic acid nanoparticles, overcoming the problems due to its dimension. Then, this nanoparticles will be modified conjugating the synthetic opioid peptide g7. Subsequently, we will study the efficiency of this system *in vitro* evaluating in our cellular model the excision activity, the transposon copy number, the expression and the activity of the recombinant GALC protein. So, if we have good results from the *in vitro* tests, we will evaluate this system in mice model. First, the *in vivo* toxicity and bio-distribution will be studied in control mice (such as Balb/c mice) to understand the injectable amount of nanoparticles and the best way of administration. Then the efficiency of the Sleeping Beauty will be tested *in vivo* using the Twitcher mouse, the animal model of the Krabbe's disease.

8 Acknowledgments

We thank the IRCCS Burlo Garofolo (Trieste) for the laboratory equipment. We thanks the Drs. Zsuzsanna Izsvák (Max Delbück Center for Molecular Medicine, Berlin, Germany), who provide us the “Sleeping Beauty” system. For the Human Oligodendrocytic (Glial) (MO3.13) Cell Line we thank Dr. Marco Cecchini (CNR-Istituto Nanoscienze, Pisa). We are grateful to the University of Modena and Reggio Emilia that provide the PLGA nanoparticles. For the chitosan nanoplexes we thank the Dr Danilo Perin (Protos research Institute, Trieste) and the Institute of Bioscience and BioResources (CNR, Naples) for the chitosan/TPP-hyaluronic acid nanoparticles. For the in vivo experiments we thank the Connecting Bio-research and Industry (CBM, Trieste).

9 Bibliography

1. McClintock, Barbara. Mutable loci in maize: The mechanism of transposition of the Ds Locus. The origin of Ac-controlled mutable loci. Transposition of the Ac locus. The action of Ac on the mutable loci it controls. Mutable loci *c m-2* and *wx m-1*. Conclusions. Carnegie Institution of Washington Year Book; (1949) No. 48 142-154.
2. Lander et al.. Initial sequencing and analysis of the human genome. *Nature*; (2001) 409(6822): 860-921
3. Thomas Wicker, François Sabot, Aurélie Hua-Van, Jeffrey L. Bennetzen, Pierre Capy, Boulos Chalhouh, Andrew Flavell, Philippe Leroy, Michele Morgante, Olivier Panaud, Etienne Paux, Phillip SanMiguel, Alan H. Schulman. A unified classification system for eukaryotic transposable elements. *Nature Reviews Genetics*; (2007) 8, 973-982
4. Georgii P. Georgiev. Mobile genetic elements in animal cells and their biological significance. *Eur. J. Biochem.*; (1984) 145, 203-220
5. Ivics Z., Izsvák S.. Molecular Reconstruction of Sleeping Beauty, a Tc1-like Transposon from Fish, and Its Transposition in Human Cells. *Cell.*; (1997) Vol.91, 501-510.
6. Martín Muñoz-López and José L. García-Pérez. DNA Transposons: Nature and Applications in Genomics. *Current Genomics*; (2010) 11, 115-128
7. J. Arvid Ågren. Evolutionary transitions in individuality: insights from transposable elements. *Trends in Ecology & Evolution*; Volume 29, Issue 2, (2014), 90–96
8. Wilber A, Frandesn JL, Geurts JL, Largaespada DA, Hackett PB, McIvor RS. The Sleeping Beauty transposon system: a non-viral vector for gene therapy. *Mol Ther* 13 (2006) 625-630
9. Zsuzsanna Izsvák, Zoltán Ivics. Sleeping Beauty Transposition: Biology and Applications for Molecular Therapy. *Molecular Therapy*; (2004) Volume 9, Issue 2, February 2004, Pages 147–156

- 10.Lampe, D. J.; Churchill, M. E.; Robertson, H. M.. A purified mariner transposase is sufficient to mediate transposition in vitro. *EMBO J*; (1996) 15(19), 5470-5479
- 11.Miskey, C.; Izsvak, Z.; Plasterk, R. H.; Ivics, Z.. The Frog Prince: a reconstructed transposon from *Rana pipiens* with high transpositional activity in vertebrate cells. *Nucleic Acids Res.*; (2003) 31(23), 6873-6881
- 12.Miskey, C.; Papp, B.; Mates, L.; Sinzelle, L.; Keller, H.; Izsvak, Z.; Ivics, Z.. The ancient mariner sails again: transposition of the human Hsmar1 element by a reconstructed transposase and activities of the SETMAR protein on transposon ends. *Mol. Cell. Biol.*; (2007) 27(12), 4589-4600
- 13.Brillet, B.; Bigot, Y.; Auge-Gouillou, C.. Assembly of the Tc1 and mariner transposition initiation complexes depends on the origins of their transposase DNA binding domains. *Genetica*; (2007) 130(2), 105-120.
- 14.Ivics Z., et al.. Identification of functional domains and evolution of Tc1-like transposable elements. *Proc Natl Acad Sci U S A*; (1996) 93:5008-5013
- 15.Haren I. Ton-Hoang B, Chandler M.. Integrating DNA: transposase and retroviral integrases. *Annu Rev Microbiol*; (1999) 53:245-281
- 16.Claire E Carpentier, Jeffrey M Schreifels, Elena L Aronovich, Daniel F Carlson, Perry B Hackett, Irina V Nesmelova. NMR structural analysis of Sleeping Beauty transposase binding to DNA. *Protein Sci.*; (2014 Jan) 23(1): 23–33. Published online 2013 Oct 30. doi: 10.1002/pro.2386
- 17.Zayed H., Ivics Z.. Development of Hyperactive Sleeping Beauty Transposon Vectors by Mutational Analysis. *Molecular Therapy*; (2003) Vol.9, 292-304.
- 18.Ivics Z., Izsvak Z., et al.. Molecular evolution of a novel hyperactive Sleeping Beauty transposase enables robust stable gene transfer in vertebrates. *Nat Genet*; (2009) 41:753-761
- 19.Izsvák Z, Ivics Z, Hackett PB. Characterization of a Tc1-like transposable element in zebrafish (*Danio rerio*). *Mol Gen Genet*; (1995) 247:312-322

20. Izsvák Z., Khare D, Behlke J, Heinemann U, Plasterk RH, Ivics Z.. Molecular reconstruction of Sleeping Beauty, a Tc1-like transposon from fish, and its transposition in human cells. *Cell*; (2002) 91:501-510
21. Walisko O, Jursch T, Izsvák Z, Ivics Z.. Transposon-host cell interactions in the regulation of Sleeping Beauty transposition , p 109-132. In Volff J-N, Lankenau D-H (ed), *Transposon and the Dynamic Genome*, Springer Berlin Heidelberg; (2008)
22. Suneel A. Narayanavari, Shreevathsa S. Chilkunda, Zoltán Ivics & Zsuzsanna Izsvák. Sleeping Beauty transposition: from biology to applications. *Critical reviews in biochemistry and molecular biology*, (2017) vol. 52, no. 1, 18–44
23. Izsvák Z, Ivics , Plasterk RH. Sleeping Beauty, a wide host-range transposon vector for genetic transformation in vertebrates. *J Mol Biol*; (2000) 302:93-102
24. Ivics Z and Izsvák Z. Sleeping Beauty Transposition. *Microbiol Spectrum*; (2014) 3(2):MDNA3-0042-2014
25. Hackett PB. Integrated DNA vectors for gene therapy. *Mol Ther*; (2007) 15(1): 10-12
26. Bustin M, 1999. Regulation of DNA-dependent activities by the functional motifs of the high-mobility-group chromosomal proteins. *Mol Cell Biol* 19:5237-5246
27. Zayed H, Izsvák Z, Khare D, Heinemann U, Ivics Z. The DNA-bending protein HMGB1 is a cellular cofactor of Sleeping Beauty transposition. *Nucleic Acids Res*;(2003) 31:2313-2322
28. Mizuuchi K. Polynucleotidyl transfer reactions in transpositional DNA recombination. *J Biol Chem*; (1992) 267:21273-21276
29. Izsvák Z, Stuwe EE, Fiedler D, Katzer A, Jeggo PA, Ivics Z. Healing the wounds inflicted by sleeping beauty transposition by double-strand break repair in mammalian somatic cells. *Mol Cell*; (2004) 13:279-290
30. Kolacsek O, et al.. Excision efficiency is not strongly coupled to transgenic rate: cell type-dependent transgenic efficiency of sleeping beauty and piggyback DNA transposons. *Human Gene Therapy Methods*; (2013) 25:241-252

31. Vigdal TJ, Kaufman CD, Izsvack Z, Voytas DF, Ivics Z. Common physical properties of DNA affecting target site selection of sleeping beauty and other Tc1/mariner transposable elements. *J Mol Biol*; (2002) 323:441-452
32. Liu G, Geurts AM, Yae K, Srinivasan AR, Fahrenkrug SC, Largaespada DA, Takeda J, Horie K, Olson WK, Hackett PB. Target-site preferences of sleeping beauty transposons. *J Mol Biol*; (2005) 346:161-173
33. Li X, et al.. A resurrected mammalian hAT transposable element and a closely related insect element are highly active in human cell culture. *Proc Natl Acad Sci U S A*; (2013) 110:E478-487
34. Ivics Z, et al.. Retargeting sleeping beauty transposon insertions by engineered zinc finger DNA-binding domains. *Mol Ther*; (2012) 20:1852-1862
35. Liu G, et al. Target-site preferences of sleeping beauty transposons. *J Mol Biol*; (2005) 346:161-173
36. Wang Y, Wang J, Devaraj A, Singh M, Jimenez Orgaz A, Chen JX, Selbach M, Ivics Z, Izsvak Z. Suicidal autointegration of sleeping beauty and piggyback transposons in eukaryotic cells. *PLoS Genet*; (2014) 10:e1004103
37. Yaa-Jyuhn James Meir, Sareina Chiung-Yuan Wu. Transposon-based Vector Systems for Gene Therapy Clinical Trials: Challenges and Considerations. *Chang Gung Med J.*; (2001) 34(6):565-79
38. Vand Rajabpour F, Raoofian R, Habibi L, Akrami SM, Tabrizi M. Novel trends in Genetics: transposable elements and their application in medicine. *Arch Iran Med*; (2014) 17(10): 702-712
39. Stephen R. Yant, Leonard Meuse, Winnie Chiu, Zoltan Ivics, Zsuzsanna Izsvak, Mark A Kay. Somatic integration and long-term transgene expression in normal and hemophilic mice using a DNA system. *Nature Genetics*; (2000) 25, 35-41
40. Ohlfest JR, Frandsen JL, Fritz S, Lobitz PD, Perkinson SG, Clark KJ, et al. Phenotypic correction and long-term expression of factor VIII in hemophilic mice by

- immunotolerization and nonviral gene transfer using the Sleeping Beauty transposon system. *Blood*; (2005) 105:2691-2698
- 41.Liu L, Mah C, Fletcher BS. Sustained FVIII expression and phenotypic correction of hemophilia A in neonatal mice using and endothelial target sleeping beauty transposon. *Mol Ther*; (2006) 13:1006-1015
- 42.Kren BT, Unger GM, Sjeklocha L, Trossen AA, Korman V, DiethelmOkita BM, et al. Nanocapsule-delivered Sleeping Beauty mediates therapeutic Factor VIII expression in liver sinusoidal endothelial cells of hemophilia A mice. *J Clin Invest.*; (2009) 119: 2086 – 2099
- 43.He CX, Shi D, Wu WJ, Ding YF, Feng DM, Lu B, et al. Insulin expression in livers of diabetic mice mediated by hydrodynamics-based administration. *World J Gastroenterol.*; (2004) 10: 567 – 572.
- 44.Aronovich EL, Bell JB, Belur LR, Gunther R, Koniar B, Erickson DC, et al. Prolonged expression of a lysosomal enzyme in mouse liver after Sleeping Beauty transposon-mediated gene delivery: implications for non-viral gene therapy of mucopolysaccharidoses. *J Gene Med.*; (2007) 9: 403 – 415
- 45.Ohlfest JR, Lobitz PD, Perkinson SG, Largaespada DA. Integration and long-term expression in xenografted human glioblastoma cells using a plasmid-based transposon system. *Mol Ther.*; (2004) 10: 260 – 268.
- 46.Ohlfest JR, Demorest ZL, Motooka Y, Vengco IOh S, Chen E, et al. Combinatorial antiangiogenic gene therapy by nonviral gene transfer using the sleeping beauty transposon causes tumor regression and improves survival in mice bearing intracranial human glioblastoma. *Mol Ther.*; (2005) 12: 778 – 788
- 47.Bao Q, Zhao Y, Niess H, Conrad C, Schwarz B, Jauch KW, et al. Mesenchymal stem cell-based tumor-targeted gene therapy in gastrointestinal cancer. *Stem Cells Dev.*; (2012) 21: 2355 – 2363.

48. Fujiwara M, Kashima TG, Kunita A, Kii I, Komura D, Grigoriadis AE, et al. Stable knockdown of S100A4 suppresses cell migration and metastasis of osteosarcoma. *Tumour Biol.*; (2011) 32: 611 – 622
49. Huang G, Yu L, Cooper LJ, Hollomon M, Huls H, Kleinerman ES. Genetically modified T cells targeting interleukin-11 receptor α -Chain Kill Human Osteosarcoma Cells and Induce the Regression of Established Osteosarcoma Lung Metastases. *Cancer Res.*; (2012) 72: 271 – 281.
50. David A Williams. Sleeping Beauty Vector System Moves Toward Human Trials in the United States. *Molecular therapy*; (2008) vol. 16 (9), 1515-1516
51. Huls, M.H., Figliola, M.J., Dawson, M.J., Olivares, S., Kebriaei, P., Shpall, E.J., Champlin, R.E., Singh, H., Cooper, L.J.N. Clinical Application of Sleeping Beauty and Artificial Antigen Presenting Cells to Genetically Modify T Cells from Peripheral and Umbilical Cord Blood. *J. Vis. Exp.*; (2013) (72), e50070, doi:10.3791/50070
52. Singh H, Figliola MJ, Dawson MJ, Olivares S, Zhang L, et al.. Manufacture of Clinical-Grade CD19-Specific T Cells Stably Expressing Chimeric Antigen Receptor Using Sleeping Beauty System and Artificial Antigen Presenting Cells. *PLoS ONE*; (2013) 8(5): e64138. doi:10.1371/journal.pone.0064138
53. Harjeet Singh, Helen Huls, and Laurence JN Cooper. A new approach to gene therapy using Sleeping Beauty to genetically modify clinical-grade T cells to target CD19. *Immunol Rev.* (2014 January) ; 257(1): 181–190. doi:10.1111/imr.12137
54. Begley DJ. Delivery of therapeutic agents to the central nervous system: the problems and the possibilities. *Pharmacol Ther*; (2004);104:29-45.
55. Pathan, S.A. et al.. CNS drug delivery systems: novel approaches. *Recent Patents on Drug Delivery & Formulation*; (2009) 3(1); 71–89.
56. Abbott NJ, Patabendige AA, Dolman DE, et al. Structure and function of the blood-brain barrier. *Neurobiol Dis*; (2010) 37:13-25.
57. University of Minnesota College of Pharmacy, Duluth: Blood Brain Barrier

58. Tachikawa M, Hosoya K, Ohtsuki S, Terasaki T. A novel relationship between creatine transport at the blood-brain and blood-retinal barriers, creatine biosynthesis, and its use for brain and retinal energy homeostasis. *Subcell Biochem.*; (2007) 46:83-98
59. William M Pardridge. Drug transport across the blood–brain barrier. *Journal of Cerebral Blood Flow & Metabolism* (2012) 32, 1959–1972
60. Y. Chen, G. Dalwadi, H. Benson, Drug delivery across the blood–brain barrier. *Curr. Drug Deliv.* 1 (2004) 361–376
61. Y. Chen, L. Liu. Modern methods for delivery of drugs across the blood–brain barrier. *Advanced Drug Delivery Reviews* 64 (2012) 640–665
62. W.M. Pardridge, J. Eisenberg, J. Yang, Human blood–brain barrier transferrin receptor, *Metabolism* 36 (1987) 892–895
63. L. Frolich, D. Blum-Degen, H.G. Bernstein, S. Engelsberger, J. Humrich, S. Laufer, D. Muschner, A. Thalheimer, A. Turk, S. Hoyer, R. Zochling, K.W. Boissl, K. Jellinger, P. Riederer, Brain insulin and insulin receptors in aging and sporadic Alzheimer's disease, *J. Neural Transm.* 105 (1998) 423–438.
64. B. Dehouck, L. Fenart, M.P. Dehouck, A. Pierce, G. Torpier, R. Cecchelli, A new function for the LDL receptor: transcytosis of LDL across the blood–brain barrier, *J. Cell Biol.* 138 (1997) 877–889.
65. J. Herz, D.K. Strickland, LRP: a multifunctional scavenger and signaling receptor, *J. Clin. Invest.* 108 (2001) 779–784.
66. K. Mishima, S. Higashiyama, Y. Nagashima, Y. Miyagi, A. Tamura, N. Kawahara, N., Taniguchi, A. Asai, Y. Kuchino, T. Kirino, Regional distribution of heparin-binding epidermal growth factor-like growth factor mRNA and protein in adult rat forebrain, *Neurosci. Lett.* 213 (1996) 153–156.
67. P.J. Gaillard, A. Brink, A.G. de Boer, Diphtheria toxin receptor-targeted brain drug delivery, *Int. Congr. Ser.* 1277 (2005) 185–198

68. Allhenn D, Alsadat M, Boushehri S, Lamprecht A. Drug delivery strategies for the treatment of malignant gliomas. *Int J Pharm*; (2012) 436, 299-310
69. Brasnjevic, I. et al.. Delivery of peptide and protein drugs over the blood-brain barrier. *Progress in Neurobiology*; (2009) 87(4), pagg.212–251
70. N.J. Abbott, L. Ronnback, E. Hansson, Astrocyte-endothelial interactions at the blood–brain barrier, *Nat. Rev. Neurosci.* 7; (2006) 41–53.
71. V.H. Tam et al.. Nanomedicine as a non-invasive strategy for drug delivery across the blood brain barrier. *International Journal of pharmaceutics*; (2016) 515, 331-342
72. Tej d. Azad, BA, James pan, Bs, ian d. Connolly, ms, Austin remington, BA, Christy m. wilson, phd, and gerald A. grant, md. Therapeutic strategies to improve drug delivery across the blood-brain barrier. *Neurosurg Focus*; (2015) 38 (3):E9,
73. Rapport SI, Robinson PJ. Tight-junctional modification as the basis of osmotic opening of the blood-brain barrier. *Ann N Y Acad Sci*; (1986) 481:250-267
74. Stockwell J, Abdi N, Lu X, Maheshwari O, Taghibiglou C. Novel central nervous system drug delivery systems. *Chem Biol Drug Des*; (2014) 83,507-520
75. Bellavance M A, Blanchette M, Fortin D. Recent advances in blood-brain barrier disruption as a CNS delivery strategy. *AAPS J*; (2008) 10,166-177
76. Kullervo Hynynen, PhD, Nathan McDannold, BS, Natalia Vykhodtseva, PhD, and Ferenc A. Jolesz, MD Noninvasive MR Imaging–guided Focal Opening of the Blood-Brain Barrier in Rabbits. *RSNA Radiology*; (2000) Volume 220, Issue 3
77. Lisa H. Treat, Nathan McDannold, Natalia Vykhodtseva, Yongzhi Zhang, Karen Tam and Kullervo Hynynen Targeted delivery of doxorubicin to the rat brain at therapeutic levels using MRI-guided focused ultrasound *Int. J. Cancer*: 121, 901–907 (2007)
78. Hao-Li Liu, Ching-Hsiang Fan, Chien-Yu Ting, Chih-Kuang Yeh. Combining Microbubbles and Ultrasound for Drug Delivery to Brain Tumors: Current Progress and Overview. *Theranostics*, (2014) 4(4):432-444. doi:10.7150

79. Cloughesy, Timothy F. MD; Black, Keith L. MD; Gobin, Y. Pierre MD; Farahani, Keyvan PhD; Nelson, Gillian PA; Villablanca, Pablo MD; Kabbinavar, Fairouz MD; Viñeula, Fernando MD; Wortel, Cornelius H. MD, PhD. Intra-arterial Cereport (RMP-7) and Carboplatin: A Dose Escalation Study for Recurrent Malignant Gliomas. *Neurosurgery*; (1999) - Volume 44 - Issue 2 - pp 270-278
80. Frnac I, Lipinski A, Feeney PJ. Experimental and computational approaches to estimate solubility and permeability in drug discovery and development setting. *Adv Drug Deliv Rev*; (2001) 46,3-26
81. Yong-Eun Lee Kooa, G. Ramachandra Reddyb, Mahaveer Bhojanic, Randy Schneiderd, Martin A. Philbertd, Alnawaz Rehemtullac, Brian D. Rosse, Raoul Kopelman. Brain cancer diagnosis and therapy with nanoplatfoms. *Advanced Drug Delivery Reviews*; (2006) Volume 58, Issue 14, Pages 1556–1577
82. Marilena Hadjidemetriou, Zahraa Al-Ahmady, Mariarosa Mazza, Richard F. Collins, Kenneth Dawson, and Kostas Kostarelos. In Vivo Biomolecule Corona around Blood-Circulating, Clinically Used and Antibody-Targeted Lipid Bilayer Nanoscale Vesicles. *ACS Nano*, (2015) 9 (8), pp 8142–8156
83. Joseph D Meyers, Tennyson Doane, Clemens Burda James P Basilion. Nanoparticles for imaging and treating brain cancer. *Nanomedicine*; (2013) Vol. 8, No. 1, Pages 123-143
84. Zhao M, Chang J, Fu X, Liang S, Yan R, Li A. Nano-sized cationic polymeric magnetic liposomes significantly improve drug delivery to the brain in rats. *J Drug target*; (2012) 20, 416-421
85. Bhatt Neha, Bhatt Ganesh, Kthiyal Preeti. Drug delivery to the brain using polymeric nanoparticles: a review. *Int J of Pharm and Life Scien*; (2013) vol 2 Issue 3
86. Franc I, Lipinski A, Feeney P J. experimental and computational approaches to estimate solubility and permeability in drug discovery and development settings. *Adv Drug Deliv Rev*; (2001) 46, 3-26

87. Béduneau A, Saulnier P, Benoit JP. Active targeting of brain tumors using nanocarriers. *Biomaterials*; (2007) 28, 4947-4967
88. Trapani A, Denora N, Sitterberg J, Bakowsky U, Kissel T. Methotrexate-loaded chitosan- and glycol chitosan-based nanoparticles: a promising strategy for the administration of the anticancer drug to brain tumors. *AAPS PharmSciTech*; (2011) 12, 1302-1311
89. Barbu E, Molnár E, Tsibuklis J, Górecki DC. The potential for nanoparticle-based drug delivery to the brain: overcoming the blood-brain barrier. *Expert Opin Drug Deliv*; (2009) 6, 553-565
90. Howe P, Green M, Bowers A, Parker D, Varma G, Kallumadil M, Hughes M, Warley A, Brain A, Botnar R. Magnetic conjugated polymer nanoparticles as bimodal imaging agents. *J Am Chem Soc*; (2010) 132, 9833-9842
91. Peckys D., Landwehrmeyer G.B. Expression of mu, kappa, and delta opioid receptor messenger RNA in the human CNS: a 33P in situ hybridization study. *Neuroscience*. (1999) 88(4):1093–135
92. Polt, D.R. & Palian, M.M.. Glycopeptide analgesics. *Drugs of the Future*, (2001) 26(6), pag.561.
93. Costantino, L. et al.. Peptide-derivatized biodegradable nanoparticles able to cross the blood– brain barrier. *Journal of Controlled Release*, (2005) 108(1), pagg.84–96
94. Tosi, G. et al.. Glycopeptide-Decorated Nanoparticles as Drug Carriers for CNS: Effects of Surface Coverage and Carbohydrate Type. *Journal of Nanoneuroscience*, (2009) 1(2), pagg.152–157
95. Tosi, G. et al.. Brain-targeted polymeric nanoparticles: in vivo evidence of different routes of administration in rodents. *Nanomedicine (London, England)*, (2013) 8(9), pagg.1373–1383.
96. G. Tosi, B. Bortot, B. Ruozi, D. Dolcetta, M.A. Vandelli, F. Forni, G.M. Severini. Potential Use of Polymeric Nanoparticles for Drug Delivery Across the Blood-Brain Barrier. *Curr Med Chem*. 2013;20(17):2212-25

- 97.Vilella, A. et al.. Insight on the fate of CNS-targeted nanoparticles. Part I: Rab5-dependent cell-specific uptake and distribution. *Journal of Controlled Release*, (2014) 174, pagg.195–201
- 98.Jiménez AJ, Domínguez-Pinos MD, Guerra MM, FernándezLlebrez P, Pérez-Fígares JM. Structure and function of the ependymal barrier and diseases associated with ependyma disruption. *Tissue Barriers* 2014
- 99.Kara Rogers. Ependymal cell Anatomy. *Encyclopedia Britannica*. 9-26-2016
- 100.Clas B. Johansson, Stefan Momma, Diana L. Clarke, Maarten Risling, Urban Lendahl, and Jonas Frisén. Identification of a Neural Stem Cell in the Adult Mammalian Central Nervous System. *Cell*, Vol. 96, 25–34, January 8, 1999
- 101.Coskun et al.. CD133⁺ neural stem cells in the ependyma of mammalian postnatal forebrain. *PNAS*, January 22, 2008, vol. 105, 1026–1031
- 102.Yoshiyuki Yamazaki, Yukihiro Hirai, Koichi Miyake & Takashi Shimada. Targeted gene transfer into ependymal cells through intraventricular injection of AAV1 vector and long-term enzyme replacement via the CSF. *SCIENTIFIC REPORTS*; 4 : 5506
- 103.Margaret F. Bennewitz and W. Mark Saltzman. Nanotechnology for Delivery of Drugs to the Brain for Epilepsy. *Neurotherapeutics: The Journal of the American Society for Experimental NeuroTherapeutics*. Vol. 6, 323–336, April 2009
- 104.Mihir B. Chauhan and Neelima B. Chauhan. Brain Uptake of Neurotherapeutics after Intranasal versus Intraperitoneal Delivery in Mice. *J Neurol Neurosurg*. 2015; 2(1): 009.
- 105.Anaísa Pires, Ana Fortuna, Gilberto Alves and Amílcar Falcão. Intranasal Drug Delivery: How, Why and What for?. *J Pharm Pharmaceut Sci*, 12(3) 288 - 311, 2009
- 106.S. Talegaonkar, P. R. Mishra. Intranasal delivery: An approach to bypass the blood brain. *Indian J Pharmacol*; June 2004 Vol 36 Issue 3 140-147
- 107.Vilella A, Ruozi B, Belletti D, Pederzoli F, Galliani M, Semeghini V, Forni F, Zoli M, Vandelli MA, Tosi G. Endocytosis of Nanomedicines: The Case of Glycopeptide Engineered PLGA Nanoparticles. *Pharmaceutics*. (2015) Jun 19;7(2):74-89.

108. Salvalaio M, Rigon L, Belletti D, D'Avanzo F, Pederzoli F, Ruozi B, Marin O, Vandelli MA, Forni F, Scarpa M, Tomanin R, Tosi G. Targeted Polymeric Nanoparticles for Brain Delivery of High Molecular Weight Molecules in Lysosomal Storage Disorders. *PLoS One*. (2016 May 26) 11(5):e0156452.
109. P. Sciau, C. Mirguet, C. Roucau, D. Chabanne, M. Schvoerer. Nanoparticles in Ancient Materials: The Metallic Lustre Decorations of Medieval Ceramics. *J. Nano Res.* 8 (2009) 133.
110. The New York Times article of February 22, 2005 see: http://www.nytimes.com/imagepages/2005/02/21/science/20050222_NANO1_GRAPHIC.html
111. Jorg Kreuter. Historical Perspectives Nanoparticles—a historical perspective. *International Journal of Pharmaceutics* 331 (2007) 1–10
112. Merkle, H.P., Speiser, P.. Preparation and in vitro evaluation of cellulose acetate phthalate coacervate microcapsules. *J. Pharm. Sci.* (1973) 62, 1444–1448
113. Anirban Samantaa,b and Igor L. Medintz. Nanoparticles and DNA – a powerful and growing functional combination in bionanotechnology. *Nanoscale*, (2016) 8, 9037-9095
114. Cupaioli, F.A. et al.. Engineered nanoparticles. How brain friendly is this new guest? *Progress in Neurobiology*, (2014) 119–120, pagg.20–38
115. Muro, S.. Challenges in design and characterization of ligand-targeted drug delivery systems. *Journal of Controlled Release*, (2012)164(2), pagg.125–137
116. Maria Justina Roxana Virlan, Daniela Miricescu, Radu Radulescu, Cristina M. Sabliov, Alexandra Totan, Bogdan Calenic and Maria Greabu. Organic Nanomaterials and Their Applications in the Treatment of Oral Diseases. *Molecules* 2016, 21(2), 207
117. ZORZI, Giovanni Konat et al . On the use of nanotechnology-based strategies for association of complex matrices from plant extracts. *Rev. bras. farmacogn.*, Curitiba , v. 25, n. 4, p. 426-436, Aug. 2015

- 118.J. Prasad Raoa, Kurt E. Geckelera. Polymer nanoparticles: Preparation techniques and size-control parameters. *Progress in Polymer Science*. Volume 36, Issue 7, July (2011), Pages 887–913
- 119.Mohanraj, V.J. and Chen, Y.. Nanoparticles-a review. *Tropical Journal of Pharmaceutical Research*, (2007) 5(1), pagg.561–573.
- 120.Panyam, J. and Labhasetwar, V. Dynamics of Endocytosis and Exocytosis of Poly(D,L-Lactide<i>>co</i>-Glycolide) Nanoparticles in Vascular Smooth Muscle Cells. *Pharmaceutical Research*, (2003) 20(2), pagg.212–220.
- 121.Van Oss CJ. Phagocytosis as a surface phenomenon. *Annu Rev Microbiol* 32 (1978) 19-39
- 122.Muller H, Willis KM. Surface modification of i.v. injection able biodegradable nanoparticles with poloxamer polymers and polyxmine 908. *Int J Pharm* 89 (1993) 25-31
- 123.Moghimi SM, Hunter Ac, Murray JC. Long-circulating and target-specific nanoparticles: theory to practice. *Pharmacol Rev* (2001), 53: 283-318
- 124.Chen C, Yang T, Liang W, Zhang Q. In vitro and in vivo study of two types of long circulating solid lipid nanoparticles containing Paclitaxel. *Chem Pharm Bull* 49 (2001) 1444-1447
- 125.Schroeder U, Sabel BA, Schroeder H. *Life Sci* (2000) 66, 495
- 126.Vyas SP, Singh A, Sihorkar V. Ligand-receptor mediated drug delivery: an emerging paradigm in cellular drug targeting. *Crit Rev Ther Drug Carr Syst* (2001) 189:1-76
- 127.Barichello, J.M. et al.. Encapsulation of Hydrophilic and Lipophilic Drugs in PLGA Nanoparticles by the Nanoprecipitation Method. *Drug Development and Industrial Pharmacy*, (1999) 25(4), pagg.471–476
- 128.Dinarvand, R. et al.. Polylactide-co-glycolide nanoparticles for controlled delivery of anticancer agents. *International Journal of Nanomedicine*, (2011) 6, pagg.877–895.

- 129.Muthu, M.. Nanoparticles based on PLGA and its co-polymer: An overview. *Asian Journal of Pharmaceutics*, (2009) 3(4), pag.266
- 130.Rao, J.P. and Geckeler, K.E.. Polymer nanoparticles: Preparation techniques and size-control parameters. *Progress in Polymer Science*, (2011) 36(7), pagg.887–913.
- 131.Makadia, H.K. and Siegel, S.J.. Poly Lactic-co-Glycolic Acid (PLGA) as Biodegradable Controlled Drug Delivery Carrier. *Polymers*, (2011) 3(3), pagg.1377–1397.
- 132.Fredenberg, S. et al.. The mechanisms of drug release in poly(lactic-co-glycolic acid)-based drug delivery systems—A review. *International Journal of Pharmaceutics*, (2011)415(1–2), pagg.34–52.
- 133.Bala, I., Hariharan, S. and Kumar, M.N.V.R.. PLGA nanoparticles in drug delivery: the state of the art. *Critical Reviews in Therapeutic Drug Carrier Systems*, (2004) 21(5), pagg.387–422.
- 134.Estey, T. et al.. BSA degradation under acidic conditions: a model for protein instability during release from PLGA delivery systems. *Journal of pharmaceutical sciences*, (2006) 95(7), pagg.1626–1639
- 135.Fu, K. et al.. Visual evidence of acidic environment within degrading poly(lactic-co-glycolic acid) (PLGA) microspheres. *Pharmaceutical research*, (2000) 17(1), pagg.100–106.
- 136.Vasir, J.K. and Labhasetwar, V.. Biodegradable nanoparticles for cytosolic delivery of therapeutics. *Advanced Drug Delivery Reviews*, (2007) 59(8), pagg.718–728
- 137.Breunig, M., Bauer, S. and Goepferich, A.. Polymers and nanoparticles: Intelligent tools for intracellular targeting? *European Journal of Pharmaceutics and Biopharmaceutics* (2008) 68(1), pagg.112–128.
- 138.Panyam, J. et al., 2002. Rapid endo-lysosomal escape of poly(DL-lactide-co-glycolide) nanoparticles: implications for drug and gene delivery. *FASEB journal: official publication of the Federation of American Societies for Experimental Biology*, 16(10), pagg.1217–1226

139. Aiman O Abbas, Maureen D Dnovan, Aleasger K Salem. Formulating Poly(Lactide-co-Glycolide) Particles for Plasmid DNA Delivery. *Journal of Pharmaceutical Sciences* (2008) Vol 97, NO 7
140. Prabha S, Labhasetwar V. Critical determinants in PLGA/PLA nanoparticle-mediated gene expression. *Pharm Res* (2004) 21:354-364
141. Walter E, Moelling K, Pavlovic J, Merkle HP. Microencapsulation of DNA using poly(D,L-lactide-co-glycolide): Stability issues and release characteristics. *J Control Release* (1999) 61:361-374
142. Cohen H, Levy RJ, Gao J, Fishbein I, Kousaev V, Sosnowski S, Slomkowski S, Golomb G. Sustained delivery and expression of DNA encapsulated in polymeric nanoparticles. *Gene Ther* (2000) 7: 1896-1905
143. Murakami H, Kawashima Y, Niwa T, Hino T, Takeuchi H, Kobayashi M. Influence of the degrees of hydrolyzation and polymerization of poly(vinylalcohol) on the preparation and properties of poly(D,L-lactide-co-glycolide) nanoparticle. *Int J Pharm* (1997) 149:43–49.
144. Zhuang FF, Liang R, Zou CT, Ma H, Zheng CX, Duan MX. High efficient encapsulation of plasmid DNA in PLGA microparticles by organic phase self-emulsification. *J Biochem Biophys Methods* (2002) 52:169–178.
145. Sinha VR, Kumria R. Polysaccharides in colon-specific delivery, *Int J Pharm* 224 (2001) 19-38
146. Saravanakumar, G.; Jo, D.G.; Park, J.H. Polysaccharide-Based Nanoparticles: A Versatile Platform for Drug Delivery and Biomedical Imaging. *Curr. Med. Chem.* (2012) 19, 3212–3229
147. Farnaz Sadat Mirzazadeh Tekie, Fatemeh Atyabi, Masoud soleimani, Ehsan Arefian, Amir Atashi, Melika Kiani, Mohammad Reza Khoshayand, Mohsen Amini, Rassoul Dinarvand. Chitosan polyplex nanoparticle vector for miR-145 expression in MCF-7: optimization by design of experiment. *International Journal of Biological Macromolecules* 81 (2015) 828-837

148. Kubra Kaban, Emine Salva and Julide Akbuga. In vitro dose studies on Chitosan nanoplexes for microRNA delivery in Breast Cancer Cells. *Nucleic Acid Therapeutics* (2016)
149. Andrew M Louw, Mallappa K Kolar, Liudmila N Novikova, Paul J Kingham, Mikael Wiberg, Jørgen Kjems, Lev N Novikov. Chitosan polyplex mediated of miRNA-124 reduces activation of microglial cells in vitro and in rat models of spinal cord injury. *Nanomedicine: Nanotechnology, Biology and Medicine*; 12 (2016) 643-653
150. Sachiko Kaihara Nitta and Keiji Numata. Biopolymer-Based Nanoparticles for Drug/Gene Delivery and Tissue Engineering. *Int. J. Mol. Sci.* (2013) 14, 1629-1654; doi:10.3390/ijms14011629
151. Mumper R, Wang J, Claspell J, Rolland A. novel polymeric condensing carriers for gene delivery. *Proc Int* (1995) 22, 178-179
152. Elena Fernández Fernández, Beatriz Santos-Carballal, Wolf-Michael Weber, Francisco M Goycoolea. Chitosan as non-viral co-transfection system in cystic fibrosis cell line. *International Journal of Pharmaceutics* (2016) 502: 1-9
153. Khalil, I.A.; Kogure, K.; Akita, H.; Harashima, H. Uptake pathways and subsequent intracellular trafficking in nonviral gene delivery. *Pharmacol. Rev.* (2006) 58, 32–45
154. Xiang, S.; Tong, H.; Shi, Q.; Fernandes, J.C.; Jin, T.; Dai, K.; Zhang, X. Uptake mechanisms of non-viral gene delivery. *J. Controll. Release* (2012) 158, 371–378
155. Marc Thibault, Surendra Nimesh, Marc Lavertu and Michael D Buschmann. Intracellular Trafficking and Decondensation Kinetics of Chitosan–pDNA Polyplexes. *Molecular Therapy* vol. 18 no. 10, 1787–1795 oct. 2010
156. Florence Croisier, Christine Jérôme. Chitosan-based biomaterials for tissue engineering. *European Polymer Journal*. Volume 49, Issue 4, April 2013, Pages 780–792
157. Mireia Agirre, Jon Zarate, Edilberto Ojeda, Gustavo Puras, Jacques Desbrieres, Jose Luis Pedraz. Low Molecular Weight Chitosan (LMWC)-based Polyplexes for pDNA

- Delivery: From Bench to Bedside. *Polymers* (2014) 6, 1727-1755; doi:10.3390/polym6061727
158. Duceppe, N.; Tabrizian, M. Factors influencing the transfection efficiency of ultra low molecular weight chitosan/hyaluronic acid nanoparticles. *Biomaterials* (2009) 30, 2625–2631
159. Huang, M.; Fong, C.; Khor, E.; Lim, L. Transfection efficiency of chitosan vectors: Effect of polymer molecular weight and degree of deacetylation. *J. Control. Release* (2005), 106, 391–406
160. Lee, M.; Nah, J.W.; Kwon, Y.; Koh, J.J.; Ko, K.S.; Kim, S.W. Water-soluble and low molecular weight chitosan-based plasmid DNA delivery. *Pharm. Res.* (2001), 18, 427–431
161. Gary L. Peterson. Review of the Folin Phenol Protein Quantitation Method of Lowry, Rosebrough, Farr and Randall. *Analytical Biochemistry* (1979) 100, 201-220
162. Inoue Y, Izawa K, Kiryu S, Tojo A, Ohtomo K Diet and abdominal autofluorescence detected by in vivo fluorescence imaging of living mice diet. *Mol Imaging* (2008) 7:21–27
163. Ausubel, F.M., Brent, R., Kingston, R.E., Moore, D.D., Seidman, J.G., Smith, J.A., Struhl, K. (2000): *Current Protocols in Molecular Biology*. Vol. I, section 2 and 3, John Wiley and Sons, Inc., New York, USA: 1-10
164. Dan M Close, Tingting Xu, Gary S Sayler and Steven Ripp. In Vivo Bioluminescent imaging (BLI): noninvasive visualization and interrogation of biological processes in living animals. *Sensors* (2011) 11, 180-206
165. Kolacsek O, Krizsik V, Schamberger A, Erdei Z, Apati A, Várady G, Mates L, Izsvák Z, Ivics Z, Sarkadi B, Orban TI. Reliable transgene-independent method for determining sleeping beauty transposon copy numbers. *Mob DNA*; 2011. 2:5
166. Geyi Liu, Elena L. Aronovich, Zongbin Cui¹, Chester B. Whitley, Perry B. Hackett. Excision of SleepingBeauty transposons: parameters and applications to gene therapy. *J Gene Med* (2004); 6: 574–583

167. Nasti A, Zaki NM, de Leonardis P, Ungphaiboon S, Sansongsak P, Rimoli MG, Tirelli N. Chitosan/TPP and chitosan/TPP-hyaluronic acid nanoparticles: Systematic optimisation of the preparative process and preliminary biological evaluation. *Pharm. Res.* (2009) 26:1918.
168. Yousefpour et al. Targeted delivery of doxorubicin-utilizing chitosan nanoparticles surface-functionalized with anti-Her2 trastuzumab. *International Journal of Nanomedicine* 2011;6 1977–1990
169. Yuliana Monsalve¹, Giovanni Tosi^{*2}, Barbara Ruozi², Daniela Belletti², Antonietta Vilella³, Michele Zoli³, Maria Angela Vandelli², Flavio Forni², Betty L López¹ & Ligia Sierra. PEG-g-chitosan nanoparticles functionalized with the monoclonal antibody OX26 for brain drug targeting. *Nanomedicine*; June 2015, Vol. 10, No. 11, Pages 1735-1750
170. MacLaughlin FC, Mumper RJ, Wang J, Tagliaferri JM, Gill I, Hinchcliffe M, Rolland AP. Chitosan and depolymerized chitosan oligomers as condensing carriers for in vivo plasmid delivery. *J. Controlled Release.* (1998) 56:259
171. Karimi et al. Evaluation of Chitosan-Tripolyphosphate Nanoparticles as a pshRNA Delivery Vector: Formulation, Optimization and Cellular Uptake Study. *J Nanopharm Drug Deliv.* (2013) 1(3): 266–278
172. So-Jung Gwak, Jong Kwon Jung, Sung Su An, Hyo Jin Kim, Jin Soo Oh, William A Pennant, Hye Yeong Lee, Min Ho Kong, Keung Nyun Kim, Do Heum Yoon, Yoon Ha. Chitosan/TPP-Hyaluronic acid nanoparticles: a new vehicle for gene delivery to spinal cord. *Journal of Biomaterials Scienc.* (2012) Vol 23, Issue 11
173. Alessandro Nasti, Noha M. Zaki, Piero de Leonardis, Suwipa Ungphaiboon, Proramate Sansongsak, Maria Grazia Rimoli, Nicola Tirelli. Chitosan/TPP and Chitosan/TPP-hyaluronic Acid Nanoparticles: Systematic Optimisation of the Preparative Process and Preliminary Biological Evaluation. *Pharm Res* (2009) 26: 1918
174. G. Tosi, A.V. Vergoni, B. Ruozi, L. Bondioli, L. Badiali, F. Rivasi, L. Costantino, F. Forni, M.A. Vandelli. Sialic acid and glycopeptides conjugated PLGA nanoparticles

- for central nervous system targeting: In vivo pharmacological evidence and biodistribution. *Journal of Controlled Release* 145 (2010) 49–57
175. Krauland A and Alonso M. Chitosan/cyclodextrin nanoparticles as macromolecular drug delivery system *Int. J. Pharm.* (2007) 340 134–42
176. Eratalay A, Coskun-Ari F F, Öner F and Özçengiz E. In vitro and in vivo evaluations of PLGA microsphere vaccine formulations containing pDNA coexpressing Hepatitis B surface antigen and Interleukin-2 *J. Microencapsul* (2010) 27 48–56
177. Moghimi SM, Symonds P, Murray JC, Hunter AC, Debska G, Szewczyk A. A two-stage poly(ethylenimine)-mediated cytotoxicity: implications for gene transfer/therapy. *Mol Ther.* 2005;11(6):990–995
178. Yanliang Zhu, Gaofeng Liang, Bo Sun, Tian Tian, Feihu Hu, Zhongdang Xiao. A novel type of self-assembled nanoparticles as targeted gene carriers: an application for plasmid DNA and antimicroRNA oligonucleotide delivery. *International Journal of Nanomedicine* 2016;11 399–411
179. M.N.V. Ravi Kumar, U. Bakowsky, C.M. Lehr. Preparation and characterization of cationic PLGA nanospheres as DNA carriers. *Biomaterials* 25 (2004) 1771–1777
180. J.H. Park, G. Saravanakumar, K. Kim. Targeted delivery of low molecular drugs using chitosan and its derivatives. *Adv. Drug Deliv. Rev.*, 62 (2010), pp. 28–41
181. Krabbe, K.A.. New familial, infantile form of diffuse brain-sclerosis. *Brain*; (1916) 39, 74–114.
182. Suzuki K. Globoid cell leukodystrophy (Krabbe disease): update. *J Child Neurol*; (2003) 18(9):595-603.
183. Matsuda, J., Suzuki, K.. Krabbe disease (globoid cell leukodystrophy). In: Barranger, J.A., Cabrera-Salazar, M. (Eds.), *Lysosomal Storage Disorders*. Springer, US; (2007) pp. 269–283
184. Suzuki, K., Suzuki, K.. The twitcher mouse. A model of human globoid cell leukodystrophy (Krabbe's disease). *Am. J. Pathol.*; (1983) 111, 394–397

185. Suzuki, K., Suzuki, K.. Genetic galactosylceramidase deficiency (globoid cell leukodystrophy, Krabbe disease) in different mammalian species. *Neurochem. Pathol.*; (1985) 3, 53–68.
186. Suzuki, K.. Krabbe disease. In: Lazzarini, R.A., Lassman, H., Nave, K.A., Miller, R., Trapp, B. (Eds.), *Myelin Biology and Disorders*. Elsevier/Academic Press, San Diego, CA; (2004) pp. 841–850.
187. Pritchard, D.H., Napthine, D.V., Sinclair, A.J.. Globoid cell leukodystrophy in polled Dorset sheep. *Vet. Pathol.*; (1980) 17, 399–405
188. Spratley J.. Molecular Mechanisms of Disease Pathogenesis differ in Krabbe Disease Variants. *Traffic*; (2016) 17(8):908-22
189. Luzzi, P., Rafi, M.A., Wenger, D.A.. Structure and organization of the human galactocerebrosidase (GALC) gene. *Genomics*; (1995) 26, 407–409
190. Sakai, N., Tatsumi, N., Fukushima, H., Nishigaki, T., Taniike, M., Nishimoto, J., Tsukamoto, H., Yanagihara, I., Ozono, K., Okada, S.. Molecular cloning and expression of cDNA for murine galactocerebrosidase and mutation analysis of the twitcher mouse, a model of Krabbe's disease. *J. Neurochem.*; (1996) 66, 1118–1124
191. Wenger, D.A.. Krabbe disease (globoid cell leukodystrophy), In: Rosenberg, R.N., Prusiner, S., Di Mauro, S., Barchi, R.L. (Eds.), *The Molecular and Genetic Basis of Neurological Disease*, 2nd ed. Butterworth-Heinemann, Boston; (1997) pp. 421–431.
192. Deane, J.E., Graham, S.C., Na Kim, N., Stein, P.E., McNair, R., Begoña Cachón-González, M., Cox, T.M., Read, R.J.. Insights into Krabbe disease from structures of galactocerebrosidase. *Proc. Natl. Acad. Sci. U. S. A.*; (2011) 108, 15169–15173.
193. Chen, Y.Q., Wenger, D.A.. Galactocerebrosidase from human urine: purification and partial characterization. *Biochim. Biophys. Acta*; (1993) 1170, 53–61.
194. Lefebvre, S., Vartanian, T.. Molecular basis of myelin. In: Dangond, F., Heinemann, B. (Eds.), *Disorders of Myelin in the Central and Peripheral Nervous Systems*. Chapter 2. Butterworth Heinemann, Woburn; (2002).

195. Costantino-Ceccarini, E., Morell, P.. Biosynthesis of brain sphingolipids and myelin accumulation in the mouse. *Lipids*. (1972) 7, 656–659.
196. Austin, J.H., Lehfeldt, D.. Studies in globoid (Krabbe) leukodystrophy. III. Significance of experimentally-produced globoid-like elements in rat white matter and spleen. *J. Neuropathol. Exp. Neurol.*; (1965) 24, 265–289.
197. Suzuki, K., Tanaka, H., Suzuki, K.. Studies on the pathogenesis of Krabbe's leukodystrophy: cellular reaction of the brain to exogenous galactosylsphingosine, monogalactosyl diglyceride and lactosylceramide. In: Volk, B.W., Schneck, L. (Eds.), *Current Trends in Sphingolipidoses and Allied Disorders*. Plenum Press, New York; (1976) pp. 99–113.
198. Borda, J.T., Alvarez, X., Mohan, M., Ratterree, M.S., Phillippi-Falkenstein, K., Lackner, A.A., Bunnell, B.A.. Clinical and immunopathologic alterations in rhesus macaques affected with globoid cell leukodystrophy. *Am. J. Pathol.*; (2008) 172, 98–111.
199. Hawkins-Salsbury, J.A., Parameswar, A.R., Jiang, X., Schlesinger, P., Bongarzone, E., Ory, D. S., Demchenko, A.V., Sands, M.S.. Psychosine, the cytotoxic sphingolipid that accumulates in globoid cell leukodystrophy, alters membrane architecture. *J. Lipid Res.*; (2013) 54, 3303–3311.
200. Yedda Li BA and Mark S. Sands. Experimental Therapies in the Murine Model of Globoid Cell Leukodystrophy. *Pediatric Neurology*; (2014) 51(5): 600–606.
201. Wenger, D.A., Rafi, M.A., Luzi, P., Costantino-Ceccherini, E.. Krabbe disease: genetic aspects and progress toward therapy. *Mol. Genet. Metab.*; (2000) 70, 1–9.
202. Wenger, D.A.. Intravenous injection of AAVrh10-GALC after the neonatal period in twitcher mice results in significant expression in the central and peripheral nervous systems and improvement of clinical features. *Mol Genet Metab.*; (2015) 114(3):459–66.
203. Ursula M.. Non Viral Gene Transfer Approaches for Lysosomal Storage Disorders. *Non-Viral Gene Therapy*; (2011)

- 204.Sergey S. Sergin and Amalfitano A., 2011. Immune Recognition of Gene Transfer Vectors: Focus on Adenovirus as a Paradigm. *Front Immunol.*; (2011) 2: 40.
- 205.Hawkins-Salsbury et al.. Triple Treatment for Murine GLD. *J. Neurosci.*; (2015) 35(16):6495– 6505.
- 206.Christina R. Mikulka, Mark S. Sands. Treatment for Krabbe’s Disease: Finding the Combination. *Journal of Neuroscience Research*; (2016) 94:1126–1137
- 207.JacquelineA.Hawkins-Salsbury and MarkS.Sands. Mechanism-Based Combination Treatment Dramatically Increases Therapeutic Efficacy in Murine Globoid Cell Leukodystrophy. *TheJournalofNeuroscience*; (2015) 35(16):6495–6505.
- 208.Sakai, N., Tatsumi, N., Fukushima, H., Nishigaki, T., Taniike, M., Nishimoto, J., Tsukamoto, H., Yanagihara, I., Ozono, K., Okada, S.. Molecular cloning and expression of cDNA for murine galactocerebrosidase and mutation analysis of the twitcher mouse, a model of Krabbe's disease. *J. Neurochem.*; (1996) 66, 1118–1124.
- 209.Fletcher TF, Kurtz HJ. Animal model: globoid cell leukodystrophyin the dog. *Am J Pathol*; (1972) 66:375–378.
- 210.Victoria T, Rafi MA, Wenger DA. Cloning of the canine GALCcDNA and identification of the mutation causing globoid cell leukodys-trophy in West Highland and Cairn terriers. *Genomics*; (1996) 33:457–462.
- 211.Luzi P, Rafi MA, Victoria T, Baskin GB, Wenger DA. Characteri-zation of the rhesus monkey galactocerebrisdase (GALC) cDNA andgene identification of the mutation causing globoid cell leukodystrophy(Krabbe disease) in this primate. *Genomics*; (1997) 42:319–324.
- 212.D. Zheng, C. Duan, D. Zhang, L. Jia, G. Liu, Y. Liu, F. Wang, C. Li, H. Guo, Q. Zhang. Galactosylated chitosan nanoparticles for hepatocyte-targeted delivery of oridonin. *Int J. Pharm.*, 436 (2012), pp. 379–386
- 213.Zsuzsanna Izsvák, Marinee K.L., Thierry VandenDriessche, Zoltàn Ivics. Efficient stable gene transfer into human cells by the Sleeping Beauty transposon vectors. *Methods* 49 (2009) 287–297

- 214.T.S.C. Lia, T. Yawata, K. Honke. Efficient siRNA delivery and tumor accumulation mediated by ionically cross-linked folic acid-poly(ethylene glycol)-chitosan oligosaccharide lactate nanoparticles: for the potential targeted ovarian cancer gene therapy. *Eur. J. Pharm Sci.*, 52 (2014), pp. 48–61
- 215.X. Zhao, Z. Li, W. Liu, W. Lam, P. Sun, R.Y.T.K. Keith, D.K. Luk, W.W. Lu. Octaarginine-modified chitosan as a nonviral gene delivery vector: properties and in vitro transfection efficiency. *J. Nanopart. Res.*, 13 (2011), pp. 693–702
- 216.Mao S, Sun W, Kissel T. Chitosan-based formulations for delivery of DNA and siRNA. *Adv. Drug Deliv. Rev.* (2010) 62:12
- 217.Evanko SP, Wight TN. Intracellular localization of hyaluronan in proliferating cells. *J Histochem Cytochem* (1999) 47: 1331–1341